NON-BOLTZMANN MONTE CARLO STUDY OF CONFINED LIQUID CRYSTALS AND LIQUID CRYSTAL ELASTOMERS

A dissertation submitted to the faculty of

University of Hyderabad

for the award of degree of

Doctor of Philosophy

by

D. Jayasri

School of Physics

University of Hyderabad

June 2009

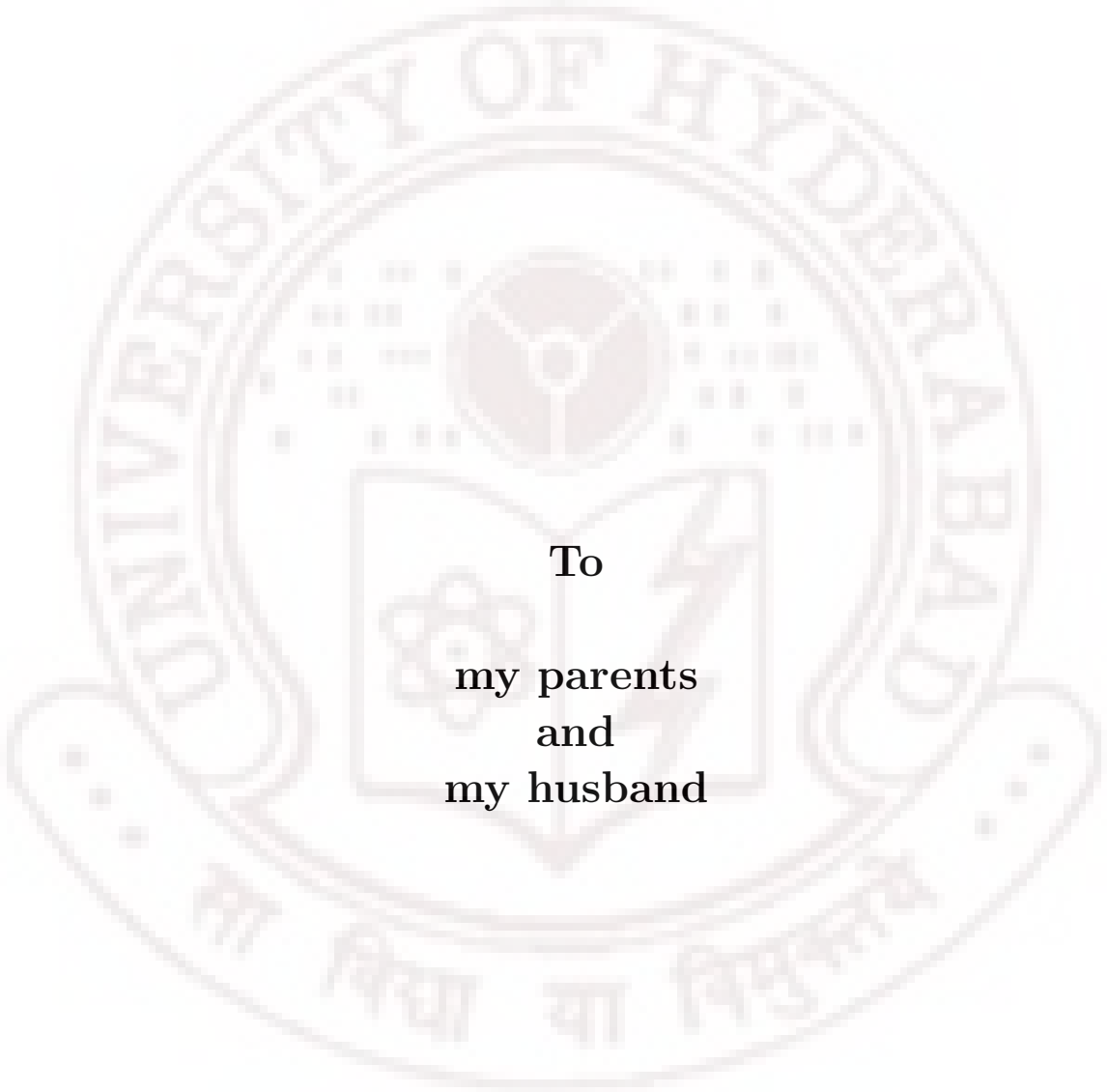

To

my parents
and
my husband

Declaration

I hereby declare that the work presented in this thesis titled 'Non-Boltzmann Monte Carlo study of confined liquid crystals and liquid crystal elastomers' has been carried out by me under the supervision of Prof. V. S. S. Sastry, School of physics, University of Hyderabad, Hyderabad, India, as per the Ph.D ordinances of the University. I declare, to the best of my knowledge, that no part of this thesis has been submitted for the award of a research degree of any other University.

D. Jayasri

Reg. no: 04PHPH05

Certificate

This is to certify that the thesis work entitled "Non-Boltzmann Monte Carlo study of confined liquid crystals and liquid crystal elastomers" being submitted to the University of Hyderabad by D. Jayasri (Reg. No. 04PHPH05), for the award of the degree of Doctor of Philosophy in Physics, is a record of *bona fide* work carried out by her under my supervision.

The matter embodied in this dissertation has not been submitted to any other University or Institution for the award of any degree or diploma.

Prof. Vipin Srivastava,

Dean,

School of Physics,

University of Hyderabad,

Hyderabad - 500 046.

Prof. V. S. S. Sastry,

Supervisor,

School of Physics,

University of Hyderabad,

Hyderabad - 500 046.

Acknowledgements

"If I have seen farther, it is by standing on the shoulders of giants"

-Sir Isaac Newton.

First and foremost, I would like to express my profound gratitude to my mentor, teacher and thesis advisor, Prof. V. S. S. Sastry, who has been supportive with his invaluable knowledge, supervision and useful suggestions through out this research work. I attribute the knowledge attained during my research starting from my M. Tech, to his constant encouragement and effort. Sir, without you this thesis would not have been written or completed. Your patience and continuous guidance enabled me to learn physics as well as the much needed lessons in life.

It is an honour for me to express my gratitude to Prof. K. P. N. Murthy, whose support and guidance made my thesis work possible. He has been actively interested and involved in my work and has always been available to advice me starting from my M.Tech project. Sir, I thank you so much for teaching me the nuances of various Monte Carlo methods and other memorable discussions on thermodynamics and statistical physics. Your enthusiasm and zeal for physics and your readiness to share your knowledge with others always kept me motivated.

I wish to thank the faculty of School of Physics, Prof. A. Chatterjee, Prof. S. R. Shenoy, Prof. A. K. Kapoor, Prof. S. Chaturvedi, Prof. B. A.

Bambah, Dr. Anantha Lakshmi, Dr. P. K. Suresh and others who taught me various aspects of physics during my stay in this University. It is with great pleasure, I would like to express my gratitude to Prof. N. Satyavathi (Osmania University) for showing interest in my work and for whom I have a high regard. She has always been supportive and encouraging during our discussions.

I am grateful to Prof. Vipin Srivastava, the Dean, School of Physics, for providing the facilities of the school I would like to thank the office staff of School of Physics, Mr. Abraham and others who helped me in more than one way during the period of my PhD here.

It is my pleasure to thank Prof. Arun Agarwal, Director, CMSD, University of Hyderabad, for allowing me to use the computing and other facilities at the Centre and also for providing financial assistance for participating in various conferences and workshops across the country, which greatly helped in enriching my knowledge. I would also like to express my gratitude to CMSD staff, Mr. Murali, Mr. Vinod and others for giving me timely help in administration related affairs during my visits to conferences abroad.

I gratefully acknowledge DST(HPC)-CMSD/IBM for providing me financial assistance during 2006-09 and also providing travel assistance during this period for presenting my work in various conferences. I would also like to acknowledge DAE (BRNS) for providing the fellowship during the initial years of my research.

Iam indebted to all my group mates Saipreeti, Regina Jose, Kamala Latha, Trivikram Rao, Rajeswari, Shankaraiah, Shiva, Suman, Arun and Satya (Boltzmann group) for being a constant source of support and also for making my days here filled with fun and frolic. I would like to specially thank Saipreeti

for being a great companion during all these days of my stay here. I wish to thank my colleagues Niranjan, Mikki (K. Jayasri), Sudha, Anjan, Juby, Sridhar, Sathish, Sundarayya and many others who made my stay here memorable. I wish to offer my sincere thanks to my lab mate Regina for reviewing my entire draft of thesis and offering her invaluable suggestions during the process.

I owe a lot to my loving parents, Prof. D. Bhaskara Murti and D. Parvati, for their patience, love and understanding all through my life. Their love and blessings helped me in completing this endeavour successfully. I would like to specially thank my loving sister D. Aparna for being my constant support, inspiration and for being my best companion all through my life. If there is any driving force that kept me going and which has not changed over time, it is the love, support and encouragement of my dearest husband G. Rejeesh, to whom I dedicate this compilation. I owe my deepest gratitude to my parents-in-law, P. Gangadharan and G. Thangam, with out whose constant support and encouragement, this PhD would have not been complete. I would like to mention a special note here to my loving sisters-in-law Reena and Sheena. My sincere thanks to Reena for her timely help in the most needed time of my thesis compilation and also for being a great companion.

Above and beyond all, I owe my heart-felt gratitude to Bhagawan Sri Sathya Sai Baba for making every thing possible.

Preface

Liquid crystals constitute a cascade of intermediate phases between solids and liquids. The simplest and fascinating of these is nematic phase in which the constituent molecules (mostly rod-like or disc-like) exhibit long-range orientational order but their centres of mass are distributed randomly, resembling a liquid. In nematic phase, there exists an average direction represented by $\hat{(n)}$, called the *director* along which a statistically large number of molecules tend to align parallel to themselves. Since the translational degrees of freedom do not get affected during the nematic to isotropic (NI) transition, the order parameter depends only on the orientational degrees of freedom. In the nematic phase, the directors have head-tail symmetry, *i.e.,* $\hat{n}$ and $-\hat{n}$ are indistinguishable. More often, the distribution of molecules about the director has uniaxial symmetry and further the constituent molecules are assumed to be cylindrically symmetric. Under these simplifying conditions, the degree of orientational order is adequately represented by a scalar, and serves as the order parameter to describe the NI transition in bulk liquid crystal systems. However, it is not the case with liquid crystals confined under certain chosen boundary conditions. In such confined liquid crystal (LC) systems, there can exist additional direction of molecular alignment necessitating tensorial description of the degree of orientational order in the system.

Since liquid crystals are soft materials, surface induced ordering can lead to novel and interesting director structures on appropriate confinement. Possible transitions from one stable director structure to another (through a control pa-

rameter) make confined liquid crystals challenging objects of study, from both academic as well as technological points of view. Such systems confined to, for example, patterned substrates have been receiving considerable attention in the recent years due to their potential applications in display technology. In this thesis, one of the objectives is to investigate the effect of such confinement on the NI transition, through Monte Carlo simulations.

Elastic materials obtained by cross-linking polymers made up of liquid crystalline monomers (liquid crystal elastomers) have been receiving considerable attention recently owing to the coupling between the orientational degree of freedom of the LC constituents in the polymer chains and the strain. Manifestation of thermally induced orientational liquid crystalline order (across the isotropic-nematic phase transition) in terms of observable strain makes these systems potential candidates for applications as for example actuators. From conceptual view point, it is challenging to look for simple Hamiltonian models which provide a reasonable microscopic (or even mesoscopic) basis to capture the macroscopic observations. In this context, the other objective of this thesis is to investigate two such recently proposed (coarse grained) lattice models through detailed Monte Carlo simulations, with a view to examining their implementations in accounting for the experimental observations.

In principle, liquid crystals (as well as liquid crystal elastomers) should be simulated using off-lattice models, wherein it is possible to vary translational as well as orientational coordinates. But since the nematic-isotropic (NI) transition primarily influences only the orientational degrees of freedom, it has become customary to employ lattice-based Hamiltonian models to capture the curious behaviour of the orientational order across the transition. Lebwohl-Lasher lattice model based on Maier-Saupe theory accounts for the

observed weak first order NI transition by prescribing a suitable orientation dependent interaction among nearest neighbours. Canonical simulation methods applied to this model provide a simple tool to investigate the NI transition computationally.

An interesting consequence of a first order transition is the possibility of coexistence of the two phases over an appreciable range of the control parameter bracketing the transition. In terms of a free-energy description this corresponds to the onset of two free-energy minima (corresponding to the two phases) seperated by a barrier in the appropriate order parameter space, which rapidly increases with the size of the system. Canonical sampling techniques, which require that the elementary steps in the random walk of the system in the configurational space are *a priori* unbiased, but for the natural bias provided by the density of states of the system, are thus rendered inefficient in the presence of such barriers, as they make the corresponding configurational space quasi-ergodic. In realistic terms such sampling methods are not well suited to investigate details near such first order transitions. An important step in partially resolving this issue was the recognition of the fact that a carefully guided walk of the system, so as to make the resultant probability distribution uniform with respect to its energy, can be rendered insensitive to the energy barriers, and consequently can encompass all microstates including those which are expected to be visited only rarely under conventional excursions. Implementation of this novel idea needs on one hand development of suitable algorithms to create such energy-wise uniform ensembles (so called non-Boltzmann ensembles) and, on the other deriving physically meaningful (canonical) ensembles corresponding to actual observations by appropriate extraction (re-weighting) methods from the grand ensemble of microstates. In

this context, this thesis attempts to adopt the so-called entropic sampling techniques to different Hamiltonian models of liquid crystals, based on a recent and efficient procedure (Wang-Landau (WL) algorithm), originally suggested for lattice models with discrete degrees of freedom. Suitable modifications to the WL algorithm to make it applicable to liquid crystal system of moderately large sizes, as well as its application to investigate phase transitions in liquid crystal elastomers and certain confined liquid crystals are objectives of this study.

The above work is reported in the thesis divided into six Chapters. While Chapter 1 provides a brief introduction to the physics of liquid crystals and related elastomers with specific focus on the phenomena near the NI transition, Chapter 2 reviews the Monte Carlo simulation methodologies providing motivation to look for multi-canonical sampling techniques to deal with issues connected with the chosen systems of study. Chapter 3 describes the development of computational methodology based on WL algorithm, to suit LC systems. In simple terms, it corresponds to providing algorithmic guidance to the random walk of the system in its configurational space so that it visits progressively regions of lesser probability at the cost of naturally occuring more probable regions. A careful implementation of this procedure, with a provision to withdraw this guidance asymptotically, leads to a reasonable estimate of density of states (DoS) of the system. This representative DoS is then utilized to bias a long walk (so called production run) in such a way the system performs a random walk which is reasonably uniform with respect to energy. Such collection of microstates, while not corresponding to any physical ensemble, can be used to project out the required canonical ensemble (at the appropriate temperatures) by known re-weighting techniques. In this

Chapter, finer details of the implementation of this modified algorithm, as well as of introduction of other strategies like the frontier sampling (reported earlier for magnetic systems) are presented. The applicability and efficacy of this procedure is tested first on a lattice Hamiltonian model (Lebwohl-Lasher) with a size of $20 \times 20 \times 20$, and the results are compared with known data from canonical sampling procedures. The methodology is further validated with confined liquid crystals in a porous medium. The effect of confinement to different pore sizes is mimicked by the introduction of appropriate doses of randomly quenched disorder. The depressions in the NI transition temperatures at different degrees of confinements are computed, and they are found to compare very well with those reported earlier. The sampling procedure so optimized is adopted for all the simulations reported subsequently.

Experimental evidence in liquid crystal elastomers (LCE) shows that the thermally induced NI transition involving mesogenic units, and the resultant changes in the strain parameter, correspond at best to a non-singular crossover from the isotropic to the nematic phase. It may be noted that NI transition in a simple liquid crystal itself is a (weak) first order transition. Attempts to understand the origin for these observations in LCE were first based on the analysis of Landau free energy expansion in the appropriate space of order parameters (orientational order and strain), and it was concluded that the smoothening of this transition could be due to the presence of heterogeniety within the sample (radom-bond or random-field type), in preference over the other plausible cause of having large (internal) stresses imparting super critical elastic behaviour to the sample. In this connection two lattice models were proposed to take into account the interaction energy between different mesogenic units (on a coarse grained level), and their interaction with the global strain.

The energy contribution from the strain itself was derived from the established theory of rubber elasticity. The first such lattice Hamiltonian, say Model-A, (proposed by Selinger and Ratna, in 2004) was proposed encompassing different contributions existing from purely energetic considerations. For simplicity it is assumed that the nematic directors of the different polymer chains are located at the sites of a cubic lattice, and are appropriately coupled to the global strain. Their Monte Carlo simulations on this model correspond to performing a random walk in the combined space of orientational degrees and strain. In their simulations the coupling between these two order parameters were set to its maximum value (unity) corresponding to maximal anisotropy of the polymer chain shape tensor. The conclusions were that a homogeneous sample (without invoking either random-bond or random-field type quenched disorder) described by this Hamiltonian leads to a strong first-order NI transition (and hence the corresponding strain transition), and in order to make contact with the observed behaviour certain degree of heterogenity needs to be introduced. The second Hamiltonian model, say Model-B (proposed by Pasini, *et. al.*, in 2005) also describes this system on a coarse grained level, by assuming a cubic lattice of cross-linking points connected by polymer chains with Gaussian statistics. While the mesogenic units with directors located at the centres of each cell of this elastic lattice interact much the same way as in the earlier model (Lebwohl-Lasher interactions), the terms representating the elastic energy and the interaction between the two orders are included as explicitly due to entropic contributions. As a result, the Hamiltonian contains the so-called pseudo-terms as far as strain degrees of freedom are concerned. This model further provides for a moderation of the interaction term depending on the state of deformation, by introducing a strain-dependent prefactor in

the corresponding expression. Additional pre-factor introduced by the authors in this context is to take into account other attributes of a real system, like cross-link density, type of the polymer formed, etc.

Chapter 4 reports results of simulations on the above two lattice models, employing sampling technique outlined in Chapter 3. Since Model-A has pure energetic contributions, it does not present any conceptual problem in the construction of non-Boltzmann ensemble via entropic sampling. It actually provides an opportunity to extend the random walk in the configuration space to a higher dimension, and consequent construction of canonical ensemble in this enhanced parameter space. Primary objective of the study of Model-A thus is to investigate the effect of stronger orientational order on the strain of the system by extending the simulations to much lower temperatures than reported. The motivation arises from the fact that the earlier investigations reporting strong first order transition in a homogeneous sample were carried out imposing an extreme condition on the shape anisotropy of the polymer chain ($\gamma = 1$ in the model). The present studies show that the first order transition as reported under these conditions is also evidenced by the free-energy profiles obtained from the density of states estimated through this entropic sampling method. However, the strain expected from this model even at moderately high orientational order is found to be highly non-linear. This led to further simulations, changing γ progressively from 1 to 0 in very small steps. Such a variation can be looked upon as a cumulative effect of one or more of the following physical scenarios: presence of local mesogenic units with different degrees of anisotropy, variable density of cross-links in the system, effect of the nature of polymerization of the mesogenic units, etc. The results indicate that on progressively decreasing the value of γ certain consequenses follow: the

transition temperature changes and the transition softens; the strain dependence on orientational order becomes progressively linear; the low temperature behaviour of this model LCE recovers the experimental observation; and the initial barrier (at $\gamma = 1$) in the free energy profiles gradually disappears. It emerges from these observations that apart from the introduction of heterogeneity in the system as a means of softening the simulated transition to relate to experimental observations, introduction of a variable coupling strength, necessitated by compulsions imposed by realistic systems, is another plausible device to make contact with the experiment.

The second LCE Hamiltonian (Model-B) differs qualitatively from the earlier one in two respects. The elastic energy and its interaction with orientational degrees are explicitly included as entropic contributions, making them (linearly) temperature-dependent pseudo Hamiltonian terms. Secondly, the coupling strength between the two interacting variables is made a function of the degree of strain, and as a consequence this interaction strength is instantaneously moderated for a given strain. Monte Carlo simulations (canonical sampling) already reported based on this Hamiltonian, are found to account for experimental observations satisfactorily. The interest in studying this model in this context arises from a different perspective: application of entropic sampling technique (which is originally employed for Hamiltonians with purely energetic terms) to systems with pseudo (temperature dependent) terms. While such a structure does not pose problems during canonical sampling for obvious reasons, qualitatively different methodology needs to be developed to estimate DoS in the combined space of the two order parameters. The DoS of the orientational degrees arising from the pure enrgetic contribution is suitably augmented with that generated from the elastic terms, so as to result in a

two dimensional DoS surface. Canonical ensembles are then extracted at the desired temperature, and averages of physical properties are computed from the two-dimensional canonical ensembles. Details of these simulations and comparison of results so obtained with the canonical methods are presented. Finally, this Chapter concludes with a few observations on the two models based on the present simulations.

Chapter 5 reports results on the phase behaviour of a liquid crystal in contact with a chemically patterned and geometrically structured substrate, as it undergoes a transition from isotropic to nematic phase. While experimental as well as theoretical investigations of nematic liquid crystals (NLC) in contact with geometrically structured substrates or with chemically patterned substrates have been fairly extensive and well reported, such studies on NLC confined by geometrically structured as well as chemically patterned substrates are of recent origin. In particular, prediction of new phase diagrams involving transitions between distinct director configurations under varied geometrical structures, based on continuum models, is particularly interesting due to possible implications in their application to display purposes. The control parameter space spanning these predicted transitions encompasses typically the relative anchoring strengths at the different chemical patterns, the relative length scales of the geometric structures perturbing the system in the plane representing the cross section of the geometric structure (like groove depth *versus* the pitch of the pattern), and in principle the relative phase of the chemical pattern with respect to the geometrical structure. Monte Carlo studies on these new systems have been rare. In this context, the present work attempts this problem to examine whether the MC simulations results conform to the continuum theory predictions, the role of finite temperature

effects on the director structures as the sample is gradually cooled, the effect of inter-molecular interactons in a real system spanning the 3-dimensional space (in contrast to the 2-dimensional description in the continuum theory restricted by the chosen boundary conditions), and detection of other possible metastable states by computing representative free-energy profiles in the appropriate parameter space (as afforded by the entropic sampling technique).

Two such systems were investigated with these objectives. System-1 is a NLC embedded between two solid substrates: one has planar geometry and is expected to induce anchoring with the desired tilt angle with respect to the substrate normal (θ_D), and the second has a corrugated geometry with a sinusoidal cross section. This substrate induces alternately both planar and homeotropic anchoring (like repeating stripes) over chosen regions along the sinusoidal curve. Restricting the problem to the two dimensional space of the cross section of the substrate, minimization of the Frank-Oseen energy predicts two stable director structures (homeotropic H and hybrid aligned nematic HAN), between which transition can be induced either by varying the relative strength of the two alternating stripes of planar and homeotropic anchoring, or even by varying the anchoring angle (θ_D) at the other planar substrate. In this context, MC simulations are carried out on this system, represented by a cubic lattice with Lebwohl-Lasher interaction among the nearest neighbours. The prescribed boundary conditions are imposed by introducing ghost layers with appropriate orientations, as is done typically in such studies. Some of the interesting observations from this work include: significant (temperature dependent) deviations from the expected homeotropic (H) structure with large director excursions (away from the substrate normal) being observed in the middle of the sample (away from anchoring effects from either substrate); onset

of phase biaxiality for tilt angles $\theta_D > 30^0$; evidence from the microstates collected in the entropic ensemble to the effect that there are at least two distincticly observable director structures with the same energy, free energy curves computed as a function of temperature; and sensitivity of all these features to the relative phase of the chemical pattern with respect to the underlying geometrical structure.

The second example in this category (System-2) is a thin film of liquid crystal pasted on a spherical substrate. The substrate is modelled to induce homeotropic anchoring with variable strength, and the outer surface experiences free boundary conditions. After preliminary studies to arrive at optimum dimensions of the sample (radius of the substrate and the thickness of the film), detailed MC studies were carried out to compute the two relevant order parameters corresponding to the axial and radial director structures of the system and their variances, as a function of temperature, for a wide range of anchoring strengths. The results indicate a clear anchoring transition from axial to radial director structure at low enough temperatures, while just below the NI transition temperature both structures are observed to coexist with relative probabilities determined (at the given temperature) by the anchoring strength. These features are evident from the collection of microstates in the entropic ensemble displayed with respect to the energy of two systems. The outcome of MC simulations on these two textured systems point out to the potential application of entropic sampling based MC simulations in investigating possible metastable states, and the role of finite temperature on the predicted phase diagrams.

Salient features of application of multi-canonical Monte Carlo techniques to liquid crystal systems, by suitably modifying the WL algorithm, are sum-

marized in Chapter 6. While recounting the potential gains achieved through such novel sampling methods, as illustrated by the modest investigations reported here on liquid crystal elastomers and textured liquid crystal films, the need to speed up the algorithm to deal with bigger systems through appropriate parallelization schemes, as well as the potential for new information that this type of simulations can lead to when applied to off-lattice models (like Gay-Berne interactions) are noted.

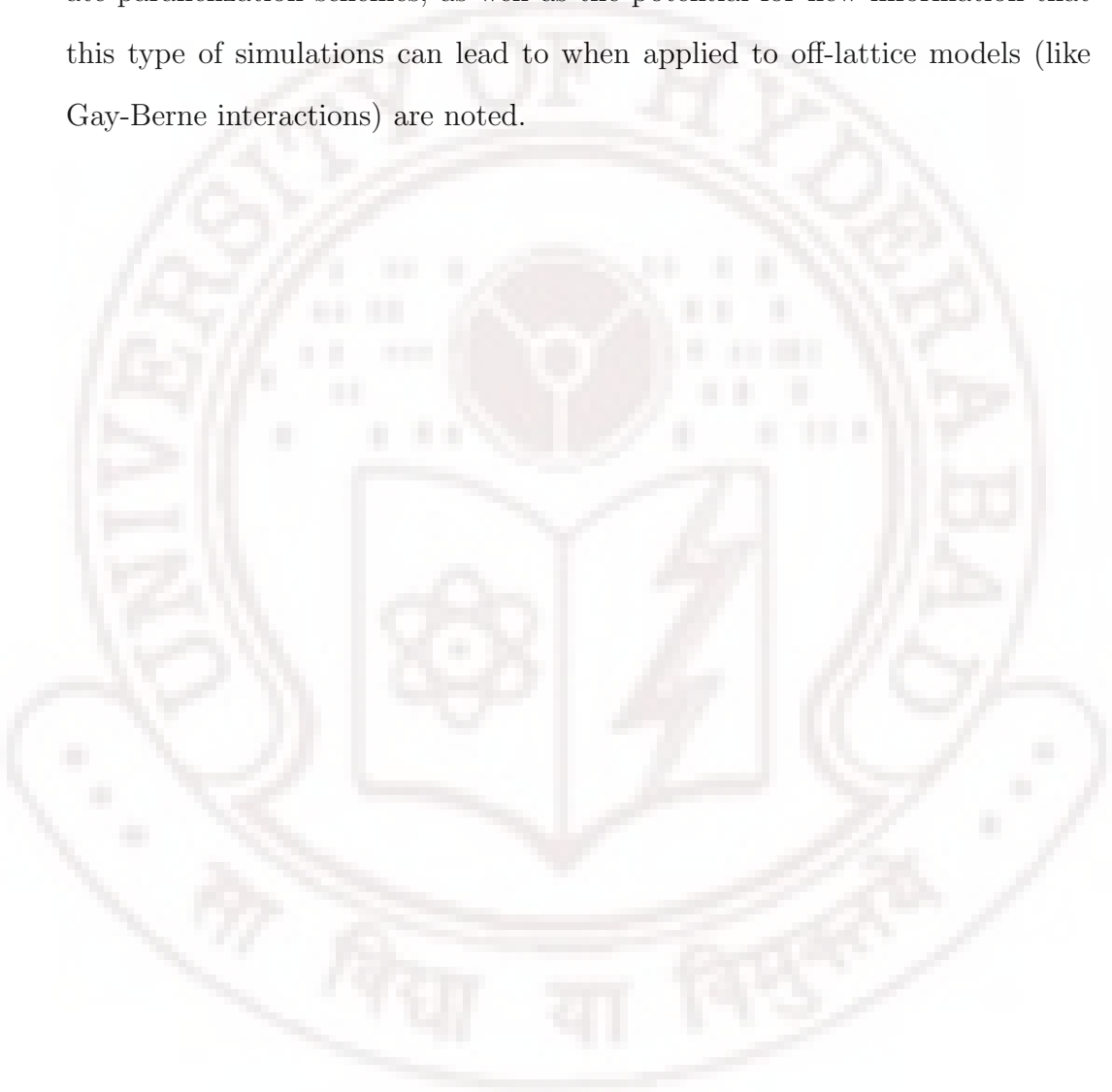

Contents

List of Figures

Chapter 1

Introduction to liquid crystals

Matter can be classified into solid, liquid and gaseous states. The transitions between these states are not necessarily direct, and there may exist certain intermediate phases called mesophases. Liquid crystalline phases denote a series of such mesophases, between solids and liquids. The important property that differentiates the solid and liquid phases is flow. More fundamentally, spatial as well as orientational correlation lengths are of the order of system size in crystalline solids, whereas liquids exhibit short and finite correlation lengths. Liquid crystals, on the other hand, exhibit long-range orientational order while having only partial order in one or two dimensions in their translational degrees of freedom. These materials have highly anisotropic physical properties, and consist of usually either rod-like (calamatic liquid crystals) or disc-like (discotic liquid crystals) molecules.

The discovery of liquid crystals as an intermediate phase between solids and liquids is attributed to an Austrian botanist Friedrich Reinitzer. In 1888, while experimenting with certain type of cholesterol in plants, he realised that it undergoes two transitions, from solid to a cloudy liquid and then to a clear liquid. Subsequently, Otto Lehmann also observed similar behaviour in other substances. He coined the term liquid crystals

for the first time on observing that this phase shares both the properties of liquids and solids. In 1922, Georges Friedel [1] classified the liquid crystalline phases into nematic, smectic and cholesteric phases. But the liquid crystal research had been rather slow till 1960's largely due to the lack of awareness of these materials among researchers and particularly about their possible practical applications. With the advent of a discovery of switchable optical properties of liquid crystals under suitable confinements, research on liquid crystals expanded during 1970's and 80's looking particularly for display applications. Now, technologically, liquid crystals have become a part of our daily life right from wrist watches, calculators, etc, to laptops, high definition televisions, etc [3–5].

The liquid crystals can be broadly divided into two categories: thermotropic and lyotropic liquid crystals, depending on whether the ordering is driven by temperature or concentration of liquid crystalline substance in solution, respectively. The present work deals with thermotropic liquid crystals. The simplest thermotropic liquid-crystalline phase is the nematic phase. The term *nematic* originated from Greek word $\nu\eta\mu\alpha$, which means thread. The defects in nematic phase produce thread-like disclination lines when observed between crossed polarisers and hence the name. In the nematic phase, there exists an average direction, called *director* ($\hat{n}$), along which a large number of molecules tend to orient themselves. In rod-like molecules, this direction is along the long-axis whereas in disc-like molecules, it is normal to the disc. As the temperature decreases the degree of alignment and hence the order increases in the nematic phase. In the present work, we deal with rod-like molecules with perfect uniaxial symmetry about the long axis. In bulk, the angular distribution of molecules around the director is uniform which corresponds to uniaxial symmetry of the nematic phase. But when the liquid crystal system is constrained under external boundary conditions, there could also exist other characterstic and distinguishable di-

rections about which the molecules tend to align themselves, thus exhibiting biaxial symmetry. An important feature of the nematic phase is that there exists a head-tail symmetry of the director, i.e., the states with director, $\hat{n}$ and $-\hat{n}$ are indistinguishable. Even though there exists a preferred direction of orientation, the centres of mass are randomly distributed and dynamics just in the isotropic fluid, and hence the nematic phase behaves as a fluid. The main focus in this thesis is the phenomenon of transformation of isotropic phase into an orientationally ordered nematic phase on cooling.

1.1 Types of interactions between liquid crystal molecules

Typical intermolecular potential generally used to describe interactions among constituent molecules in a liquid, as a function of distance r between the centres of molecules is as shown in the figure 1.1 [22]. Such a potenital is characterized by a minimum which usually has a depth ϵ at a distance r_0. At larger values of r, the potential decays to zero, while for smaller values, it rises through zero at $r = \sigma$, rapidly to higher values. The repulsion at short range is a consequence of the overlap of the electron clouds and hence it has a form roughly like $exp(-r/\rho)$, where ρ is a distance of the order σ. The long-range interactions can be broken down into a number of distinct contributions:

a. Electrostatic term, which is a direct interaction between the charge distributions of the molecules ($\pm r^{-n}$)

b. Induction and dispersion terms, due to the perturbation of the charge distribution of one molecule owing to the presence of the other ($-r^{-n},\ n > 6$).

Dispersion term involves only the states where both the molecules are excited.

c. Resonance term, when at least any one of the molecules is in a degenerate state ($\pm r^{-n},\ n > 3$).

d. Magnetic term, when there exists electronic degeneracy ($\pm r^{-n},\ n > 3$).

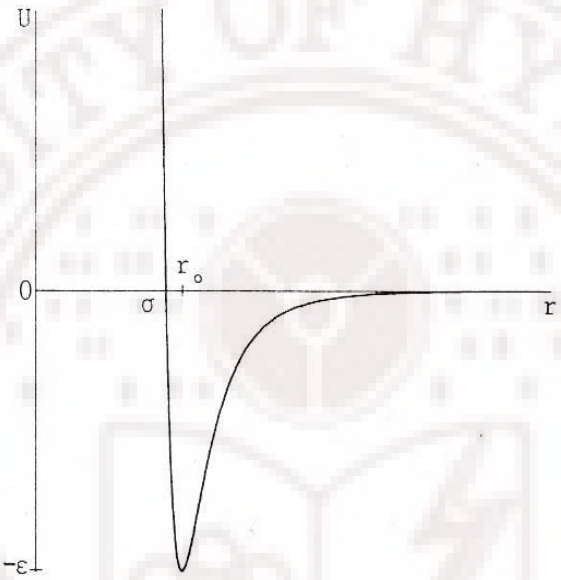

Figure 1.1 The interaction energy,U between two molecules as a function of the distance r between them.

In the case of liquid crystal molecules, the dispersion energy plays an important role as it gives rise to orientation dependent anisotropic contributions to the intermolecular potential which are crucial for explaining the isotropic to nematic transition, characterized by the onset of an orientational order parameter. Maier-Saupe theory accounts for this transition based on this long-range attractive dispersive energy while ignoring all the other energetic contributions.

1.2 Nematic-Isotropic transition

As discussed above, nematic phase is fluid and anisotropic in nature. Several experimental observations [8, 11] using various techniques [7–9] show that the order parameter decreases monotonically as the temperature is increased and drops abruptly to zero near the transition temperature (T_{NI}). In the case of uniaxial nematic (which is the subject of study in this thesis), the order parameter drops from a value in the range $(0.25 - 0.5)$ depending on the mesogenic material being considered. The nematic to isotropic transition is first order in nature though it is relatively weak thermodynamically because only orientational order is lost at T_{NI} and the heat of transition is 1 KJ/mol [13]. The changes in entropy and volume are only a few percent of the corresponding values of solid-nematic transition. In the isotropic phase, there is no long-range orientational order. But on careful observation, one finds that locally the molecules even in the isotropic phase exhibit short-range orientational order particularly near the transition temperature and this local order persists over a characteristic distance, $\xi(T)$ called the coherence length. It has been observed that just above the NI transition, and as the sample is cooled, the coherence length, $\xi(T)$ starts diverging, typically of the order of hundreds of $\mathring{A}$ which is much larger than molecular length scale. This in turn leads to large pre-transitional effects [9, 11] in thermodynamic observables like specific heat, thermal expansion, isothermal compressibilty of the medium, etc. This so-called pre-transitional phenomenon is similar to the one observed near continuous phase transitions, and hence it is conjectured that a Landau-type phenomenological theory with necessary modifications could perhaps explain the weak first order nature of the NI transition satisfactorily. Details of Landau theory are presented in subsection 1.4.1, while Maier-Saupe theory is discussed in 1.4.2.

1.3 Order Parameter

The symmetry of a simple nematic liquid crystal can be best described in terms of the order parameter, which is defined to be non-zero in the ordered phase and zero in the disordered phase. The main difference between the nematic and isotropic phases is the presence of long-range orientational order in the nematic phase, while positional order is completely absent in both the phases. A convenient way of defining orientational order parameters is to define them as expansion coefficients of the relevant orientational distribution function in an appropriate basis set [2, 7, 11, 12, 23, 41]. Let us consider a macroscopic system with N cylindrically symmetric rigid molecules, and only the singlet distribution of pure orientations of the molecules. The distribution function is given by:

$$f(\Omega) = \left(\frac{V}{Z_N}\right) \int exp[-\beta U(\{X^N\})]\{dX^N\} \tag{1.1}$$

where, V is the volume of the system, Z_N is the partition function of N particles of the system. $U(\{X^N\})$ is the potential energy of N particles with coordinates being angles $\Omega = (\theta, \phi)$. In uniaxial mesophases, the singlet distribution is invariant under rotation about the director. In this case, the distribution function $f(\Omega)$ can be expanded in a Wigner series i.e., in a basis of Wigner rotation matrices;

$$f(\Omega) = \sum f_{Lmn} D^L_{m,n}(\Omega). \tag{1.2}$$

If the director is chosen to coincide with the z-axis, it follows that $m = 0$ in $D^L_{m,n}$. In addition if the mesophase has a symmetry plane perpendicular to the director, ($D_{\infty h}$ symmetry, which is the case with liquid crystal molecules being considered here) only terms with even L can appear in $D^L_{m,n}$, denoted by $D^{l^*}_{m,n}$. The orientational order parameters are then the relevant linear expansion coefficients in eqn 1.2, and are given

by

$$\overline{D}^{l^*}_{0,n} = \int d\Omega f(\Omega) D^{l^*}_{0,n}(\Omega). \tag{1.3}$$

Let us consider the simplest case of the uniaxial nematic phase composed of molecules of cylindrical symmetry. In this case the rotation about the molecular symmetry axis should not modify the distribution which means $n = 0$ and $f(\Omega)$ has to depend only on the angle θ between the director and the molecular symmetry axis. Accordingly, we obtain

$$\overline{D}^{l^*}_{0,0}(\equiv \overline{P}_l) = \int d\Omega f(\Omega) P_l(cos\theta). \tag{1.4}$$

The $\overline{P}_l$ is the ensemble average of even Legendre polynomials. Thus a knowledge of order parameter successively leads to a progressively accurate description of the distribution function $f(\theta)$. Several experimental techniques are used to measure these order parameters. The simplest and most common orientational order parameter specified for a uniaxial nematic phase composed of cylindrical molecules is thus $\overline{P}_2$ given by

$$\overline{P}_2 = \langle P_2(cos\theta) \rangle. \tag{1.5}$$

One can in principle also consider higher order Legendre polynomials in the expansion of $f(\theta)$ and obtain the corresponding weight coefficients as the relevant order parameters. Since this particularly simple case requires just one order parameter, it is referred to as scalar parameter denoted by $S = \langle P_2(cos\theta) \rangle$. The loss of macroscopic cylindrical symmetry in a system of cylindrical molecules, brought upon by specific confining conditions, needs another parameter as a measure of this loss of symmetry, and is referred to as phase biaxiality parameter, represented by $\overline{D}_{2,0}(\theta, \phi)$. In the case of nematics composed of molecules which themselves have no cylindrical symmetry (say, biaxial molecules), the resulting orientationally ordered medium requires a more elaborate description to account for the orientational distribution function.

One needs then three independent angles (Euler angles: (ϕ, θ, ψ)) to transform from the laboratory frame to a given molecular frame, calling for an expansion in terms of Wigner functions represented in the space of Euler angles. It then turns out that one needs four order parameters as defined below to define the state of the orientational order in the system.

$$\begin{aligned}
\overline{P}_2 &= \overline{D}^{2^*}_{0,0} = \langle P_2(cos\theta)\rangle \\
\overline{\eta}_2 &= \overline{D}^{2^*}_{0,2} = \langle \frac{\sqrt{3}}{2} sin^2\theta cos2\psi\rangle \\
\overline{\mu}_2 &= \overline{D}^{2^*}_{2,0} = \langle \frac{\sqrt{3}}{2} sin^2\theta cos2\phi\rangle \\
\overline{\tau}_2 &= \overline{D}^{2^*}_{2,2} = \langle \frac{\sqrt{1}}{2}(1+cos^2\theta)cos2\phi cos2\psi - cos\theta sin^2\phi cos2\psi\rangle
\end{aligned}$$

1.4 Statistical theories of nematic order

The onset and development of the nematic phase at the NI transition have been analysed theoretically from different view points. One of the simplest and widely applied approaches is the phenomenological theory of Landau developed for LC systems by de Gennes [2], the so-called Landau - de Gennes theory (LDG theory) [24]. In this theory, Helmholtz free energy is expressed in powers of order parameters and its gradients, compatible with the symmetry of the system under consideration. In this process, typically five or more adjustable parameters are required, to be determined by experiments. This theory is physically appealing and mathematically simple, and captures characteristic features of the phase transition quite well, depending of course on the effort made in expanding the relevant free energy adequately. However, being phenomenological in nature, it lacks, microscopic basis.

In molecular field theories, one starts with developing a model in the form of inter-particle potential and solves for obtaining (anisotropic) potential acting on each

individual molecule (due to the surrounding molecules). The more the richness in the molecular structure the more elaborate should be the proposed potential, and hence needing more complex calculations. As a result, a number of simplifying approximations are proposed in making the choice of interaction potentials, and also while evaluating relevant physical properties, like, correlation functions, etc. The most widely used approximations are based on mean-field theory. The mean field approximation replaces the system of interacting molecules by a system of free molecules interacting with a field that is generated due to the presence of the other molecules. The initial version of mean-field theory is due to Onsager [15] which ascribes the nematic ordering as arising due to the anisotropic shape of the molecules. The Maier-Saupe theory [7, 9, 11, 12, 14] and its modifications introduce anisotropic attractive interactions in stabilizing the nematic phase. In reality, both these interactions are operative. Thus, in Van der Waal type theories both anisotropic hard core repulsions and angle dependent attractions are included [16–19]. Other than those mentioned above, another molecular theory was developed based on density functional approach which involves writing exact expressions for thermodynamic functions in terms of correlation functions. In the following subsections, we discuss the above-mentioned molecular theories based on Landau's phenomenological formalism and Maier-Saupe approach to appreciate the phenomenon of the isotropic to nematic transition in some detail.

1.4.1 Landau - deGennes (LDG) phenomenological theory

Landau theory is concerned with a phenomenological description of the phase transitions. These transitions involve a change of symmetry, generally in thermally driven transitions, the more symmetric (less ordered) phase corresponds to higher temperature and the less symmetric (more ordered) one to lower temperature. The differ-

ence in symmetry between the two phases is quantitatively accounted for by defining certain order parameters in such a way that they are (typically) zero in the more symmetric phase. (Such parameters are described earlier in the section 1.3). The mathematical formulation of the theory is based on the idea that the thermodynamic quantities of the less symmetric phase can be obtained by expanding the appropriate thermodynamic potential in powers of order parameters, and their spatial variations, in the neighbourhood of transition. Sufficiently close to the transition only the leading terms of the series are considered important so that the said expansion is limited to a polynomial of manageable order. The motivation for this simple and most elegant speculation is derived from the continuity of the change of state at a phase transition of the second order, i.e., the order parameters have low values near the transition point. Hence the Landau's original procedure is, in principle, restricted to second order phase transitions. The thermodynamic behaviour of the order parameters in the less symmetric phase is then determined from the condition that their values must minimize the postulated expansion of the thermodynamic potential.

The uniaxial nematic state is described by the symmetric tensor order parameter Q with zero trace, i.e., $Q_{aa} = 0$, (in this discussion we follow the usual summation convention). Since the thermodynamic potential is a scalar, the expansion can only contain terms that are invariant combinations of the elements Q_{ab} of the order parameter with respect to the symmetry operations of the system. In general, the expansion reads

$$g = g_0 + \frac{1}{2}AQ_{ab}Q_{ba} - \frac{1}{3}BQ_{ab}Q_{bc}Q_{ca} + \frac{1}{4}C(Q_{ab}Q_{ba})^2, \tag{1.6}$$

where g and g_0 represent the Gibbs free-energy density of the nematic and isotropic phases, respectively and coefficients A, B and C depend on the temperature T. The term linear in Q_{ab} does not appear in the expansion due to the difference in the

symmetry of the two phases. In principle, the gradient terms could also be included to accomodate contributions from inhomogeneties in the medium. Based on general considerations we note the following possibilities about the expansion (eqn 1.6):

1. The absence of linear term in Q_{ab} allows for the existence of an isotropic phase. In case an external field is present a linear term has to be included which makes the isotropic phase impossible.

2. Since the NI transition is first-order, odd terms of order three and higher are necessary, and are allowed.

3. The NI phase transition takes place in the neighbourhood of $A = 0$, being the leading term in the expansion for very small order parameter values. Therefore, it is assumed that the temperature dependence of free-energy is contained in the coefficient A alone and that other coefficients can be regarded as temperature independent. To describe the phase transition we write

$$A = a(T - T^*_{NI}) \tag{1.7}$$

where a is a positive constant and T^*_{NI} is a temperature close to the NI transition temperature T_{NI}.

For uniaxial nematic case, Q_{ab} reduces to

$$Q_{ab} = S(N_{ab} - \frac{1}{3}\delta_{ab}), \tag{1.8}$$

where the order parameter S has values between 0 and 1, and N_{ab} is represented by $N_{ab} = n_a n_b$, the scalar product of directors n_a and n_b. In order to facilitate a comparison with molecular statistical theory which are often performed at constant density, Helmholtz free energy density f is preferred instead of g. With the above considerations, similar expansion of f can then be written as

$$f = f_0 + \frac{1}{2}ATr(Q^2) + \frac{1}{3}BTr(Q^3) + \frac{1}{4}CTr(Q^4). \tag{1.9}$$

Near the phase transition, the temperature dependence of B and C ($C > 0$) is neglected. Free energy density for a nematic phase in terms of the scalar order parameter S is given by [9]:

$$f = f_0 + \frac{1}{3}a(T - T^*_{NI})S^2 - \frac{2}{27}BS^3 + \frac{1}{9}CS^4. \tag{1.10}$$

The equilibrium value of S is obtained by minimizing the free energy density eqn 1.10 with respect to S.

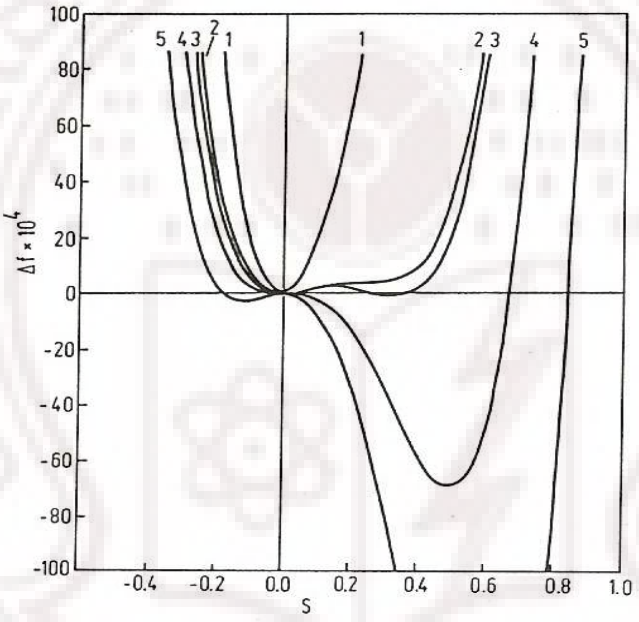

Figure 1.2 Free energy as a function of order parameter (courtesy [9])

Summarizing the solutions obtained by minimizing eqn 1.10, LDG theory distinguishes four different temperature zones (following the notations in [9]:

(i) $T > T^{\dagger}_{NI}$: S=0 and hence only isotropic phase exists (region bounded by curve 2 in figure 1.2)

(ii) $T_{NI} < T < T^{\dagger}_{NI}$: There is a small free energy barrier. Metastable nematic phase

can also be observed in this region (region between curves 2 and 3 in figure 1.2) by superheating a nematic liquid crystal.

(iii) $T^*_{NI} < T < T_{NI}$: Nematic phase is thermodynamically stable but isotropic phase can also be observed by super cooling from isotropic phase (region between curves 3 and 4 in figure 1.2).

(iV) $T < T^*_{NI}$: Nematic phase is thermodynamically stable in this region (bounded by curve 4 in figure 1.2), and isotropic phase is not possible.

LDG thus accounts for the existence of the two phase regions as simple manifestations of the features of the corresponding thermodynamic potential, as the control parameter is varied. Effect of various factors like density fluctuations, presence of non-nematic impurities, presence of external fields, etc., can also be, in principle, included in the eqn 1.10 to account for other experimental conditions. For biaxial case, the tensor nature of the order parameter has to be considered in the free energy expansion.

1.4.2 Maier - Saupe approach

Maier and Saupe (MS) [7, 9, 11, 12, 14] assumed that the existence of nematic phase is due to the anisotropic part of dispersion interaction energy between the molecules. This interaction energy is actually the second order perturbation term in the intermolecular electrostatic interaction between two liquid crystal molecules. Certain assumptions were made in this context for simplification:

i. The influence of the permanent dipoles can be neglected as far as long range nematic order is concerned.

ii. Only the effect of the induced dipole-dipole interaction needs to be considered as the higher order terms are not thought to be significant.

iii. A molecule is considered to be rotationally symmetric with respect to its long molecular axis described by a unit vector **a**.

iv. The distribution of the centres of mass of the remaining molecules with respect to a given molecule is taken to be spherically symmetric.

With these assumptions, rotational energy u_i of a molecule i can be approximated as

$$u_i = -AV^{-2}\left\langle \frac{3cos^2\theta_i - 1}{2} \right\rangle \left(\frac{3cos^2\theta_i - 1}{2} \right) \tag{1.11}$$

where θ_i is the angle which the long molecular axis makes with the preferred axis, V is the molar volume and A is a constant independent of temperature, volume and pressure. It may be noted that in order to obtain results from Maier-Saupe theory one requires only orientation-dependent interactions between the molecules.

One readily identifies the factor in angular paranthesis as the scalar order parameter, $S = \left\langle \frac{3cos^2\theta_i - 1}{2} \right\rangle$ is the scalar orientational order parameter. Free energy as a function of order parameter calculated from Maier-Saupe theory is shown in the figure 1.3. Here it is assumed that the molecules are cylindrically symmetric and hence one order parameter, S is sufficient. However, in real nematogens most molecules are not cylindrically symmetric (for example, lath shaped) and have biaxial property. In such cases, one needs to generalize the above interaction energy suitably.

Maier-Saupe theory explains the NI transition very well qualitatively. But one may wish to note two drawbacks in this theory, the first one is the exclusion of short range repulsive forces completely and the second is the use of mean-field approximation; it depends only on the long-range dispersion forces. It is interesting that this theory works well compared to other theories, like Onsagar's treatment, which are

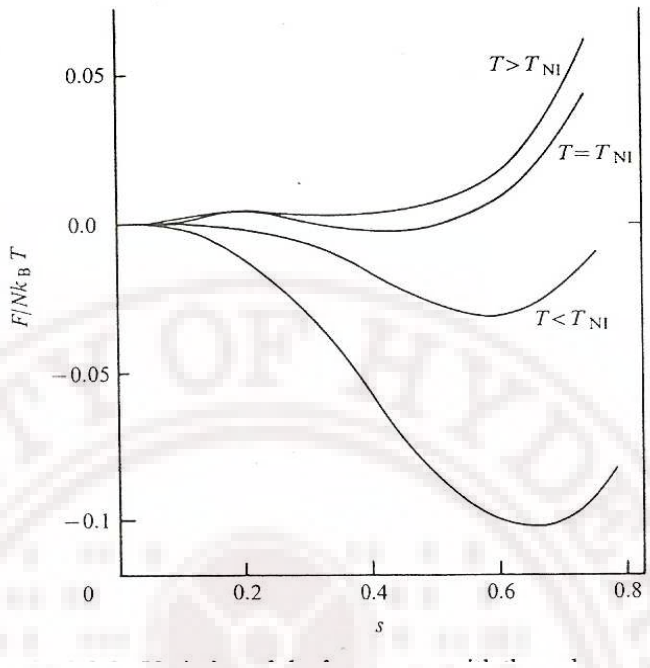

Figure 1.3 Free energy as a function of order parameter(courtesy [11])

completely based on the short-range repulsive forces. To explain this, it was conjectured that the short range repulsive forces probably give rise to highly ordered clusters [20], and hence the pair potenital employed in MS theory is to be thought as that between clusters of molecules rather than between single molecules themselves. Argument [21] that MS theory actually corresponds to the first term in the expansion of orientational part of the generalized interacting potential constituting both anisotropic (long range as well as short range) and isotropic contributions lends further support to this proposition. However, it is believed that the departure of results of MS theory from the experimental observations is largely due to the inclusion of mean-field approximation.

1.5 Continuum theory

So far we have assumed that the director field is perfectly uniform. But this is rarely the case and in general, the director varies with position. For most situations of interest, the distances l over which significant variations of order parameter occur are much larger than the molecular dimensions a (typically $l \geq 1\mu m$, while $a \sim 20\mathring{A}$). Thus this variation is extremely modest at microscopic level, and hence does not affect the orientational or positional order parameter in such a sample. Hence these distortions may be described by continuum theory, depending only on elastic energy considerations disregarding the details of the structure on the molecular scale. To construct such a theory, one possible starting point could be the free energy density F_d, expressed as a function of the order parameter Q_{ab} as in equation 1.8. When Q_{ab} becomes a function of $\mathbf{r}$, we must add in F_d new terms involving the gradients of Q_{ab}. This approach is indeed useful to study space-dependent properties above NI transition, because in this region Q_{ab} is small, and the structure of the gradient terms is simple. Below T_{NI} this approach would become rather clumsy, because for large Q_{ab}, there are many phenomenological coefficients involved. In a weakly distorted system, the order parameter can be written as

$$Q_{ab}(r) = S[n_a(r)n_b(r) - \frac{1}{3}\delta_{ab}] + \textit{terms of higher order in } a/l. \qquad (1.12)$$

This type of description was initiated by Oseen [25] and Zocher [26]. Subsequently, Frank [27] applied it to hydrostatic properties of nematics. There are certain assumptions made before we write the distortion free energy F_d in terms of the gradients of $\mathbf{n}$:

1. F_d must be even in $\mathbf{n}$, since the states $\mathbf{n}$ and $-\mathbf{n}$ are indistinguishable.

2. There are no linear terms in $\bigtriangledown\mathbf{n}$.

3. Terms that can be written as a divergence and integrated over the volume of the sample can be changed to surface integral. These contributions must be taken into account when considering the surface effects.

Based on these assumptions, distortion free energy density, F_d can be written as [2, 8]

$$F_d = \frac{1}{2}K_1(div\ n)^2 + \frac{1}{2}K_2(\mathbf{n} \cdot curl\ \mathbf{n})^2 + \frac{1}{2}K_3(\mathbf{n} \times curl\ \mathbf{n})^2 \tag{1.13}$$

where K_1, K_2 and K_3 are the Frank's elastic constants. Greater the order parameter, greater these constants are and these are associated with splay, twist and bend distortion contributions respectively represented in the figure 1.4. Each constant is positive and their values are of the order of 10^{-11} Newtons, with K_3 being two to three times larger than K_1 and K_2 in a typical system. In the continuum limit, this represents a very small value contribution to the total energy.

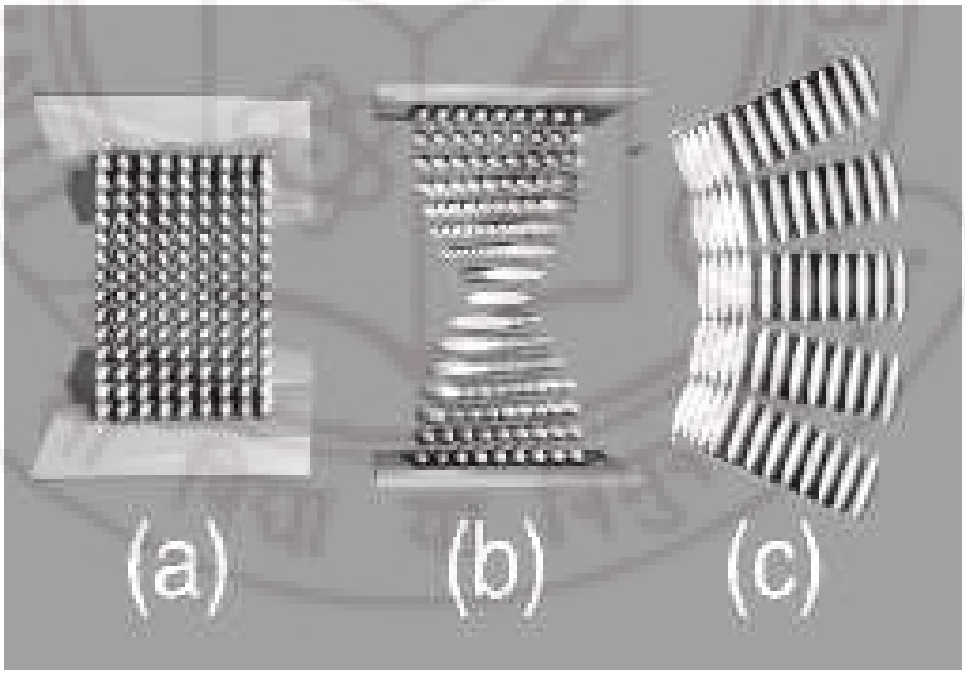

Figure 1.4 Schematic representation of Splay (a), Twist (b) and Bend (c) elastic distortions in liquid crystals

1.6 Surface effects

In the absence of surfaces and applied forces, the director field $n(r)$ of a nematic at equilibrium is uniform (independent of r) and its orientation is arbitrary. Liquid crystals are 'soft' materials i.e., the binding energy of the constituent molecules is very less compared to that of solids and hence can be easily influenced by the presence of solid substrates. Presence of a surface can anchor the direction of the orientation of the liquid crystal molecules, hence the phenomenon is called 'anchoring'. Anchoring can be *monostable* or *multistable* depending on the number of stable director orientations that these anchored liquid crystal molecules exhibit and the transitions between such directions are called anchoring transitions. One usually distinguishes three main types of liquid crystalline director alignment near solid wall or at the free surface. These are homeotropic, planar and tilted orientations. In order to orient a liquid crystal, one usually treats a solid substrate either mechanically (rubbing, lithography, etc) or by depositing chemical substances (surfactants, polymers, etc). Combined methods are also being used more recently. In the mechanical methods, glass substrates are rubbed with soft materials or photolithographic methods are used to obtain different geometric patterns like sinusoidal relief ([28] and references therein), saw-tooth pattern [30], etc. Liquid crystal molecules tend to align along the direction of the grooves rather than perpendicular to them since they are energetically more favourable. These directions are called the "easy-orientation directions". When liquid crystal is subjected to competing alignments on either side of the sample, it may undergo gradual variation in the director orientations across the sample to minimize its free energy. As these competing anchoring conditions are varied externally, the liquid crystal system undergoes transitions from one equilibrium director structure to another.

For a nematic liquid crystal, the elastic free energy density is given by the eqn 1.13. We

can simplify this by taking single-constant approximation, i.e., $K_{11} = K_{22} = K_{33} = K$. To illustrate the concept of anchoring, consider a twist deformed nematic placed between two solid substrates (labelled as, say, 1 and 2). Let the easy-orientation of one of the substrate (say, top) makes an angle τ with the other substrate. Let the director make an angle ϕ_1 and $\tau - \phi_2$ with the two substrates respectively. The surface energies at the two substrates are given by:

$$\begin{aligned} F_{1s} &= F_{1s}^a + F_{1s}^i = \frac{1}{2} W_1 \phi_1^2 + F_{1s}^i \\ F_{2s} &= F_{2s}^a + F_{2s}^i = \frac{1}{2} W_2 (\tau - \phi_2)^2 + F_{2s}^i \end{aligned} \tag{1.14}$$

Here F_{1s}^i and F_{2s}^i are the densities of the isotropic surface energy of the nematic, the functions F_{1s}^a and F_{2s}^a are the angle-dependent anisotropic parts of the surface energy. The coefficients W_1 and W_2 are the so-called anchoring strengths of the nematic liquid crystal.

In the above example the director field deformations are considered to be small and hence the surface free energy can be written in simple forms as shown in the above eqn 1.14. But in actual experiments, the deviation of the director can be considerable, thus raising the problem of real angular dependence of F_s^a. To answer this, several approximations of the angular dependencies $F_s^a(\phi)$, where ϕ is the angle of easy-axis with the substrate, are considered. The most commonly used analytical approximation for the surface free energy density is the so-called Rapini-Popoular form [31] given by:

$$F_s^a = \frac{W}{2} sin^2 \phi. \tag{1.15}$$

If $\phi \ll 1$ then equation 1.15 corresponds to eqns 1.14. The Rapini potential describes very satisfactorily many physical phenomena in liquid crystals in the presence of a surface for weak anchoring strengths. This potential is used in the present work to mimic the surface elastic energy of a system of nematic liquid crystals confined to a

geometrically and chemically patterned substrate (Chapter 5).

1.7 Liquid crystal elastomers

Liquid crystal elastomers (LCE) are weakly cross-linked polymers made of liquid crystals [32]. Polymers which are not cross-linked are fluid-like, and changes in the orientational order of constituent liquid crystal molecules do not affect the properties of the polymer. Linking the polymer chains into a gel network fixes their topology, and the melt becomes a rubber (solid). Liquid crystal elastomers exhibit fascinating properties due to the coupling between anisotropic properties of liquid crystals and the elastic properties of the polymer [32, 35]. They exhibit a continuous strain transition driven by the liquid crystalline transition of the constituent molecules from isotropic to nematic phase, as temperature is decreased.

In 1975, de Gennes [38] envisaged that polymers made of liquid crystals can lead to several fascinating properties due to the coupling of orientational order to the average shape of the nematic polymers. Without special precautions, LCE's always form polydomain textures. In contrast to the ordinary nematic liquid crystals where polydomain state is a kinetically delayed state, in elastomers this state is in thermodynamic equilibrium and is very difficult to get rid off. Hence until a robust method of producing well-aligned monodomain nematic elastomers was devised [33], the progress in understanding and development of the LCE's was very slow. In the following sub-sections some salient features of LCE's relevant to our present study are discussed briefly. The continuum description of the NI transition in LCE's and the so-called neo-classical rubber elastic theory are discussed in the subsequent section. Lattice models based on this elastic theory [36, 37] are studied employing entropic sampling methods in our present work, presented in Chapter 4.

1.7.1 Salient features

Classical liquid crystals are typically fluids with long-range orientational order. As the temperature is reduced, long polymer chains with anisotropic units also align themselves in the nematic phase. These liquid crystal polymers change shape from spherical to spheroidal as their constituent liquid crystal molecules orient parallel to each other which is shown in the schematic 1.5 [32]. In the prolate spheroidal case, the long axes point along the nematic director. In rubbers, monomers remain

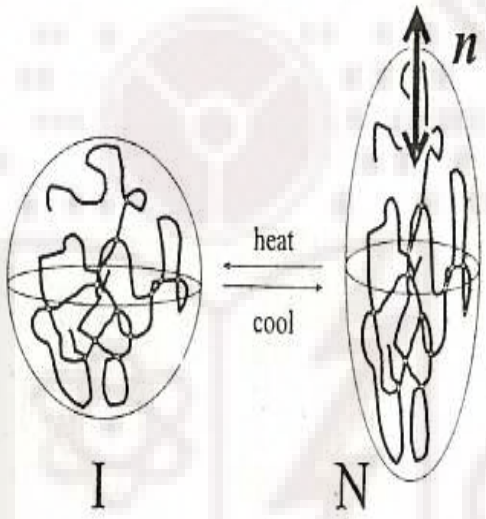

Figure 1.5 Polymers with average spherical shape in isotropic phase (I) elongates on cooling to nematic phase (N). The director **n** points along the long axis for prolate spheroid.(courtesy: [32])

highly mobile and thus behave like liquids. Thermal fluctuations move the chains as rapidly as in the melt, but only as far as their topological crosslinking constraints allow. These constraints make the rubbers into weak, highly extensible material. Nevertheless, rubbers are solids, and some amount of energy is required to change the macroscopic shape. This is due to the fact that as the rubber is deformed from its natural equilibrium shape, where its entropy is maximum, the deformation causes

the entropy to decrease (while the corresponding change in its energy is relatively negligible;)and hence the net free energy increases as, $\Delta F = -T\Delta S > 0$. This free energy is essentially dependent only on the entropy change itself driven by the chain conformations, and in this context polymers are sometimes referred to as 'entropic springs'.

Nematic-elastic coupling gives rise to some interesting properties in LCE's. It was observed that the free energy associated with the independent director rotation with respect to its macroscopic shape is periodic [32], meaning that rotating the director independently of the rubber matrix costs energy. In nematic liquid crystals, uniform rotations of the director costs no energy. It is the director gradients that suffer Frank elastic energy penalties, and thus long-wavelength spatial variations of the rotation angle cost small energy. However, in LCE's local rotations exhibit interesting elastic properties called 'soft elasticity'. If we rotate the director freely by an angle, it would not cost any energy if the whole body rotates at the same angle. There are infinite number of such intermediate deformed states to accomodate the chain distribution of the polymer with out distorting it. This phenomenon is shown in the schematic 1.6. From the figure, we observe that as the director is rotated from initial to final state, there is a possibility of several intermediate θ states which accomodate the spheroid distribution of the polymer without destroying it. This phenomenon of soft-elasticity can be observed even from stress-strain relations [34] and the director rotation curves as seen in figure 1.7 . LCE's also exhibit extreme thermo-mechanical, thermo-optical properities which make them good candidates for applications like acutators, artificial muscles, strain gauges, bifocal contacts, intra-ocular lenses, etc ([32] and references therein). The coupling between anisotropic liquid crystals and the elastic degrees of freedom gives rise to a new kind of elasticity. This so-called neo rubber elasticity

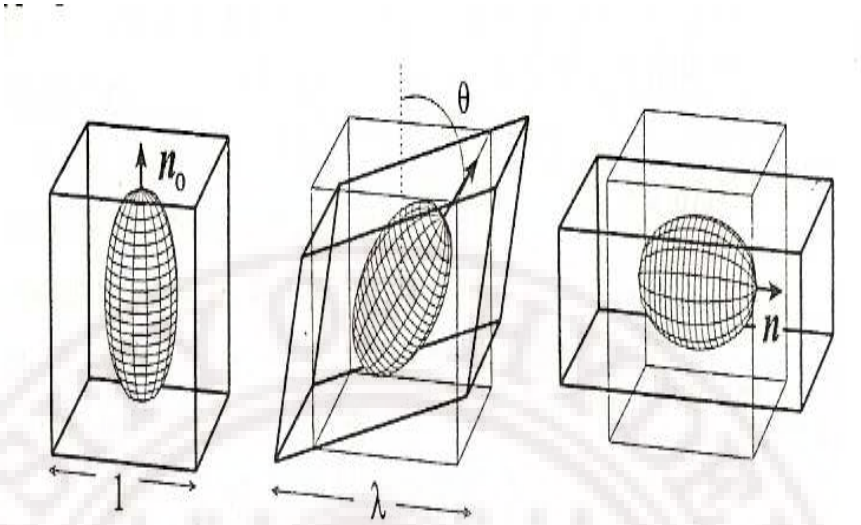

Figure 1.6 Chain shape distribution is rotated by 90^0 from n_0 to n with an intermediate θ state. (courtesy: [32])

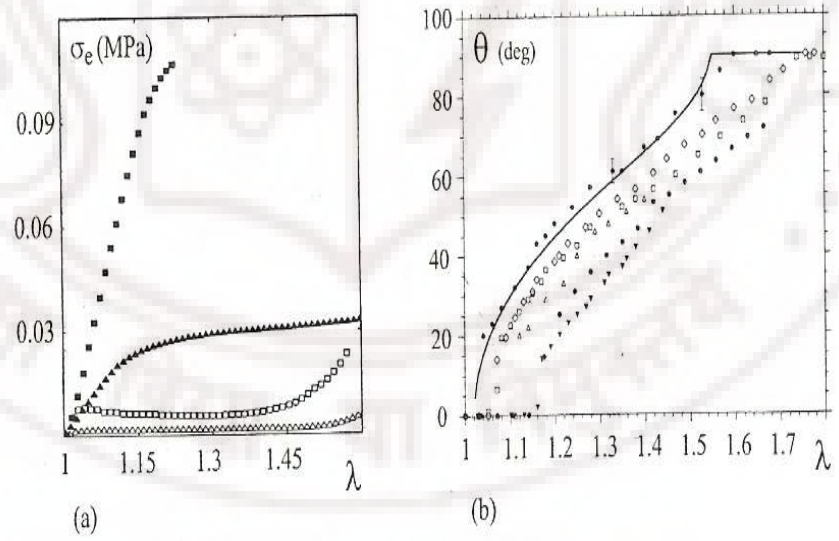

Figure 1.7 Stress deformation data for a series of rubbers with same cross-link density (a) and the angle of director rotation on stretching a piece of nematic elastomer (b) (courtesy: [32])

depends on the polymer chain lengths and takes into account the anisotropy brought about by the nematic constituents of the elastomers. This theory is discussed in the next subsection.

1.7.2 Neo-classical rubber elastic theory

Let us consider an isotropic cross-linked polymer with the cross-link density well above the threshold value and hence acts like a rubber. The free energy for such a system is purely entropy-driven. The internal energy is involved only in the distortion of chemical bonds. Let $\mathbf{R_f}$ be the end-to-end distance of a selected strand during the network formation. Let it get deformed to a new value $\mathbf{R}$. The deformation, λ is defined as below

$$\mathbf{R} = \lambda \cdot \mathbf{R_f}. \tag{1.16}$$

The free energy of this particular strand is given by,

$$F_s(\mathbf{R}) = k_B T \left(\frac{3\mathbf{R}^2}{2R_0^2} \right). \tag{1.17}$$

From the above two equations, we can write

$$F_s(\mathbf{R}) = \frac{3k_B T}{2} \frac{\mathbf{R_f} \cdot \lambda^{\mathbf{T}} \cdot \lambda \cdot \mathbf{R_f}}{R_0^2}. \tag{1.18}$$

Let the probability of having an initial end-to-end distance vector, $\mathbf{R_f}$ before cross-linking be given by

$$p(\mathbf{R_f}) = \left(\frac{3}{2\pi R_0^2} \right)^{\frac{3}{2}} e^{\frac{-3(R_f)^2}{2R_0^2}}. \tag{1.19}$$

From equations 1.17 and 1.19, the average free energy per strand F is given by

$$F = \frac{3k_B T}{2R_0^2} \langle \mathbf{R_f} \cdot \lambda^T \cdot \lambda \cdot \mathbf{R_f} \rangle_{p(\mathbf{R_f})}. \tag{1.20}$$

Solving the above equation, the free energy density of a deformed rubber is calculated by multiplying the above with average number of strands per unit volume, n_s, leading to

$$F = \frac{1}{2} n_s k_B T Tr\left(\lambda^T \cdot \lambda\right). \tag{1.21}$$

In the above equation, shear deformations are not considered and hence the matrix, λ is diagonal. The shear modulus of the rubber, μ is related to the number of strands n_s as $\mu = n_s k_B T$. Typical values of rubber modulus, μ are $10^5 Jm^{-3}$. Assuming the rubber block has extensions λ_{xx}, λ_{yy} and λ_{zz} along the coordinate axes x, y, z respectively, and imposing the condition of incompressibility, so that $\lambda_{xx} = \lambda_{yy} = 1/\sqrt{\lambda}$ where $\lambda_{zz} = \lambda$, the free energy density becomes:

$$F = \frac{1}{2}\mu\left(\lambda^2 + \frac{2}{\lambda}\right). \tag{1.22}$$

In liquid crystal elastomers, the end-to-end distance distribution becomes anisotropic. In the case of simple uniaxial nematic one obtains $\langle R_{||} R_{||}\rangle = \frac{1}{3} l_{||} L$ and $\langle R_{\perp} R_{\perp}\rangle = \frac{1}{3} l_{\perp} L$ with $L = aN$ the chain contour length and $l_{\parallel}/l_{\perp}$ is the ratio of average chain step lengths along and perpendicular to the nematic director. In the isotropic phase, one recovers $l_{\perp} = l_{\parallel} = a$. The uniaxial anisotropy of polymer chains has a principal axis along the nematic director n. The ability of this principal axis to rotate independently under the influence of network strains makes the rubber-elastic response non-symmetric. Thus, we have [32]

$$F_{el} = \frac{1}{2}\mu Tr(\lambda^T \cdot l_{\theta}^{-1} \cdot \lambda \cdot l_0) + \frac{1}{2}\tilde{B}(Det[\lambda] - 1)^2. \tag{1.23}$$

Here, l is the uniaxial matrix representing chain step length before and after the director is rotated by an angle θ.

$$l_{ij} = l_{\perp}\delta_{ij} + [l_{\parallel} - l_{\perp}] n_i n_j. \tag{1.24}$$

The last term in eqn 4.2 represents the contribution from bulk modulus ($\tilde{B} \sim 10^{10} - 10^{11} Jm^{-3}$), which is much greater than the shear modulus and independent of the chain conformations. This large energy penalty constrains the system to become physically incompressible. From these equations it is clear that the strain components will now have non-trivial effect on the system, in contrast to the isotropic rubbers. The uniqueness of nematic rubbers stems from the competing microscopic interactions and the existence of two levels of characteristic length scales: one is the anisotropy on the nematic coherence length (small) of the LC monomers, while the strains are defined on a much greater length scale, typically of polymer end-to-end chain length. This length scale separation calls for a more detailed treatment, like, multi-scale modelling, to understand various underlying phenomena exhibited by the liquid crystal elastomers.

1.8 Lattice models

Lattice spin models consist of systems with interacting spins placed at regular lattice sites. The spins can be idealized unit vectors assuming discrete or continuously varying orientations in a space of a given "spin dimensionality", s. The lattice of positions will have its own dimensionality, d. Despite their simplicity, spin models have proved to be extremely important in the study of phase transitions and critical phenomena in many fields ranging from liquids to polymers [40–42]. Although lattice systems with their intrinsic positional order are in some sense antithesis for properties of liquid crystals, they have been successfully employed in investigating various properties and phenomena in the nematic liquid crystals. These models are extensively used to investigate the properties of nematics starting from the pioneering work of Lebwohl and Lasher (LL) [39]. In LL model, each spin at a given lattice site represents a molecule or a group of molecules of the liquid crystal. Each spin will have continuous

rotational freedom, rather than a discrete set of orientations in order to mimic long range orientational behaviour. Subsequently, other models which permit the translational variables as well, like Gay-Berne model [45], are proposed, and represent more realistic description of molecular interactions in liquid crystals. But considering the fact that orientational order is the essential discriminating factor between isotropic and nematic phases, simple lattice models are still popular in modelling the liquid crystals when the properties of interest are only rotational degrees of freedom, mainly due to the much less computational effort involved while capturing the essential features of the system under consideration. Lattice models also allow us, even though in a somewhat simplified way, to investigate potentials for rather complicated systems with varying boundary conditions and field strengths. In this thesis, we employ lattice models as described below, to investigate properties of different complex liquid crystal systems.

Lebwohl-Lasher model is a simple prototype lattice model which is widely employed for investigating nematics. The particles are assumed to have uniaxial symmetry and represented by three dimensional spins located at the sites of $L \times L \times L$ cubic lattice. The nearest neighbour molecules interact through a pair potential which depends on the angle between the two molecules.

$$U_{ij} = -\epsilon_{ij} P_2(cos\beta_{ij}), \tag{1.25}$$

It is common in a homogeneous system to equate all ϵ_{ij} to a single constant ϵ representing the coupling strength of interaction between the neighbouring molecules. P_2 is the second Legendre polynomial and β_{ij} is the angle between the molecules. This potential favours the molecules to be parallel to each other and hence effectively introducing any collective phenomena exhibited as a consequence of such intermolecular interactions. Apart from this P_2 - based model, there are several lattice models pro-

posed to investigate various aspects of the liquid crystal materials like, for example, P_1P_2 model [48, 49] which can be viewed as a prototype for ferroelectric liquid crystals, P_2P_4 model in order to make a contact with the experimental observations [50], biaxial model [51, 52] to study lattice systems of biaxial particles, etc. Apart from these models, there are also lattice-based pair-potentials which incorporate explicitly the elastic constants of the liquid crystal medium within the Hamiltonian, and are used to investigate the behaviour of nematics under different external conditions [46, 47]. Lattice based models are useful to describe the behaviour of LCE as the system is cooled through the NI transition are of recent origin, and are presented separately in Chapter 4.

Bibliography

[1] G. Friedel, *Ann. Physique* **18**, 273 (1922).

[2] P.G. de Gennes and J. Prost, *The Physics of Liquid crsytals*, 2nd edition, (Clarendon press, Oxford, 1993); P.G. de Gennes, Mol. Cryst. Liquid Cryst. 12,193 (1971).

[3] M. P. Fisch, *Liquid crystals, laptops and life*, World Scientific, Vol. **23** (2004).

[4] B. Bahadur *Liquid crystals: applications and uses*, World Scientific publishing, Singapore (1993).

[5] J. S. Patel, *Ann. Rev. Mat. Sci.* **23**, 269-294 (1993).

[6] S. Martellucci and A. N. Chester, *Phase transitions in Liquid Crystals*, **290**, Plenum press, Newyork and London, (1992).

[7] G. R. Luckhurst and G. W. Gray, *The molecular physics of liquid crystals*, Academic Press, London, Newyork and SanFransisco, (1979).

[8] P. J. Collings and M. Herd, *Introduction to Liquid crystals chemistry and physics*, Taylor and Francis, (1998).

[9] G. Vertogen, and W.H. de Jeu, *Thermotropic Liquid Crystals, Fundamentals*, Springer-Verlag, (1988).

[10] Iam-choon Khoo, *Liquid crystals*, 2nd edition, Wiley-Interscience, (2007).

[11] S.Chandrasekhar, *Liquid crystals*, Cambridge University Press, Cambridge (1977).

[12] Shri Singh, *Liquid crystals, Fundamentals*, World Scientific, Singapore (2002)

[13] Shri Singh, *Phys. Rep.* **324**, 107-269 (2000).

[14] W. Maier and A. Saupe, *Z. Naturforsch.,* **13a**, 564 (1958); **14**, 822 (1959); **15a**, 287 (1960).

[15] L. Onsager, *Ann. N.Y. Acad. Sci* **51**, 627 (1949).

[16] N.V. Madhusudana, *Theories of liquid crystals*, in: B. Bahadur (Ed.), *Liquid Crystals: Applications and Uses* , Vol. 1, World Scienti"c, Singapore, 1990, p. 37 (Chapter 2).

[17] M.A. Cotter, *The Van der Waals approach to nematic liquid crystals*, in: G.R. Luckhurst, G.W. Gray (Eds.), *The Molecular Physics of Liquid Crystals*, Acad. Press, New York, 1979, p. 181 (Chapter 8); M.A. Cotter, *J. Chem. Phys.***66**, 1098, 4710 (1977) .

[18] W.M. Gelbart, B.A. Baron, *J. Chem. Phys.* **66**, 207 (1977); W.M. Gelbart, A. Gelbart, *Mol. Phys.* **33**, 1387 (1977); B.A. Baron, W.M. Gelbart, *J. Chem. Phys.* bf 67, 5795 (1977); J.G.J. Ypma, G. Vertogen, *Phys. Rev. A* **17**, 1490 (1978); W. Warner, *J. Chem. Phys.* **73**, 6327 (1980); K.L. Savithramma, N.V. Madhusudana, *Mol. Cryst. Liq. Cryst.* **62** 63 (1980) ; ibid **97**, 407 (1983); S. Singh, K. Singh, *Mol. Cryst. Liq. Cryst.* **101**, 77 (1983); K. Singh, S. Singh, *Mol. Cryst. Liq. Cryst.* **108**, 133 (1984); P.J. Flory, R. Ronca, *Mol. Cryst. Liq. Cryst.* **54**, 311 (1979); F. Dowell, *Phys. Rev. A* **28**, 1003 (1983); F. Dowell, *Phys. Rev. A* **31**, 2464, 3214 (1985) .

[19] P.J. Flory, R. Ronca, *Mol. Cryst. Liq. Cryst.* **54**, 311 (1979); A. Bellemans, *Phys. Rev. Lett.* **21**, 527 (1968); V.T. Rajan, C.W. Woo, *Phys. Rev. A* **17**, 382 (1978), L. Feijoo, V.T. Rajan, C.W. Woo, *Phys. Rev. A* **19**, 1263 (1979).

[20] P. Sheng, *J. Chem. Phys.* **59**, 1942 (1973).

[21] G. R. Luckhurst and C. Zannoni,*Nature* **267**, 412 (1977).

[22] Stone A. J, in *Molecular Physics of Liquid Crystals* (eds.: G. R. Luckhurst, G. W. Gray), chap. 2, Academic Press, London (1979)

[23] A. Sarlah, *Effect of the confining substrates on nematic order-fluctuations in liquid crystals*, PhD thesis, School of Mathematics and physics, University of Ljubljana (2001).

[24] L.D. Landau, and E.M. Lifshitz, *Statistical Physics*, Vol. 1, 3rd ed. (Pergamon, Oxford, 1980).

[25] C. W. Oseen, *Trans. Faraday Soc.* **29**, 883 (1933).

[26] H. Zocher, *Trans Faraday Soc.* **29**, 945 (1933).

[27] C. F. Frank, *Discuss. Faraday Soc.* **25**, 19 (1958).

[28] A. A. Sonin, *The surface physics of liquid crystals*, Gordon and Breach publishers, Luxembourg (1995).

[29] G. P. Crawford and S. Zumer, *Liquid crystals in complex geometries*, Taylor and Francis, London (1996).

[30] G. Barbero,, *Nuovo Cimento Lett.,* **29**, 553 (1980).

[31] A. Rapini and M. J. Popoular, *J. Phys. (France) Lett.,* t. 30, C4-54 (1969).

[32] M. Warner and E. M. Terentjev, *Liquid Crystal Elastomers*, Clarenden Press, Oxford (2003); M. Warner and E. M. Terentjev, *Prog. Polym. Sci.* **21**, 853 (1996); E. M. Terentjev, *J. Phys. : Condens. Matter* **11**, R239 (1999).

[33] J. Kupfer, H. Finkelmann, *Macromol. Chem. Rapid Commun.* **12**, 717 (1991).

[34] J. Kupfer, H. Finkelmann, *Macromol. Chem. Phys.* **195**, 1353 (1994).

[35] Y. Mao and M. Warner, *Phys. Rev. Lett.* **84**, 5335 (2000); M. Warner, E. M. Terentjev, R. B. Meyer and Y. Mao, *Phys. Rev. lett.* **85**, 2320 (2000); S. M. Clarke, A. R. Tajbakhsh, E. M. Terentjev and M. Warner, *Phys. Rev. Lett.* **86**, 4044 (2001); Y. Mao and M. Warner, *Phys. Rev. Lett.* **86**, 5309 (2001); P. Pasini, G. Skacej and C. Zannoni, *Chem. Phys. Lett.* **413**, 463 (2005); O. Stenull and T. C. Lubensky, *Phys. Rev. E* **73**, 030701(R) (2006).

[36] J. V. Selinger and B. R. Ratna, *Phys. Rev. E* **70**, 041707 (2004).

[37] P. Pasini, G. Skacej and C. Zanoni, *Chem. Phys. Lett.* **413**, 463 (2005).

[38] P. G. de Gennes, *Polymer liquid crystals*, edited by A. Ciferri, W. R. Krigbaum and R. B. Meyer (Academic, New york, 1982); C. R. Acad. Sci. Ser B, 281, 101 (1975);

[39] P. A. Lebwohl and G. Lasher, *Phys. Rev. A* **6**, 426 (1972).

[40] D. P. Landau and K. Binder, *A guide to Monte Carlo simulations in Statistical Physics*, Cambridge University Press (2000).

[41] P. Pasini and C. Zannoni, *Advances in the computer simulations of liquid crystals*, Kluwer Academic publishers, Dordrecht (2000).

[42] M.P.Allen, *Mol. Phys.* **96**, 1391?1397 (1999).

[43] B.Jerome. *Rep. Prog. Phys.* **54**, 391 (1991).

[44] Th. Rasing and I. Musevic, *Surfaces and Interfaces of Liquid Crystals*, Springer-Verlag, New York, LLC (2004).

[45] J. G. Gay and B. J. Berne, *J. Chem. Phys.,* **74**, 3316 (1981).

[46] G. R. Luckhurst and G. Saielli, *Mol. Cryst. Liq. Cryst.* **395**, 183?192 (2003).

[47] T. Gruhn and S. Hess, *Z. Naturforsch.*, **A51**, 1 (1996).

[48] T. J. Krieger and H. M. James, *J. Chem. Phys.* **22**, 796 (1954).

[49] L. Lei, *Mol. Cryst. Liq. Cryst* **146**, 41 (1987).

[50] H. Pottel, et. al., *Chem. Phys.* **102**, 37 (1986).

[51] G.R. Luckhurst and S. Romano,*Liq. Cryst.* **26**, 871 (1999).

[52] M. P. Allen, *Liq. Cryst.* **8**, 499 (1990).

Chapter 2

Introduction to Monte Carlo methods

In any condensed matter system, even if it is isolated, calculating its properties by solving equations of motion is impossible due to the sheer number of particles involved. Further, allowing the system to interact with the surroundings so as to be in thermodynamic equilibrium, makes such *ab initio* calculations even conceptually difficult to formulate. However, fortunately even such large systems display relatively simple macroscopic properties which are on one hand accessible to the time and length scales of a macroscopic experiment, and on the other are fairly deterministic (reproducible) under identical experimental conditions. While thermodynamics captures the features of such behaviour in a phenomenological way, it fits in the realm of statistical physics to provide a microscopic basis for predicting the macroscopic behaviour, based on certain intuitively appealing ansatz. A useful mathematical construct in this context is the concept of the phase space, and the probability density defined on this space. Equilibrium properties emerge as averages of physical variables taken over the stationary probability density appropriate to the equilibrium condi-

tions imposed. Thus the problem gets more conveniently transferred to that of finding the appropriate equilibrium ensemble of microstates for a given Hamiltonian system consequent to equilibrium conditions, can be compactly expressed mathematically in terms of phase space (probability) density. As we would see later in the chapter this condition, in a stricter sense, forms the basis for the development of a very microstates which asymptotically obey the detailed balance and hence conform to an equilibrium ensemble in that limit. Let the probability of a system to be in a state μ be $\omega_\mu(t)$, and let the transition probability (per unit time) for the system to transit from μ to ν be $R(\mu \to \nu)$. We now write the time variation of the probability of any state (say, μ) as follows [1]:

$$\frac{d\omega_\mu}{dt} = \sum_\nu [\omega_\nu(t) R(\nu \to \mu) - \omega_\mu(t) R(\mu \to \nu)]. \tag{2.1}$$

When the system reaches equilibrium, the left hand side becomes zero and the evolution of microstates is stationary with respect to time. Any method which mimics the evolution of microstates with this condition ensures that the system is in equilibrium. Development of microstates appropriate to a given Hamiltonian and construction of equilibrium ensembles can be carried out via computer simulations, and two methodologies are very powerful and popular: Monte Carlo sampling methods and molecular dynamics techniques [4, 6]. Methods based on molecular dynamics generate the variables sequentially in time by solving the equation of motion numerically and construct the equilibrium ensembles out of these states by imposing a standard law on the distribution of their velocities, typically. Monte Carlo methods on the other hand rely on the ability of the system to make a random walk in the appropriate configurational space which is guided on one hand by the density of states dictated by the underlying Hamiltonian and the statistical law imposed by equilibration condition on the other. We employ in the present work Monte Carlo methods to investigate

equilibrium properties of certain soft materials.

Simulations of liquid crystals which is the study of interest in this thesis started much later than corresponding theoretical and experimental studies. Investigating the properties of liquid crystals with simple models started only after 1970s [9]. Most difficult problem for molecular simulation involves linking together simulations that span different time and length scales, from the fast bond vibrations in a molecule ($\sim 1fs$), to rearrangement of liquid crystalline director in a nematic ($\sim$ several ns), to the rearrangement of small domains in liquid crystal polymers. Broadly, the simulations for different time scales can be depicted as shown in the figure 2.1 [8]. To study the collective phenomena like phase transitions in liquid crystals (e.g., nematic to isotropic phase transition), detailed atomistic or mesoscopic simulations may not be required fortunately. Simple models which capture the symmetry of the system and mimic the interactions between molecules (or a group of molecules) as a function of relevant parameters introduced in the interaction and/or imposed by external conditions is sufficient to understand these phenomena. Hence Monte Carlo methods applied to simple models, like Lebwohl-Lasher model, based on Maier-Saupe theory and mean-field arguments, still mimics fairly satisfactorily the macroscopic behaviour near nematic to isotropic transition and is widely used in this context.

2.1 Periodic boundary conditions

Since simulations are performed on finite size lattices, one important issue is how to deal with the edges or boundaries of the lattice. In any realistic system of even for a small size, the number of particles will be of the order of 10^{20} whereas simulation models which are typically attempted involve a few thousands of particles. Hence the boundary conditions of the simulated system have to be chosen in such a way that its

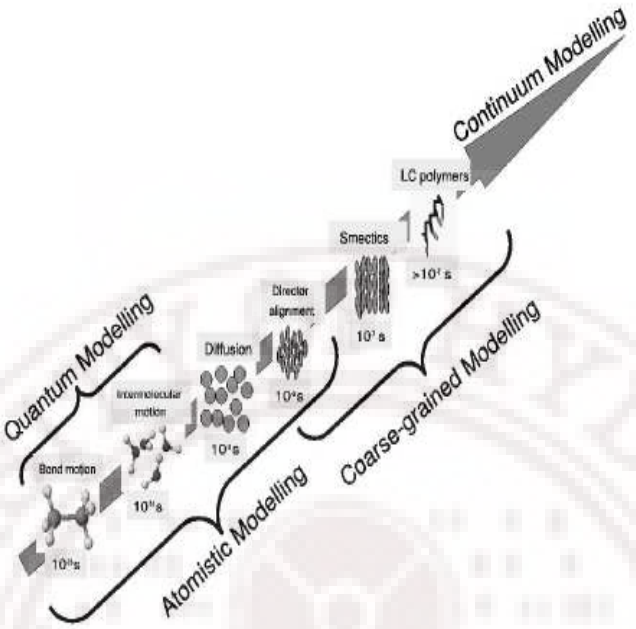

Figure 2.1 Simulations for different length and time scales (courtesy: [8])

finite size effect is minimized to the extent possible. If the boundaries are left free, they give rise to edge effects due to the dangling of the bonds at the corners of the lattice. One of the most widely used boundary conditions to mimic the system at thermodynamic limit is periodic boundary conditions. As can be seen from the figure 2.2, in this method the first spin in a row 'sees' the last spin of the row as one of the nearest neighbour, and vice versa. This can be imagined as if replicas of the lattice are placed on all the sides of the original lattice. Due to the pronounced correlations between the spins, this boundary condition has the potential to overestimate the transition temperature unless the original size of the system itself is sufficiently large where as free boundary conditions tend to underestimate it [7]. Other than these two, there are several other conditions like screw periodic boundary conditions, anti-symmetric boundary conditions, anti-periodic boundary conditions, hyper-spherical boundary conditions, etc, [2] that are used at different conditions.

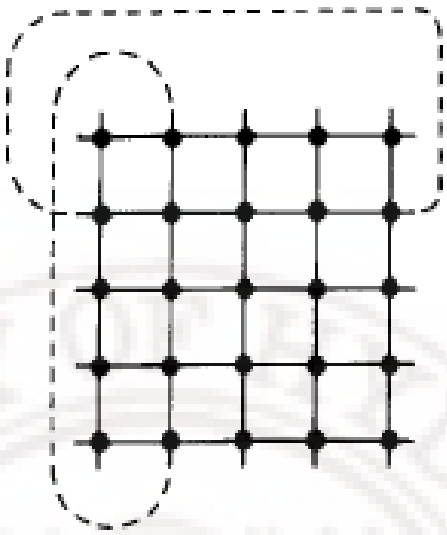

Figure 2.2 Periodic boundary conditions

2.2 Finite size effects

To appreciate the effect of finite size on the simulated behaviour, particularly near phase transitions, consider a lattice with linear dimensions L. If the correlation length $\xi(T) \ll L$, then practically a finite system can be a good approximation to a real system. In other words, interesting behaviour like signatures of phase transition can be simulated from even small lattices only if the correlation lengths are smaller compared to the size of the lattice. This happens, of course, when the temperatures are not close to the transition temperature T_C. But near the T_C the correlation lengths diverge and in the process become comparable to L at some temperature. Below this temperature, further divergence of this length scale is no more captured with this lattice size. The more the size of the lattice chosen for the simulations, the closer to T_C that one can approach before being limited by the above considerations. It is common to observe sharper variations in different response functions of the system across the transitions in bigger systems. The critical behaviour of a system in the

thermodynamic limit can be extracted from the size dependence of the singular part of the free energy at the second order transition. The scaling of various thermodynamic variables (like, magnetization, M, susceptibility χ, and specific heat C_V)is given by:

$$\begin{aligned} M &= L^{-\beta/\nu}\mathcal{M}_0(\epsilon L^{1/\nu}) \\ \chi &= L^{\gamma/\nu}\chi_0(\epsilon L^{1/\nu}) \\ C &= L^{\alpha/\nu}\mathcal{C}_0(\epsilon L^{1/\nu}) \end{aligned} \tag{2.2}$$

where $\mathcal{M}_0(x), \chi_0(x)$, and $\mathcal{C}_0(x)$ are scaling functions appropriate to the specific thermodynamic quantity. α, β, and γ are the scaling parameters. At the transition the scaling functions reduce to

$$M \propto L^{-\beta/\nu} \tag{2.3}$$

$$\chi \propto L^{\gamma/\nu} \tag{2.4}$$

$$\mathcal{C} \propto L^{\alpha/\nu} \tag{2.5}$$

In practice, we obtain these thermodynamic parameters (say M) for various system sizes and plot M vs $L^{-\beta/\nu}$. From the intercept of the best fit line to the data corresponding to various finite sizes, one estimates the transition temperature, T_C in the thermodynamic limit. The larger the sizes of the system considered, the better will be the estimate of the true T_C.

2.3 Canonical Monte Carlo methods

Let us consider a closed system in contact with a heat bath. If the system performs an unbiased random walk in the microstate space, the probability of picking up a microstate will be higher for higher energies. The density of states $D(E)$ is an increasing function of energy. But since the system is in contact with the heat bath,

and hence obeys say, the Boltzmann condition ($\beta = \frac{1}{k_B T}$), the probability is given by:

$$P_B(E) \propto D(E) exp(-\beta E). \tag{2.6}$$

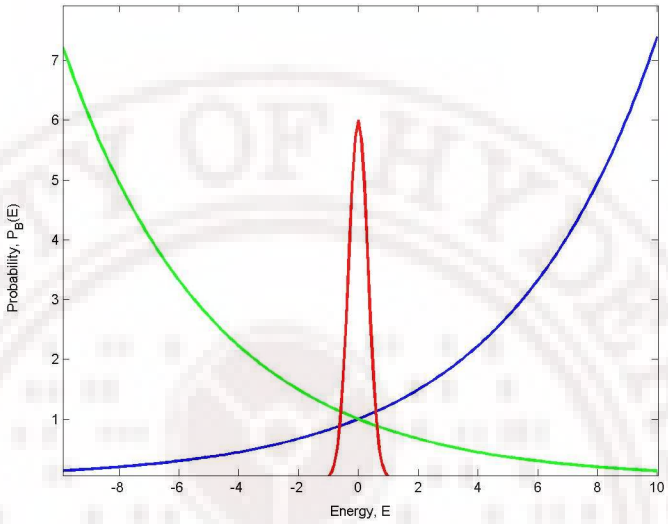

Figure 2.3 Probability density, $P_B(E)$ as a function of energy, E.

The probability distribution is depicted in the figure 2.3. As may be seen in the usual canonical sampling procedures, the given microstate is assigned two independent probablities; one is decided by the natural abundance of such microstates appropriate to the energy under consideration, and the other favouring its occupation at lower energies to respect the equilibrium condition. The resultant probability distribution, which clearly depends on the equilibrium condition (i.e., via β), will be a localised distribution around an averge energy value. Thus these microstates picked up with these resultant distribution constitute the canonical ensemble at this equilibrium condition, and any Monte Carlo method which samples such microstates is called Boltzmann Monte Carlo method or canonical sampling method. The average of the macroscopic quantities can be calculated by averaging over the sampled microstates from this canonical ensemble. But to carry out this average, we need to

know the partition function, $Z(T)$, which is not known. Metropolis, *et. al.,* [10] had given a very elegant prescription with which one constructs such ensembles without needing the knowledge of the partition funcion. The basic idea of this algorithm is given in the next subsection.

2.3.1 Metropolis algorithm

We look for an algorithm which takes the chosen system through a Markov chain of microstates starting with an initial microstate, C_0 as shown:

$$C_0 \rightarrow C_1 \rightarrow C_2 \rightarrow \cdot \cdot \cdot C_k \rightarrow C_{k+1} \rightarrow \cdot \cdot \tag{2.7}$$

In order to generate this sequence, guided by the algorithm, we select randomly one of the spins in some arbitrary configuration C_i, and flip it, thereby generating a new microstate, say C_t. We accept the trial state C_t according to the acceptance probability which is proportional to the ratio of probabilities at current C_i and the trial C_t states. Since the partition functions appear in both the numerator and denominator, the acceptance probability is independent of the partition function. The acceptance probability is given by

$$p = min\,(1, exp[-\beta \Delta E]) \tag{2.8}$$

where $\Delta E = E(C_t) - E(C_i)$ is the change in energy of the configurations. In practice, the acceptance criterion is as described below:

- if $\Delta E \leq 0$, we accept the trial state
- if $\Delta E > 0$, we draw a random number ξ.
  - If $\xi \leq exp(-\beta \Delta E)$, we accept the trial state;

- If $\xi > exp(-\beta\Delta E)$, we reject the trial state, and include the current microstate in the ensemble.

Each such trial step is called a Monte Carlo step. We perform N ($\approx$ number of lattice spins) such steps which is referred to as a Monte Carlo sweep (MCS). These MCS are performed a large number of times such that asymptotically we get a distribution of microstates given by eqn 2.6 as the system reaches equilibrium. The macroscopic variables are calculated by taking averages over this asymptotic part of microstates at each temperature. It may be noted that there can be other choices with regard to transition matrices consistent with the detailed balance condition. For example, in Metropolis algorithm, acceptance probability $p(x)$ is not continuous at $x = 0$ as shown in figure 2.4. Hence Glauber [11] proposed a dynamics where the probability, $p(x)$ is given by

$$p(x) = \frac{1}{1 + exp(x)}. \tag{2.9}$$

This choice of $p(x)$ is also consistent with the detailed balance condition.

Metropolis algorithm [10] is the most simple example for canonical sampling methods. This algorithm has been very successful in simulating a wide range of problems connected with statistical mechanics in condensed matter physics. But as the complexity of the problem increases the efficiency of this algorithm becomes an issue in addressing some of the concerns therein. For example, if the free energy surface exhibits a rugged landscape due to the inherent physical reasons, the canonical methods tend to spend unacceptably long time in sampling one of the local minima. Glassy systems, spin glass models, and other frustrated systems are good examples of such systems requiring prohibitively large computational effort based on this algorithm. Further, if the system exhibits second order phase transition, the dynamics of the system near the transition becomes very slow essentially due to the divergence of

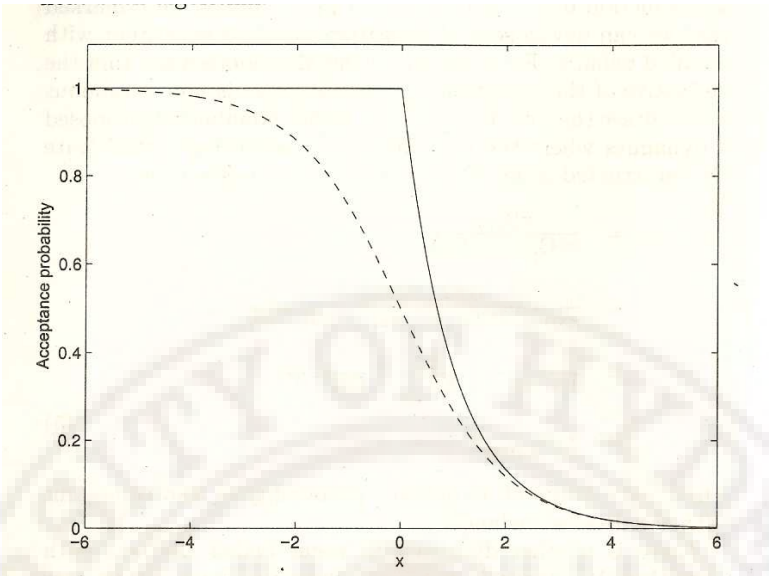

Figure 2.4 Acceptance probability, $p(x)$ as a function of change in energy between the trial and initial microstates, denoted by x. The solid line refers to the Metropolis sampling; dashed line depicts the Glauber dynamics

correlation length. This problem due to the so called critical slowing down is addressed fairly satisfactorily adopting cluster algorithms, like Swendsen and Wang algorithm [12], Wolff algorithm [13], etc. Here, instead of taking a single step in the configuration space, a cluster of carefully selected spins are flipped together while keeping the acceptance ratio reasonably high. This makes the random walk in the appropriate configurational space sample the microstate more efficiently, even in the presence of shallow free energy profiles. However, even these methods tend to fail near first order phase transitions, where the free energy develops a well-defined barrier separating two free energy minima. Canonical sampling methods now have to cope with the problem of sampling two distinct regions in the space of random walk separated by regions of relatively very low probability (quasi-ergodic) region. The barrier height increases with the system size making it increasingly difficult for canonical methods to report efficiently on the statistical properties of the system. To address this issue of super critical slowing down, non-Boltzmann sampling methods like umbrella sam-

pling [14], entropic sampling [36], multi-canonical method [30], *etc.*, were proposed. These methods allow the system to perform random walk in the microstate space in such a way that the system visits microstates in such a way as to obtain uniform distribution with respect to energy. Under those conditions, presence of energy barriers will not pose the above type of problems. The basic idea of these methods is described briefly in the following section.

2.4 Non-Boltzmann Monte Carlo methods

In any system which exhibits first order transition, the ordered and the disordered phases are seperated by a free energy barrier. The height of the barrier for a given transition increases with the size of the system, or alternatively the interfacial regions become less probable as the size of the system increases (see, fig 2.5). Conventional Monte Carlo methods like Metropolis algorithm will sample increasingly only from one of these phases and rarely cross the barrier to sample the states on the other side. This is due to the fact that Boltzmann factor suppresses configurations dominated by the interfaces between ordered and disordered phases. As a consequence, the quality of the Metropolis Monte Carlo results based on local updates deteriorates exponentially with an increase of the system size. Studies performing conventional Monte Carlo methods attempt to investigate the first order transitions by plotting hysteresis as a signature of the phase transition. More the amount of hysteresis, stronger is the first order. This hysteresis occurs because the system gets stuck for a considerable range of control parameters beyond its transition value in any one of the phases depending on the evolution of Markov chain of microstates which in turn depends on the initial conditions of the configurations (low or high temperatures, random seeds, etc.). Thus this phenomenon is a result of the inability of the system to

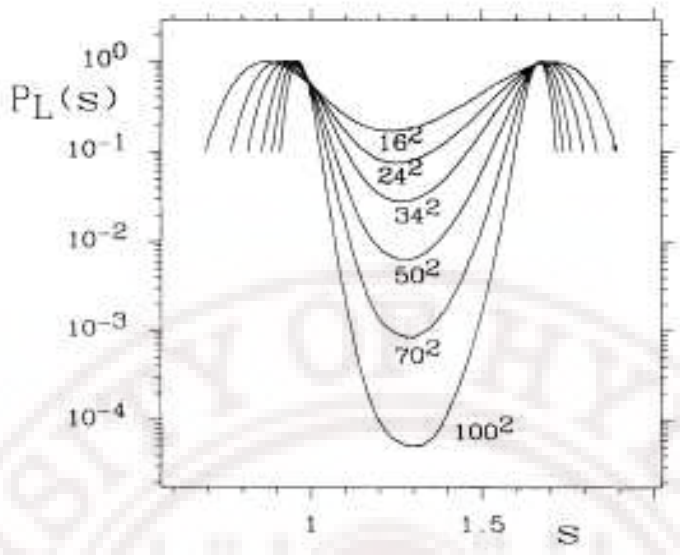

Figure 2.5 Probability distributions plotted as a function of energy for a 10-state Potts model for varying lattice sizes, L from 16^2 to 100^2(courtesy: [30])

simultaneously sample both the ordered and disordered phases which of course could differ in their relative probabilities of occupation. A generalized ensemble sampling method which samples the microstates pertaining to both the phases such that we obtain a uniform distribution in energy is called the non-Boltzmann Monte Carlo method. There are several such methods proposed to efficiently simulate systems exhibiting the first order transitions as briefly discussed in the following subsections.

2.4.1 Histogram techniques

In 1977, Torrie and Valleau proposed the so-called umbrella sampling method [14] to improve the sampling of microstates where ergodicity is hindered by the system's energy landscape, for example: interfacial events in the first order phase transition. The basic idea of the umbrella sampling is to bridge the gap between the two phases seperated by the energy barriers. In this method, Boltzmann weight factor for Monte

Carlo sampling is replaced by a potential chosen to cancel the influence of the energy barrier present. The probability distribution of the Markov chain of microstates is of the form given by

$$P(E(\mathcal{C})) = \frac{\omega(\mathcal{C})exp(-E(\mathcal{C})/k_BT)}{\sum_{\mathcal{C}_i}\omega(\mathcal{C}_i)exp(-E(\mathcal{C}_i)/k_BT)} \tag{2.10}$$

The weight function $\omega(\mathcal{C})$ is chosen such that it promotes configurations with lesser probabilities. In the case where system exhibits first order transition, the weight function is chosen high at the interfacial regions. The thermodynamic averages are then obtained by reweighting with the Boltzmann factor as shown below:

$$\langle\mathcal{O}\rangle_\beta = \frac{\sum_{\mathcal{C}}\mathcal{O}(C)\,(exp[-\beta E(\mathcal{C})]/\omega(\mathcal{C}))}{\sum_{\mathcal{C}}(exp[-\beta E(\mathcal{C})]/\omega(\mathcal{C}))} \tag{2.11}$$

The sum over microstates can be replaced by a sum over energy bins with the histogram h_i

$$\langle\mathcal{O}\rangle = \frac{\sum_i \mathcal{O}(E_i)h_i exp[-\beta E_i]/\omega_i}{\sum_i h_i exp[-\beta E_i]/\omega_i} \tag{2.12}$$

The histogram methods of Torrie and Valleau [14] and of Salzburg *et. al.* [15] are forerunners to subsequent techniques developed, belonging to this class. But this technique became popular only after the work by Ferrenberg and Swendsen [17] in 1988, and the method was applied widely to phenomena dealing with phase transitions, (for example, see [19] and references therein). In the above equation, if the weight function, ω_i is defined at a single temperature, T^* close to the reference temperature T, then it is called the single histogram method, and the probability distribution is accurate only for temperatures very close to the reference temperature. The probability distributions at these two temperatures should overlap considerably in order to get accurate results after reweighting. By generating many histograms that overlap, one can widen the temperature range. This is called the multi-histogram technique [18]. The other way of obtaining weight functions over a wide range of temperatures is to

estimate the density of states, $D(E)$ directly. This is precisely the idea behind broad histogram methods [20, 21], flat histogram methods [25] and multi-canonical Monte Carlo methods [30, 36, 44]. In these methods an estimate of the density of states, $D(E)$ is obtained in the entire energy range using iterative procedures since we have no knowledge of $D(E)$ to start with. Even though these histogram reweighting techniques are elegant, in practice they are known to give rise to errors related to poor accuracy [16].

In multi-histogram and single histogram methods, the macroscopic observables can be obtained only in a narrow energy range corresponding to that particular temperature. Hence, in systems where the free energy can have several local minima, multi-canonical methods are more efficient compared to histogram techniques. Some of the methods based on multi-canonical sampling are described in the following sections. The objective of this work is to apply one recent variant of these methods to liquid crystal systems. Before proceeding to these details, we first discuss another genre of non-Boltzmann techniques called broad histogram methods [20–22] where the density of states $D(E)$ is obtained from the probabilities of transitions between all possible states during the random walk in the energy space.

2.4.2 Broad histogram method

In the histogram reweighting techniques, the Boltzmann probability distribution is obtained as a function of energy E at a particular temperature, T. Instead of repeating the simulations for another temperature, T^1, the measured probability distribution is simply reweighted through analytical manipulations of the Boltzmann formula. The simulated Boltzmann distribution has, however, exponentially decaying tails. Therefore, statistics is poor away from the peak which is centered around the average energy. Since the peak of the new T^1 is centered somewhere on these tails,

the histogram method only works well for very small system sizes and very close to the reference temperature, T. In broad histogram method as proposed by de Oliveira, *et al.* [20–22], the system is allowed to perform a non-biased random walk along the energy E axis with long range power-law decaying tails. The density of states, $g(E)$ is measured depending on the histogram values generated on the E axis. The basic idea of this method is as follows:

Consider a lattice model of $L \times L \times L$ spins. We define a set of dynamic movements like N single spin flips starting from an initial configuration with energy E. Let us define two classes of movements $E^+ : E \rightarrow E + \Delta E$ and $E^- : E \rightarrow E - \Delta E$, where $\Delta E > 0$. If the system is left without any constraints, $g(E)$ is a monotonically increasing function of E and hence E^+ moves are more probable. In order to construct a non-biased random walk, the following dynamics is proposed:

1. If the trial movement belongs to E^- class, it is accepted and performed
2. If the trial movement belongs to E^+ class, it is accepted with probability N_{dn}/N_{up}, where N_{dn} and N_{up} are the total number of possible moves of both the classes at the current state.

Thus acceptance probability removes the bias naturally set by density of states and hence less probable moves are performed more often. Following this dynamics, we note that probability for system to jump from E to $E + \Delta E$ is same as that from $E + \Delta E$ to E. This can be written as:

$$\langle N_{up}(E)\rangle g(E) = \langle N_{dn}(E + \Delta E)\rangle g(E + \Delta E) \tag{2.13}$$

where the averages are microcanonical. From above equation one obtains:

$$lng(E + \Delta E) - lng(E) = ln\frac{\langle N_{up}(E)\rangle}{\langle N_{up}(E + \Delta E)\rangle} \tag{2.14}$$

From the above equation the density of states, $g(E)$ is obtained and canonical averages are obtained by calculating the partition function from this $g(E)$. The broad histogram covers a wide range on the energy axis, as opposed to the narrow energy windows in histogram reweighting techniques as shown in the figure 2.6. These methods were applied for example to an Ising ferromagnet (2-d lattice: 32×32 to show that the above histogram relations are exact [20–22], though some systematic errors were observed during simulations. These were subsequently reduced in their recent work [23]. Another variant of this method is the flat histogram method [24, 25] in

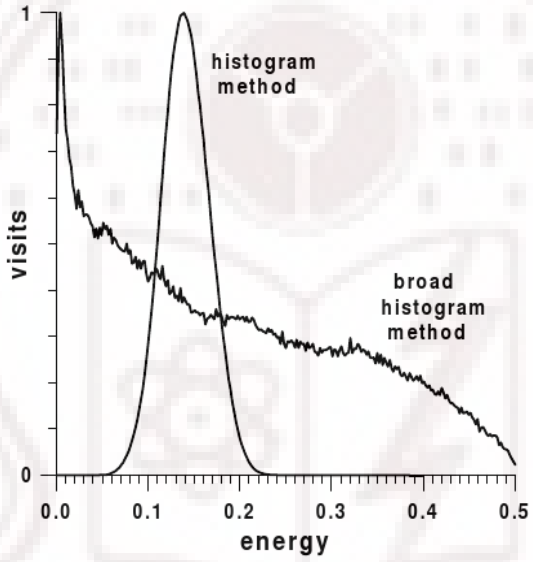

Figure 2.6 Probability distributions obtained from reweigting techniques and broad histogram method (courtesy: [22])

which the broad histogram method in combination with the transition matrix Monte Carlo method [26] is used to generate the density of states. Figure 2.7 shows the probability distributions from canonical, broad and flat histogram methods. These methods are extended to multi-parametric Hamiltonians and also to continuous systems [27–29].

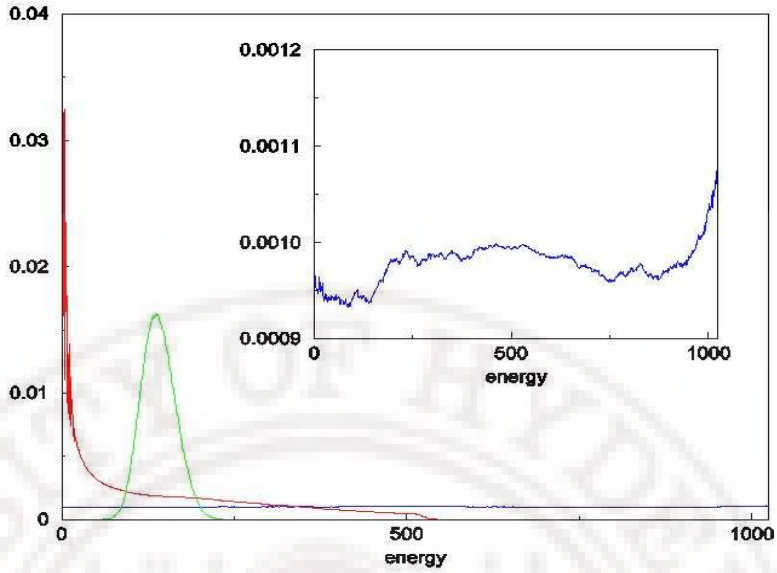

Figure 2.7 Probability distributions obtained from canonical sampling methods (green), broad histogram method (red) and flat histogram method (blue). The inset shows finer details of the probability distriubution obtained from the flat histogram methods (courtesy: [24])

2.4.3 Multi-canonical method

The broad and flat histogram methods estimate the density of states $g(E)$ from the probabilities of possible moves from one state to another. Berg and Neuhaas [30, 30, 32] came up with the idea that the density of states can also be estimated from *a priori* unknown weights which will be iteratively updated during the simulation using energy histogram entries. These methods consist of two steps:

1. Obtain a working estimate of a weight function, $w_{mu}(\mathcal{C})$, which represents the relative probability measure of the configuration $\mathcal{C}$, corresponding to a microstate. This estimate has to be good enough such that it ensures convergence to the true denstiy of states eventually and also samples the desired energy range within a feasible time.

2. Perform a Markov chain Monte Carlo simulation with these converged weights.

Canonical averages are obtained by reweighting to the Gibbs ensemble and standard jackknife methods [34] allow reliable error estimates.

In multi-canonical simulations (MUCA) the system is allowed to sample from a probability distribution

$$P_{mu}(E) \propto g(E) w_{mu}(E) \tag{2.15}$$

where $w_{mu}(E)$ is the weight function to be estimated. If $w_{mu}(E) = 1/g(E)$, then the probability distribution is uniform over all energies. In this procedure, one considers the weight functions $w_{mu}(E)$ as approximations to the corresponding weights $w_{1/g}(E(\mathcal{C}))$, as given below

$$\hat{w}_{mu}(\mathcal{C}) = w_{mu}(E(\mathcal{C})) = exp(-b(E(\mathcal{C}))E(\mathcal{C}) + a(E(\mathcal{C})). \tag{2.16}$$

to the weights

$$\hat{w}_{1/g}(\mathcal{C}) = w_{1/g}(E(\mathcal{C})) = \frac{1}{g(E(\mathcal{C}))}. \tag{2.17}$$

Here the function $b(E) = \partial S(E)/\partial E$ is the microcanonical temperature at energy E and $a(E)$ is a kind of fugacity. The desired canonical distribution is then obtained from the relation

$$P(E) \propto \frac{P_{mu}(E)}{w_{mu}(E)} e^{-\beta E}. \tag{2.18}$$

Multi-canonical simulations not only allow sampling of rare configurations in the microstate space but also improve the dynamics by allowing the system to evolve freely in the configuration space even in the presence of free energy barriers. The probability distributions in the case of 10-state Potts model obtained from both canonical and MUCA methods for a square lattice size of L=70, are shown in the figure 2.8. These methods have been successfully applied to several complex systems with characteristic rough free energy landscapes like spin glasses [31, 35, 38], protein simulations [41, 42],

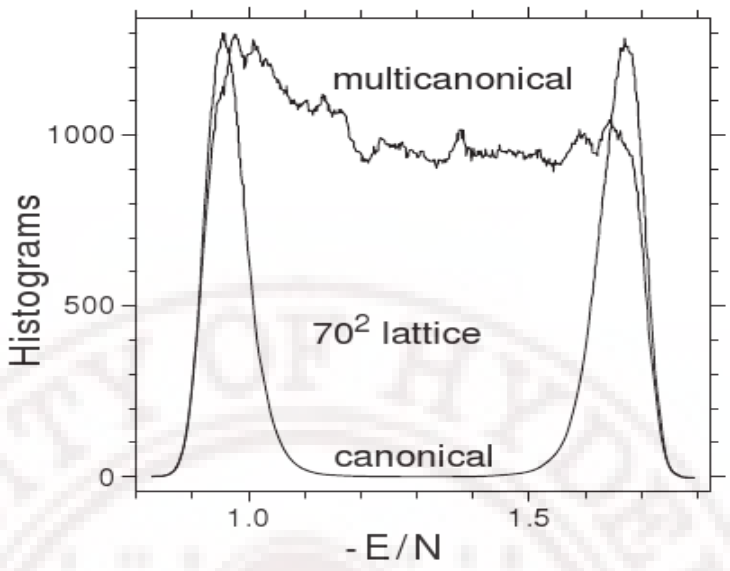

Figure 2.8 Probability distribution $P_{mu}(E)$ obtained from MUCA versus canonical probability $P(E)$ for 2D 10-state Potts model on L= 70×70 (courtesy: [30])

optimization problems [43], etc. One drawback of these methods, however, is the lack of good recursive schemes to speed up the alogorithm. The presence of two parameters to update the weight function and the density of states $g(E)$ makes it more complex in terms of initialisation and updating schemes. This problem is addressed in the entropic sampling method described in the following section. Here the probability distribution depends on only one parameter which is to be estimated during the initial learning run.

2.4.4 Entropic sampling method

The basic idea of entropic sampling method proposed by J. Lee [36] is similar to multicanonical method [30] discussed earlier. In this method, the microstates are sampled from entropy of a given system instead of canonical ensemble at infinite temperature. Since entropy is not known *a priori*, a rough estimate is made initially and corrected

iteratively till it converges to the true entropic function, $S(E)$. Let us suppose that the probability of sampling a microstate is given by:

$$P_\alpha(E) \propto exp\left[\frac{S(E)}{k_B} - \alpha(E)\right] \tag{2.19}$$

We impose the detailed balance condition given by,

$$\frac{\mathcal{W}(B \leftarrow A)}{\mathcal{W}(A \leftarrow B)} = \frac{P_\alpha(E(B))}{P_\alpha(E(A))} \tag{2.20}$$

$$= exp\left[-\{\alpha(E(B)) - \alpha(E(A))\}\right] \tag{2.21}$$

It may be noted that the contribution to the transition probabilities arising from entropic considerations is inherently taken care of during the random walk itself. This condition implies that the acceptance probability of a trial microstate, C_t from the current microstate C is given by,

$$p = min\left(1, exp\left[-\{\alpha(E(C_t)) - \alpha(E(C))\}\right]\right) \tag{2.22}$$

It is clear that if $\alpha(E) = \beta E$, then equation 2.19 reduces to conventional Boltzmann probability. Entropic sampling obtains when we set $\alpha(E) = S(E)/k_B$. This renders probability distribution, $P_\alpha(E)$ uniform over all the energies. But as we do not know the entropic function a priori, we build $\alpha(E)$ iteratively during a learning run. As a result of this procedure, since we aim to obtain a uniform distribution in the energy range, any barriers present in the energies will not affect the evolution of Markov chain of microstates. The basic idea of the simulation is given below:

Learning run:

We divide the desired energy range into number of bins (E_{min}, E_{max}). We initialize $\alpha(E_i) = 0 \; \forall \; i$. We perform a random walk with acceptance probability given by the eqn 2.22. In the first iteration, all the states get accepted. We accumulate the histogram entries h_i, after every Monte Carlo sweep (MCS,

consisting of N Monte Carlo trial steps). After M such MC sweeps, we update α_i as per the recursion given by:

$$\alpha_i^{(k+1)} = \begin{cases} \alpha_i^{(k)} \quad , & \text{if } h_i = 0, \\ \alpha_i^{(k)} + \frac{1}{k_B} ln[h_i] & \text{otherwise.} \end{cases} \tag{2.23}$$

Here, superscript k is the iteration index. We continue the iterations until energy histogram is flat in the desired energy range.

Production run:

The final α_i obtained in the learning run is used to collect a large number of microstates. This α-ensemble contains information pertaining to all the temperatures.

Reweighting:

From the α-ensemble, we obtain canonical ensembles at each temperature and calculate the average thermodynamic variables by the reweighting procedure [30, 32] described below. Let $O(\mathcal{C})$ be the macroscopic property at a desired temperature T. The average value, $\langle O \rangle_\beta$ is obtained by dividing with the factor we have introduced artificially, $exp[-\alpha(E(C_i))]$ and multiplying the Boltzmann factor, $exp[-\beta E(C_i)]$ as follows:

$$\begin{aligned} \langle O \rangle_\beta &= \lim_{N \to \infty} \bar{O}_N(\beta) \\ &= \frac{\sum_{i=1}^{N} O(\mathcal{C})\ exp[-\beta E(C_i) + \alpha(E(\mathcal{C}_i))]}{\sum_{i=1}^{N}\ exp[-\beta E(C_i) + \alpha(E(\mathcal{C}_i))]} \end{aligned} \tag{2.24}$$

In the original application [36], the partition function was calculated from α_i directly and good results were obtained for 24×24 2D ten-state (Q=10) Potts model and $4 \times 4 \times 4$ 3D Ising model. In principle, one can attempt to obtain the average values from the entropic function α_i by calculating the partition function, provided of

course α_i is accurate and also we have the knowledge of the normalization constant. For systems with discrete degrees of freedom this procedure is in principle possible. Since for systems with continuous degrees like liquid crystals, which is the focus of study in this thesis, we can not compute the normalization constant, we follow the procedure of carrying out a long production run and reweighting at the desired temperatures to obtain the canonical ensembles. However, like any other flat histogram methods described earlier, this method works very well generally for small systems only. Density of states grows exponentially with energy whereas the histogram entries hitherto are updated linearly. Hence, such recursive methods [30, 31, 37, 39–41] which update the density of states based on the histogram entries are not found to be efficient in converging the update function to its asymptotic value [44].

2.4.5 Wang-Landau algorithm

Recently, a simple and flexible variant of the entropic sampling method was proposed [44]. This procedure offers substantial advantage over others in speeding up the convergence of the density of states. It is based on the same idea as the earlier flat histogram methods in that if we perform a random walk in the microstate space according to the acceptance probability proportional to the inverse of density of states $(1/g(E))$, we generate a uniform distribution of states in the energy space. In this new method, each time an energy level E is visited, the density of states $g(E)$ is updated by $g(E) \rightarrow g(E) \times f$, where f is the so-called modification factor. In practice, the simulation is performed on log-scale and hence the entropy $\alpha(E)$ is updated as $\alpha(E) \rightarrow \alpha(E) + ln(f)$. This is to avoid over-flow errors while accumulating the histogram entries. If the trial step is rejected, then also $\alpha(E)$ is updated, in keeping with the prescriptions of Metropolis algorithm. The modification factor is initialized with a positive value $f = f_0 = e$. If f_0 is too small, the random walk will spend

an extremely long time to reach all possible energies. However, too large a choice of f_0 will lead to statistical errors. In [44], authors check the histogram values for flatness after every 10000 MCS, following which the modification factor is updated as $f_i = \sqrt{f_{i-1}}$, where i is the iteration index. The histogram values are reset and the next level of random walk is started. These iterations are continued until the modification factor, f approaches unity, in practice to a predefined value $f_{final} = exp(10^{-8})$. Any other protocol [48] to update the modification factor which decreases monontonically to unity is also valid. This method was applied succesfully to 2D Q=10 Potts model of size 200×200 and also 2D Ising model of size 256×256 [44]. It was also shown that this procedure can be adopted to complex systems like spin-glass systems for 3D EA model of size $L = 4, 6$ and 8 [44].

WL algorithm found readily applications in various discrete systems [45–47]. When applied to continuous systems (i.e., systems involving random walks with continuous step sizes), it was observed that this technique requires modifications to overcome the problem of under-sampling and slow dynamics. Thus in our liquid crystal studies, we needed to modify this algorithm to improve its efficiency, and make it applicable to at least moderately large lattice systems (upto $25 \times 25 \times 25$). Modifications proposed in this context and application of the modified WL algorithm to some complex systems are the results reported in this thesis, in the subsequent chapters.

2.5 Macroscopic observables

As has already been mentioned, the main interest in the thesis is to study nematic-isotropic phase transition in liquid crystals and related systems. We adopt Lebwohl-Lasher potential as described in Chapter 1 to mimic the interactions between the liquid crystal molecules. Here we mention briefly the procedures followed to compute

different macroscopic observables as averages over the respective canonical ensembles.

2.5.1 Average energy and specific heat

Average energy is calculated by taking the canonical average of the large collection of the microstates generated during the production run of the simulation. Thus average energy is obtained from

$$\langle E \rangle = \frac{\sum_{i=1}^{n} E_i exp(-\beta E + \alpha E)}{\sum_{i=1}^{n} exp(-\beta E + \alpha E)} \tag{2.25}$$

Specific heat at constant volume is obtained from the mean square fluctuations in energy given by:

$$C_V = \frac{1}{k_B T^2}(\langle E^2 \rangle - \langle E \rangle^2) \tag{2.26}$$

where k_B is the Boltzmann constant. The temperature is always represented in reduced units in terms of T^* given by

$$T^* = \frac{k_B T}{\epsilon} \tag{2.27}$$

where ϵ represents the coupling strength between two neighbouring mesogenic units in the LL model, and sets the energy scale of the computation.

2.5.2 Orientational order parameter

Since during the nematic to isotropic transition only the orientational degrees of freedom are affected, one needs to define the order parameter which depends only on the orientations of the molecules. Let us consider a system of N liquid crystal molecules which are cylindrically symmetric, and allocate a unit vector to each of these molecules along the respective symmetry axis. Let $e_x^{(i)}$, $e_y^{(i)}$ and $e_z^{(i)}$ represent the projections of the unit vector of i^{th} molecule with respect to a chosen laboratory

reference frame (x, y, z). We now construct an ordering matrix from these components and arrange the same over the sample, presented as

$$Q_{zz} = \frac{1}{N}\sum_{i=1}^{N}\begin{pmatrix} e_x^{(i)}e_x^{(i)} - 1/3 & e_x^{(i)}e_y^{(i)} & e_x^{(i)}e_z^{(i)} \\ e_y^{(i)}e_x^{(i)} & e_y^{(i)}e_y^{(i)} - 1/3 & e_y^{(i)}e_z^{(i)} \\ e_z^{(i)}e_x^{(i)} & e_z^{(i)}e_y^{(i)} & e_z^{(i)}e_z^{(i)} - 1/3 \end{pmatrix} \tag{2.28}$$

where Q_{zz} is symmetric and is made traceless. The diagonalization of the Q_{zz} matrix by appropriate rotational transformations leads to principal axes system in which director frame can be identified. We calculate the eigen values and eigen vectors of this matrix. The maximum eigen value (λ_{max}) gives a measure of the amount of order and the corresponding eigen vector indicates the direction of the director. The second rank scalar order parameter is defined as $S = \langle P_2 \rangle_\lambda = \frac{3}{2}\lambda_{max}$. The absolute value of the difference in the other two eigen values provides a measure of the phase biaxility in the system.

Orientational susceptibility originating from the fluctuations in the order parameter is given by

$$\chi = \frac{1}{k_B T}(\langle S^2 \rangle - \langle S \rangle^2). \tag{2.29}$$

The response functions C_V and χ show divergences near the nematic-isotropic phase transition. The location of the peaks determine the transition temperature, T_{NI}. These parameters are very useful in examining quantitatively the phase behaviour of the system when perturbed by boundary conditions or other external effects.

Bibliography

[1] M. E. J. Newman and G. T. Barkema, *Monte Carlo methods in statistical physics*, Clarendon press, London (2002).

[2] D. P. Landau and K. Binder, *A guide to Monte Carlo simulations in statistical physics*, Cambridge University press, 2nd edition (2005).

[3] K. P. N. Murthy, *Monte Carlo methods in statistical physics*, Universities press, India (2004).

[4] M. P. Allen, D. J. Tildesley, *Computer simulation of liquids*, Clarendon, Oxford (1991).

[5] B. A. Berg, *Markov chain Monte Carlo- Innovations and Applications*, edt by W. S. Kendall, F. Liang and J-S. Wang, World Scientific, Singapore (2005).

[6] M. P. Allen, *Advances in the computer simulations of liquid crystals*, edited by P. Pasini and C. Zannoni, Kluwer Acad publishers (2000).

[7] P. Pasini, C. Chiccoli and C. Zannoni, *Advances in the computer simulations of liquid crystals*, edited by P. Pasini and C. Zannoni, Kluwer Acad publishers (2000).

[8] M. R. Wilson, *Int. Rev. Phys. Chem.* **24**, 3-4, 421 (2005).

[9] P. A. Lebwohl and G. Lasher, *Phys. Rev. A.* **6**, 426 (1972).

[10] N. Metropolis, A. W. Rosenbluth, M. N. Rosenbluth, A. H. Teller and E. Teller, *J. Chem. Phys.* **21**, 1087 (1953).

[11] R. J. Glauber, *J. Math. Phys.* bf 4, 294 (1963).

[12] R. H. Swendsen and J-S. Wang, *Phys. Rev. Lett* **58**, 86 (1987).

[13] U. Wolff, *ibid* **62**, 361 (1989).

[14] G. Torrie and J. P. Valleau, *Chem. Phys. Lett* **28**, 578 (1974).

[15] Z. W. Salzburg, *et. al.*, *J. Chem. Phys.* **30**, 65 (1959).

[16] A. M. Ferrenberg and D. P. Landau, *Phys. Rev. B.* **44**, 5081 (1991).

[17] A. M. Ferrenberg and R. H. Swendsen, *Phys. Rev.Lett* **61**, 2635 (1988); **63**, 1195 (1989).

[18] A. M. Ferrenberg and R. H. Swendsen, *Phys. Rev.Lett* **63**, 1195 (1989).

[19] K. Venu, V. S. S. Sastry and K. P. N. Murthy, *Europhys. Phys. Lett.* **58**, 646 (2002).

[20] P. M. C. de Oliveira, T. J. P. Penna and H. J. Herrmann, *Braz. J. Phys.* **26**, 677 (1996).

[21] P. M. C. de Oliveira, T. J. P. Penna and H. J. Herrmann, *Eur. J. Phys. B.* **1**, 205 (1998).

[22] P. M. C. de Oliveira, *Eur. Phys. J. B*, **6**, 111 (1998).

[23] P. M. C. de Oliveira, *Braz. Phys. J.*, **30**, 4659 (2000).

[24] J. S. Wang and L. W. Lee, *Comput. Phys. Commun.* **127**, 131 (2000).

[25] J-S. Wang, arxiv: cond-mat/9909177v1 (1999).

[26] J-S. Wang and R. H. Swendsen, *J. Stat. Phys* **106**, 245 (2002).

[27] L. W. Lee and J-S. Wang, *Phys. Rev. E* **64**, 056112 (2000).

[28] J. D. Munoz, H. J. Herrmann, *Comput. Phys. Comm.* **13**, 121 (1999).

[29] A. R. Lima, P. M. C. de Oliveira and T. J. P. Penna, *Solid. State. comm.* **114**,8, 447 (2000).

[30] B. A. Berg and T. Neuhaas, *Phys. Rev. Lett* **68**, 9 (1992).

[31] B. A. Berg and T. Celik, *Phys. Rev. Lett*, **69**, 2292 (1992).

[32] B. A. Berg and T. Neuhaas, *Phys. Lett. B* **267**, 249 (1991).

[33] W. Janke and S. Kappler, *Phys. Rev. Lett* **74**, 212 (1995).

[34] B. A. Berg, *Comput. Phys. Comm.* **69**, 7-15 (1992); B. Efron, *The Jackknife, the Bootstrap and other resampling plans*, SIAM, Philadelphia (1982).

[35] B. A. Berg, U. H. Hansmann and T. Celik, *Phys. Rev. B.***50**, 16444 (1994).

[36] J. Lee, *Phys. Rev. Lett* **71**, 2 (1993).

[37] B. A. Berg, U. Hansmann and T. Neuhaas, *Phys. Rev. B* **47**, 497 (1993).

[38] B. A. Berg and W. Janke, *Phys. Rev. Lett* **80**, 4771 (1998).

[39] B. A. Berg, *Nucl. Phys. B*, **63**, 982 (1998).

[40] U. Hansmann, *Phys. Rev. E* **56**, 6200 (1997).

[41] U. Hansmann and Y. Okamoto, *Phys. Rev. E* **54**, 5863 (1996).

[42] M. -H. Hao and H. A. Scheraga, *J. Chem. Phys.* **98**, 4940 (1994).

[43] Y. Lee and M. Y. Choi, *Phys. Rev. E* **50**, R651 (1994).

[44] F. Wang, and D. P. Landau, *Phys. Rev. Lett.* **86** 2050 (2001); F. Wang and D. P. Landau, *Phys. Rev. E.* **64** 056101 (2001).

[45] D. P. Landau and F. Wang, *Braz. J. Phys.* **34**, 2A (2004).

[46] H. K. Lee, Y. Okabe and D. P. Landau, *arxiv:cond-mat/0506555 v1*, (2005).

[47] T. Surungan, Y. Okabe and Y. Tomita, *J. Phys. A: Mathematical and general* **37**, 4219 (2004).

[48] A. Huller, e-print cond-mat/011379.

Chapter 3

Wang-Landau Monte Carlo simulation of nematic-istotropic phase transition in liquid crystals

3.1 Application of WL algorithm to continuous systems

Wang-Landau (WL) algorithm [1] as mentioned in the chapter I was initially proposed for systems with discrete energy spectrum like Ising model, q-state Potts model, *etc.* It was found to be very efficient in generating density of states (DoS), and hence free energy profiles, accurately for reasonably large sizes of such discrete systems. There were also attempts to apply WL algorithm to continuous systems like simulations of proteins [3–7], fluids represented by Lennard-Jones potential [8–19], polymers [20–24], liquid crystals [25], binary Lennard-Jones glasses [26], solid-liquid equilibria [27], of Heisenberg model [28, 29], and XY model [30]. Most of the above studies suggest that the WL algorithm (in its original form) as applied to continuous systems is not

that efficient and requires certain modifications to get accurate estimates of DoS over the energy range of interest. The main issues concerned with the continuous systems are convergence of DoS within an acceptable and realistic time frame, and diffiulties in accessing lower energy regions with significantly less probability. Also, there are issues connected with numerical computations like overflow errors and rounding-off errors due to truncation which limit the efficiency of the algorithm. As the system size increases these become more prominent and accute. The reason is that the number of microstates in continuous systems is prohibitively large, so much so that, the number of steps needed for the system to sample over the desired energy range tends approximately to infinity, particularly as the system size grows. Moreover, the difference between degeneracies at lower and higher entropy regions is so high that, practically system needs additional algorithmic guidance to force it towards lower energy regions.

In the original WL algorithm, the modification factor is decreased exponentially until it reaches a negligible value so as to lead to a final random walk satisfying the detailed balance condition. However in this scheme, configurations generated at different stages of the simulation do not contribute equally to the DoS. In the final stages of iteration, the factor will be so small that it practically does not contribute to the DoS estimate. Continuous systems with the above difficulties are thus less susceptible to ready application of WL algorithm, relative to discrete energy systems. To overcome such problems, there were suggestions to determine the running estimate of DoS from the configurational information rather than the energy histogram [4, 10]. In some studies it was suggested that WL algorithm has to be combined with other methods like multi-bondic cluster algorithm, multi-canonical method, broad histogram method, transition matrix method, N-fold way rather than a single spin flip, parallel tempering, etc to increase its efficiency. In the present study, we apply

WL algorithm to study liquid crystal systems which has continuous orientational degrees of freedom, with focus on the study of the nematic-isotropic phase transition. We will briefly recall in the next section the original WL algorithm as proposed in [1]. Further, certain modifications are proposed to adapt the WL algorithm to liquid crystal systems, and these are discussed in detail in the subsequent sections.

3.2 Wang-Landau algorithm

In order to generate an ensemble of microstates distributed uniformly with respect to energy, the random walk in the configurational space should be appropriately biased, based on the knowledge of the representative density of states. However, DoS is not known a priori, and needs to be estimated, as accurately as possible, as a part of the computation. The WL algorithm addresses this problem by including the calculation of DoS as a part of the initial learning process, made efficient so as to span very low probable states through an algorithmic guidance. This is eventually withdrawn asymptotically following a protocol, leading to the evaluation of DoS on one hand, and consequent construction of an entropic ensemble over a large enough production run.

However, to initiate the computation the DoS represented by $g(E)$ is set to be uniform over the energy range of interest, which is conveniently divided into a large enough number of bins. It is customary to set $g(E)$ to be unity at the begining of the learning run. To start with, we divide the desired energy range into N number of bins. We initialize $g(E_i)\ \forall\ i \in N$ to a positive number (say 1) or alternatively we can initialize $\alpha(E_i) = log[g(E_i)]$ to e. Let us consider a set of molecules distributed over a cubic lattice of size $L \times L \times L$. To map the calculation to a LC system we assume an orientation dependent nearest neighbour interaction among the molecules.

We perform a random walk in the space of the microstates of the system by randomly changing the orientation of a randomly chosen molecule. Let the energy of the initial state be E_i.The probability of accepting a trial state of energy, E_t is prescribed in this algorithm as

$$p = \min\left[1, \frac{g(E_i)}{g(E_t)}\right]. \tag{3.1}$$

After every such Monte Carlo step, $g(E)$ is updated by the so-called modification factor f, (referred to as Wang-Landau factor in [32]), $g(E) \rightarrow g(E) \times f$.Alternatively, we can write it in terms of its logarithm as $\alpha(E) \rightarrow \alpha(E) + ln(f)$, where α represents the entropy of the system. The energy histogram $H(E)$ is collected in the desired energy range. After a large number of Monte Carlo sweeps (termed as one iteration), each sweep consisting of L^3 Monte Carlo steps, we decrease the value f monotonically until it becomes equal to 1. Wang and Landau in original work [1] suggested taking the square root of f as a protocol to decrease progressively the value of f. But any other method which ensures f to decrease monotonically to 1 can be used [31]. As $f \rightarrow 1$, long enough walk guided by the prescription in eqn 3.1 will eventually make $g(E)$ converge to the true density of states, $D(E)$. It should be noted though, that detailed balance condition is satisfied only in the final iterations when $f \approx 1$.

Once the DoS is accurately known, the relevant thermodynamic observables can be in principle be estimated via the computation of the associated partition function. But, in the case of systems with continuous degrees of freedom it has been found more practical to construct an entropic ensemble, comprising of microstates obtained by a long random walk (during a production run) guided by the DoS computed earlier. This should lead to a reasonably uniform distribution of microstates with respect to energy, the degree of uniformity reflecting the accuracy in the estimation of DoS. Though such an ensemble does not correspond to a physically observable

macrostate, canonical ensemble at any desired temperature can now be extracted from this collection of microstates by the so-called reweighting procedure (described in Chapter 2). It essentially corresponds to accepting each microstate of energy E in the entropic ensemble with a combined probability determined by the DoS, $g(E)$ and the Boltzmann factor $exp(-\beta E)$. An interesting outcome of using the DoS for this purposes is that any minor inaccuracies involved in its estimation (which would have been reflected in a deviation from uniform distribution along the energy axis) are corrected for in the reweighting process. Thus it has been found possible to allow moderate deviations in the energy histogram without perceptibly affecting the extracted behaviour of macroscopic obervables with respect to temperature.

We present the results obtained for Ising model of size $100times100$ simulated using WL algorithm described above. The density of states, $g(E)$ and energy histogram describing the distribution of microstates in the entropic ensembles, $H(E)$ for this system are shown in the figure 3.1. It may be seen that the DoS has spanned the entire energy range and the energy histogram is reasonably flat.

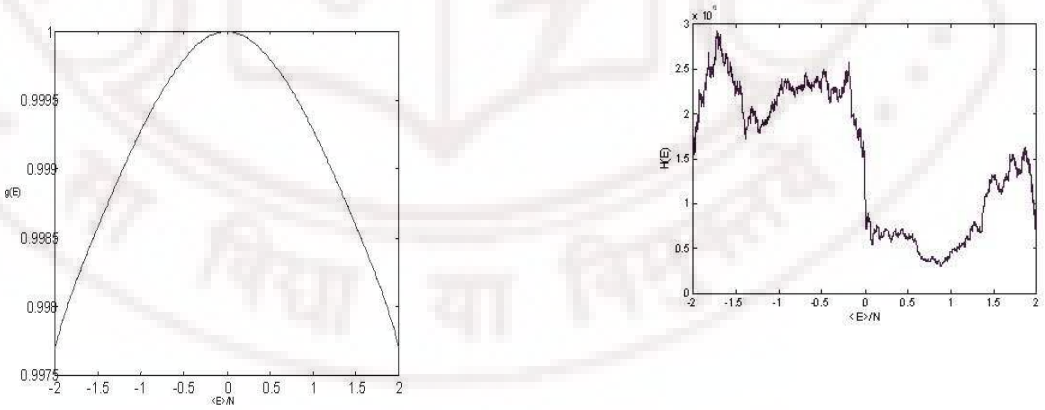

Figure 3.1 Density of states, g(E) (left) and energy histogram, H(E) (right) for Ising model of size, 100 × 100.

3.3 Modified Wang-Landau method

The Wang-Landau algorithm as proposed in [1] proved to be efficient to study discrete systems, particularly involving first order transitions. The important signature of the first order transition is the existence of a free energy barrier separating ordered and disordered phases. In order for any algorithm to simulate first order phase transitions efficiently, the tunneling times between ordered and disordered phases have to be short. In simple systems, short tunneling times are considered to be a good indication for a succesful flat-histogram method [33]. Canonical simulations at a fixed temperature sample the states from a peaked distribution in a very narrow region at a fixed temperature and hence the tunneling times will be very large. As the system size increases, the tunneling time increases exponentially because the barrier height scales linearly with the linear size of the system. WL algorithm, like the other flat histogram methods, samples the states from a broad range of energies and hence reduces the tunneling time. The tunneling time in WL algorithm seems to exhibit a power-law scaling with the system size [35] and hence found to be efficient to study first order transitions compared to the canonical as well as other flat-histogram based simulations. However, it has been observed that in all the flat-histogram based methods the time required to go from higher entropy regions to lower ones is longer than viceversa.

Liquid crystals as modeled by Lebwohl-Lasher potential [2] defined on a cubic lattice with free wheeling molecules at each lattice site is one such system which exhibits first order transition from isotropic to nematic phase as we reduce the temperature. Application of the Wang-Landau algorithm to this system in its original form proved to be inefficient [31], particularly beyond a typical system size of $6 \times 6 \times 6$ After examining in detail the converging trends of DoS under different protocols of

modification process through the factor f we find that a slightly different strategy works for the LC systems, and one can study systems with sizes upto $25 \times 25 \times 25$ within an acceptable time frame. We present below the details of this modified algorithm [32]. In this connection, it may be noted that there are also a number of other modifications proposed independently to improve the perfomance of the algorithm as applied to continuous systems. It is common experience that these modifications and improvements are mostly problem-specific.

Let us consider a cubic lattice of liquid crystals. Free wheeling spins with head-tail symmetry are placed at each lattice point. Initially we divide the desired energy range $[-3L^3, 1.5L^3]$ into N number of bins. It should be noted that if the bin width is more, the system tends to get stuck in the same energy bin and the dynamics becomes slow. On the other hand, if the bin width is too narrow larger computational times are required to obtain a reasonable amount of statistics in the energy histogram. In practice, the bin width is usually chosen depending on the temperature resolution at which one would like to calculate the thermodynamic observables. In all our simulations, we have taken the total number of bins as twice the number of particles in the system. Bin width is then calculated as the desired energy range divided by the number of bins. Let us represent the orientation of each spin by polar angle θ and azimuthal angle ϕ. We initialize the orientations of the spins on the lattice by randomly generating direction cosines from $[cos\theta, \phi]$. $g_i(E)\ \forall\ i = 1, N$ is initialized with a positive value (say e). Let $\mathcal{C}_0$ denote the initial microstate and its energy belongs to, say, μ^{th} bin. Let us now pick up a spin either randomly (or via type-writer fashion) and change its orientation by employing Barker's method [41]. In this method, one of the three coordinate axes is chosen randomly. The spin is rotated about this chosen axis by a small angle $\Delta\theta$. In all our simulations, $\Delta\theta$ varies between -0.5 to $+0.5$.

Let $\mathcal{C}_t$ be the trial microstate so obtained and its energy belongs to ν^{th} bin. If $g_\nu \leq g_\mu$, then the trial state is accepted. If $g_\nu > g_\mu$, the trial state is accepted only if $g_\nu/g_\mu \geq r$ where r is a random number generated from the uniform distribution in the range $[0, 1]$. If $g_\nu/g_\mu < r$ then the trial state is rejected. This constitutes one Monte Carlo step. L^3 such moves constitute one Monte Carlo sweep (MCS). Since g_i are chosen to have the same initial value, all the moves during the first MCS will be accepted. After one such MCS, we update g_i to $g_i \times f$. In the original algorithm [1], g_i is updated after every Monte Carlo step, rather than sweep. Since the energy difference between two consecutive Monte Carlo steps is very less in continuous systems, updation of $g(E)$ after every Monte Carlo step would spike up the $g(E)$ entries in a narrow energy region, thus leading to slower dynamics. We perform $P = 10000$ such Monte Carlo sweeps which constitute one iteration. After each iteration we update $f \rightarrow f^{0.9}$. The final g_i obtained after each iteration is used as an initial value for the next one. We perform M (160) such iterations so that $f_M - 1 = 10^{-7}$, for an initial value of f, $f_0 = 10$. Let us call M such iterations as one Wang-Landau run. f is reset to f_0 in the next WL run. The value of g_i and the microstate obtained from each such WL run are carried forward to the next WL run as initial values. We performed a total of 50 such WL runs. The value of f_0 is 100 for the first 40 runs, 10 for the next 9 and $f_0 = e$ for the last run. These values are chosen after some experimentation such that the final g_i spans totally the desired energy range and the final histogram in energy is almost flat. In the first sub-stage of 40 runs, f_0 is initialized to a higher value. This is required to sample a wider energy region. But the penalty we pay is in the accuracy of $g(E)$, since error introduced in the $g(E)$ away from the true DoS increases with increase in f. Once the $g(E)$ spans the desired energy range, then we reduce the value of f_0 in the subsequent runs. In the last stage, we perform a long smoothening run with minimum f_0 so that

$g(E)$ converges to the true DoS. It should be noted here that the values of f_0 and the number of iterations to be employed completely depend on the characteristics of the system like system size, complexity etc and hence for a given system exploratory computations are needed before optimizing the parameter values. A detailed flow chart of this algorithm for one WL run is shown in the figure 3.2. A description of the scheme of WL runs employed by us is shown in figure 3.3.

The final g_i obtained after completing the required WL runs is used without further modifications (i.e., $f = 1$) for performing a long run of about one million, or more Monte Carlo sweeps, also called the production run. During this process, we collect a large number of microstates constituting the non-Boltzmann ensemble obtained from the entropic sampling. These microstates contain information pertaining to all regions of configurational space encompassing all the temperatures. From this ensemble, we extract all the thermodynamic observables like average energy (E), orientational order parameter (S), specific heat at constant volume (C_V), orientational susceptibility (χ) and Binder's cumulant (V_4) at any temperature by appropriate reweighting procedure.

3.3.1 Flatness criteria

In this algorithm, the energy histogram is checked for flatness only after each substage of WL runs unlike in original WL algorithm where the flatness is checked after every MCS. In the original algorithm, the energy histogram is considered to be flat if all the accessible states were populated by more than 90% of the average number of visits [1]. However, this flatness criterion seems to be too restrictive for continuous systems as the system size becomes large. In many cases, it is found sufficient if there are atleast a minimum number of visits in each energy bin particularly in the lower energy bins [8]. The minimum value to be set, however, depends on the complexity of

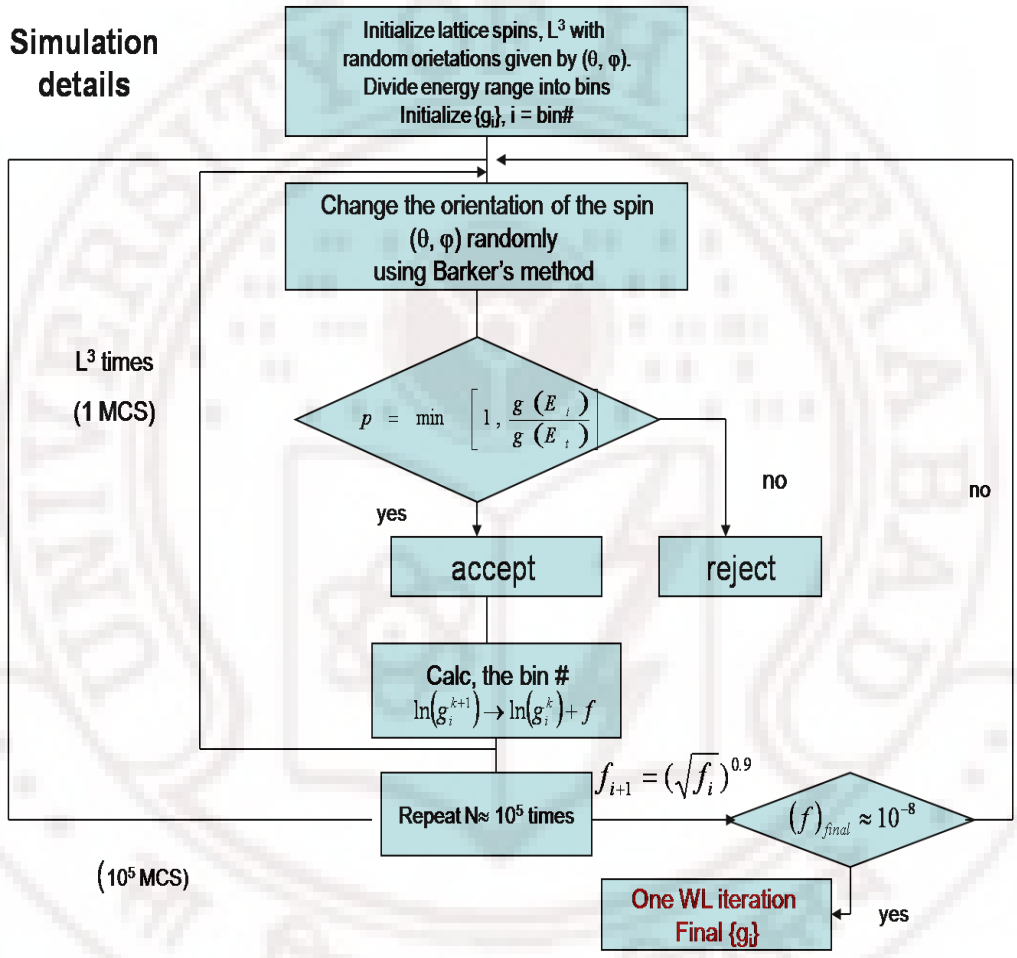

Figure 3.2 Flow chart of the basic WL algorithm

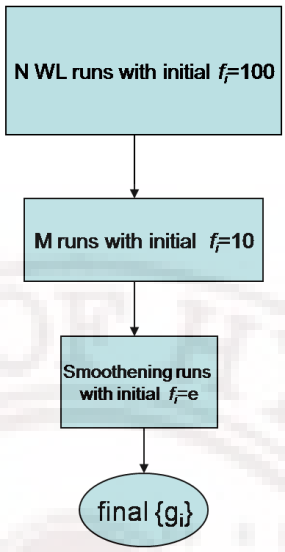

Figure 3.3 Scheme of WL runs employed in the modified version

the problem. Shell *et. al* [8] suggested a minimum value of 20, whereas, Parsons and Williams [24] suggested about 4000 samples per bin for polymer models. It has also been suggested that one can consider a histogram to be flat enough (for purposes of reweighting) in continuous systems if all the higher energy bins on the right side of the empty bins are completely filled [24]. However, the flatness criterion in continuous systems is still an open question. The reason that one can manage even with not-so-flat a histogram of states is the self-correcting opportunity afforded during the reweighting process.

We observed that there are certain numerical problems associated with this kind of iterative procedures even for moderately large systems, arising from the representation of data on computer like over flow errors and loss of precision due to the truncation errors. In order to reduce these errors we reformulated this algorithm on a log-log scale (i.e., in the representation of logarithm of entropy) and performed the simulations accordingly. These involve calculating g_i in terms of $\xi = log(\alpha) = log(log(g_i))$. The acceptance probability, updation of ξ, unweighting-reweighting procedure, etc., are

also calcualated in the same log-log scale following the numerical tricks suggested by Berg [42]. The details of these numerical tricks are given in Appendix A. We find significant improvement in the efficiency of the algorithm due to this change of scale and we could attempt simulations on a $20 \times 20 \times 20$ system.

3.3.2 Modification factor, f

It has been observed that modification factor, f as well as the scheme adapted to update f plays a crucial role in the convergence of DoS. In a recent study [34], it was observed that the convergence of $g(E)$ to the true DoS scales as $\sqrt{lnf}$. In other words, a good convergence criterion in simulations could be that each bin is visited at least a number of times which scales with modification factor as $\frac{1}{\sqrt{lnf}}$. This scheme seems to increase the accuracy of DoS at later stages of the iterations as more time is spent in constructing the DoS. However, when the system exhibits rugged energy landscape, it takes longer time to escape from the local energy minima. Moreover, it was observed [36] that the effect of initial value f_0 on the accuracy of $g(E)$ is felt only for shorter times. As the number of Monte Carlo runs increases, the efficiency as well as accuracy of final $g(E)$ is not influenced much by the value of f_0. In the present study, we have adapted a scheme where the factor f is scaled to its initial value after every few iterations, each iteration consisting of large number of Monte Carlo runs, and repeat the procedure until DoS converges satisfactorily as evidenced by successive DoS profiles. Even though in this scheme, the accuracy of DoS is compromised whenever f is scaled to a higher value, it has the distinct advantage of driving the system out of local energy minima in doing so. The comparative graph between original and modified WL algorithms is shown in figure 5.18. The figure shows the updation scheme of modification factor f in the two algorithms.

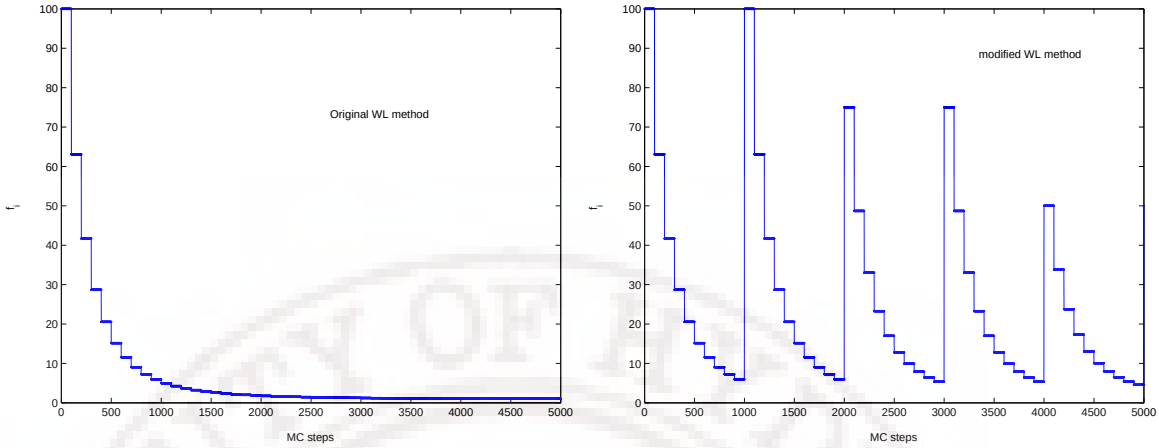

Figure 3.4 Updation schemes of f for original and modified WL algorithms respectively

3.3.3 Results and Discussion

Figure 3.5 represents the logarithm of density of states $log(g(E)) = \alpha(E)$ obtained after each WL run as a function of energy for a system of size, $L = 12$. From the figure, it is clear that as the iteration index increases from one WL run to another, the span in energy range increases. The increase in energy span is more for the initial stages and decreases gradually as $g(E)$ converges to the true DoS. The accumulation of $g(E)$ in later stages is very less and helps only in smoothening the DoS by removing any remaining discontinuities. This smoothening run is essential for achieving the desired accuracy of DoS, since large discontinuus deviations are introduced in the initial stages of modification protocol. As the system size increases further, the DoS becomes steeper making the low energy microstates relatively that much less probable and hence requires higher number of WL runs at different stages. The initial values f_0 should also be larger in order to drive the system towards low probable regions.

We calcuate orientational order parameter averaged over canonical ensemble of microstates, $\langle S \rangle$ at various temperatures. The resolution in temperatures for all the macroscopic quantities is chosen to be 0.001. The advantage of WL algorithm over

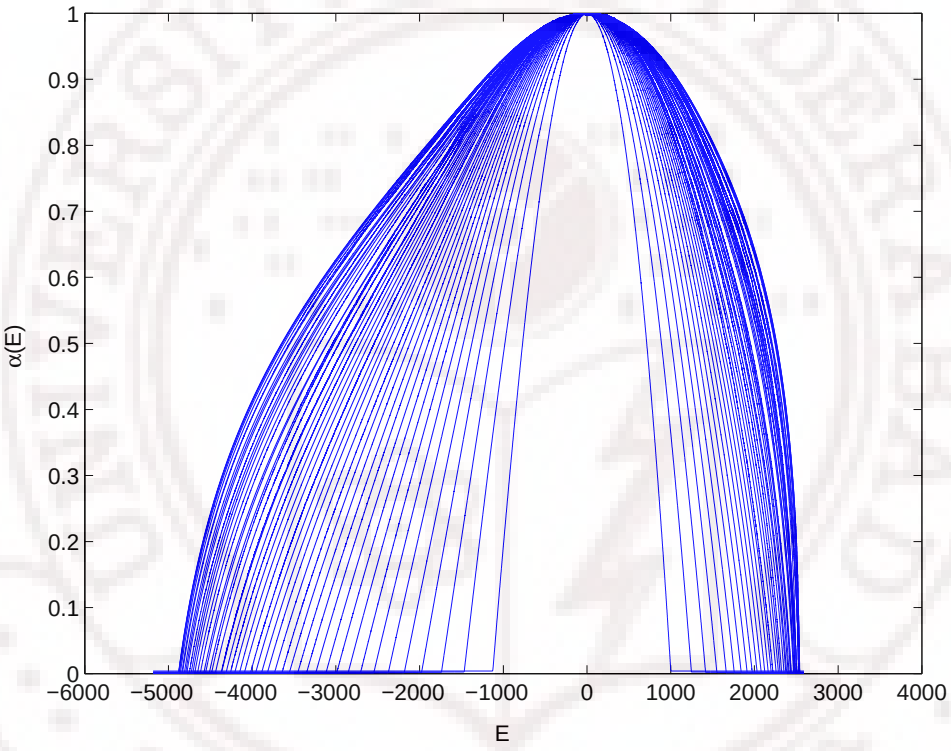

Figure 3.5 Logarithm of DoS plotted against energy, after every WL run for a cubic system of size, $L = 12$

canonical simulations lies in being able to calculate all the thermodynamic observables at any desired resolution of temperature simultaneously. Figures 3.6 and 3.7 represent specific heat and Binder's cumulant for various lattice sizes, L=4, 6, 8, 10 and 12, respectively. We observe that for L = 4 and 6 the transition is not sharp due to the finite size effects. But as the size of the system increases, we find that the specific heat profiles become sharper. The transition temperature (T_{NI}) obtained from the peak value of specific heat $T_{NI} = 1.126 \pm 0.005$ for a system of size $L = 12$ confirms with the earlier experimental and numerical results [43, 44].

Figure 3.8 represents the free energy profiles generated during the simulation for L=12. The three curves represent the profiles below, at and above the transition temperature, T_{NI} respectively. It can be observed that exactly at the transition, i.e., when both the ordered and disordered phases have equal probability, the two minima are separated by a free-energy barrier. For temperatures below and above T_{NI} the respective ordered or disordered phase is more probable. From the free-energy profiles, we deduce that the transition is first order. Figure 3.9 represents the scaling behaviour of transition temperatures, T_{NI} obtained from specific heat profiles, nematic susceptibility and Binder's cumulant profiles.

3.4 Further improvements and modifications of WL method

An important concern connected with the application of WL algorithm to even moderately large systems is that one has to sample extremely large number of microstates in the phase space to be able to span the desired energy range which may turn out to be prohibitively expensive in terms of the computational effort needed. To overcome this problem, in the original WL algorithm [1] and in several subsequent

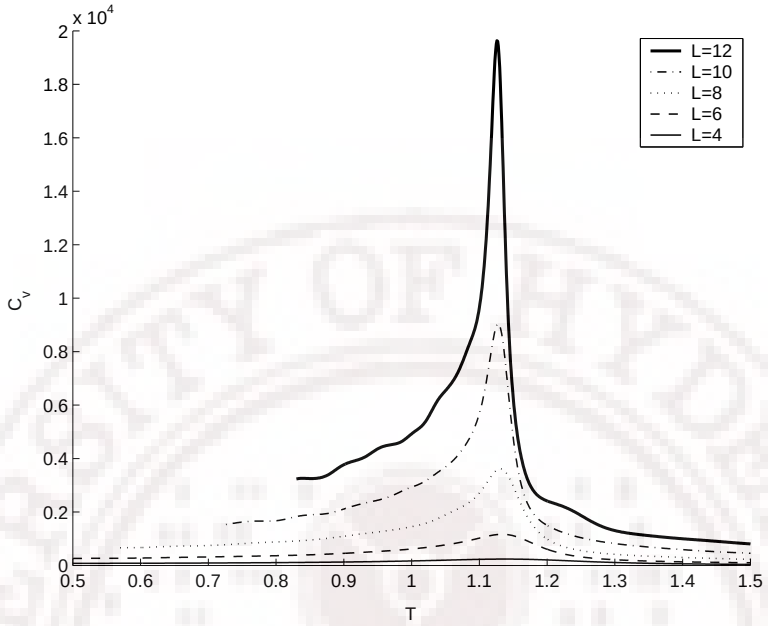

Figure 3.6 Specific heat profiles for a liquid crystal system of linear sizes L= 4, 6. 8, 10 and 12

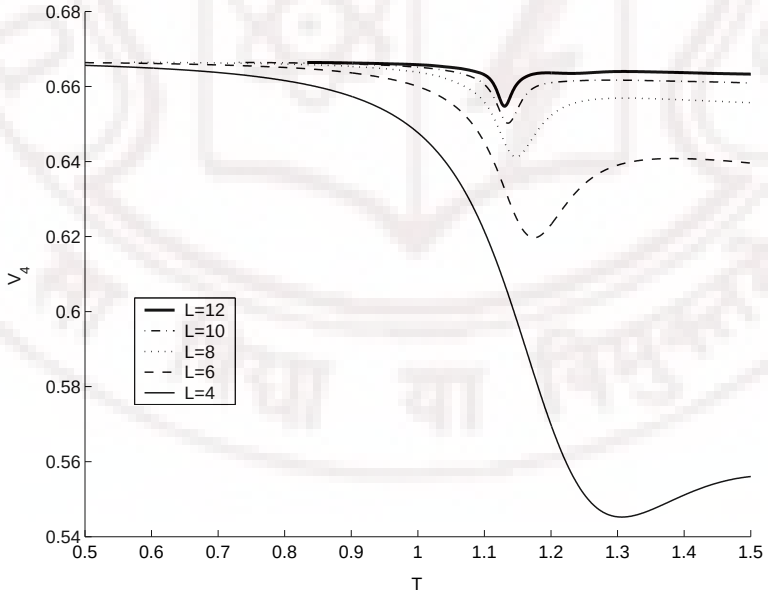

Figure 3.7 Binder's cumulant profiles for liquid crystal system of linear sizes L= 4, 6. 8, 10 and 12

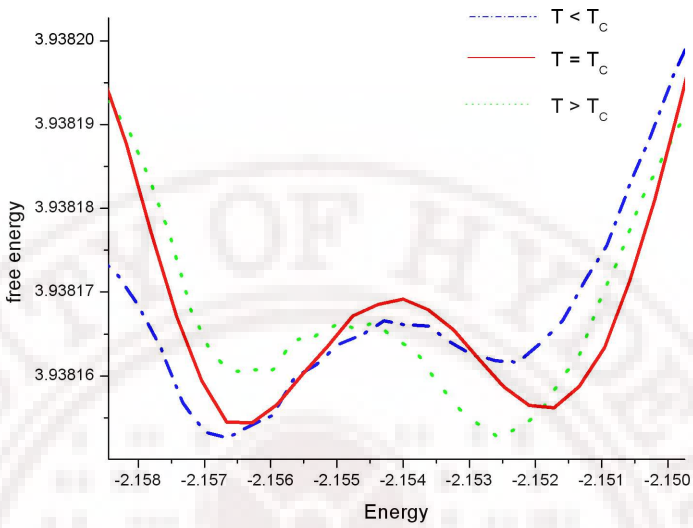

Figure 3.8 Free energy profiles below, at and above the T_{NI} for liquid crystal system of linear size, L= 12

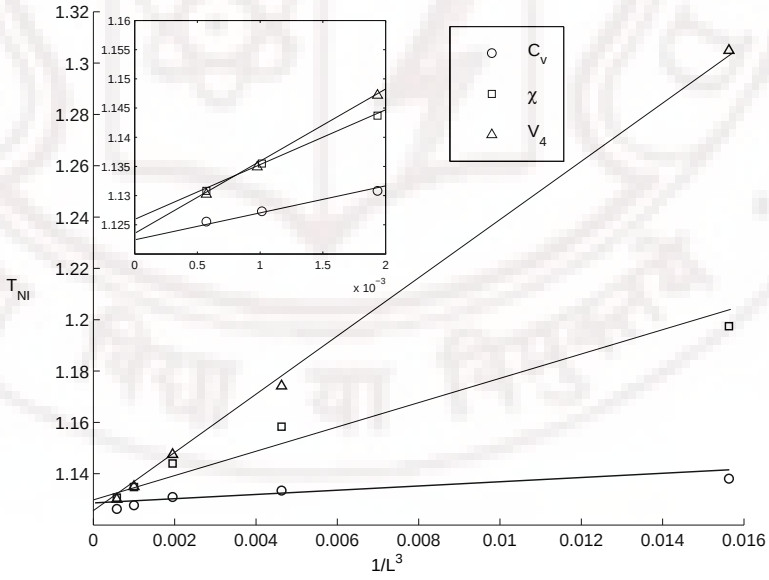

Figure 3.9 Transition temperatures from specific heat, susceptibility and binder's cumulant versus $1/L^3$ for liquid crystal system of linear sizes

studies [4, 8, 27, 29, 37, 38, 45–48], it was suggested to divide the desired energy range into a number of sub-regions and perform the WL algorithm in each energy window independently to speed-up the simulation. Each sub-region is simulated in different processors and the resulting $g(E)$ is appropriately combined together to get the final DoS. But by restricting the random walk to a sub-energy region, the states tend to get accumulated near the right edge of the energy range (corresponding to the higher energy side) and give rise to systematic errors [1]. To reduce these so-called edge effects, Schulz *et.al.* [49] have suggested to update $g(E)$ and the energy histogram, $H(E)$ even when the trial Monte Carlo step is rejected. Moreover, in continuous systems, it is observed that during the updation of $g(E)$, more number of Monte Carlo steps are utilized in sampling already explored energy range, while, only a fraction of that number is used in extending $g(E)$ to unexplored regions. An innovative way of updating $g(E)$ is given in [29] wherein $g(E)$ is updated by a continuous global update function till the values of $g(E)$ satisfies a pre-defined cut-off criterion, and then local updates are performed over the cut-off region (referred to as frontier). This in essence forces the system to sample from the energy regions beyond the frontier, corresponding to less visited configurational space. This global update process, conveniently referred to as *frontier sampling* hereafter, is discussed in detail in the subsequent sections.

More often one needs to study the phase transitions exhibited by a system as a function of more than one parameter. This is essential when one has to investigate the system near triple points or tricritical points. Simulation of multi-dimensional DoS and hence obtaining free-energy as a function of two or more parameters simultaneously is appealing since all the information is obtained from a single simulation. For example, DoS can be obtained as a function of energy and magnetization in magnetic systems like Heisenberg model [28, 29], energy and reaction-coordinate or the

end-to-end distance in protein models [29], energy and volume while investigating solid-liquid equilibria [27], energy and number of particles in simulation of fluids [9], *etc.* However, calculation of such joint DoS for continuous systems is computationally very challenging and also gives rise to several numerical issues. Therefore such methods have to be restricted to small systems [8, 48] or a carefully chosen small region in the parameter space [9, 10, 27]. Less costly alternative methods have been introduced, *e.g.,* EXEDOS [3–5], which restricts the simulation at a fixed temperature in place of at a fixed external force field. In the present work, we have generated a multi-dimensional DoS as a function of orientational order and elastic strain while investigating the nematic-isotropic transition in liquid crystal elastomers which will be discussed in detail in Chapter 3.

The DoS $g(x)$ is a continuous function (in the case of a system of any size with a continuus MC step, or even in system with a discrete MC step of sufficiently large size) and the simple binning scheme used in the above-mentioned procedure effectively approximates $g(x)$ with a piece-wise constant function. By using sufficient number of bins, as discussed above, this method can be made to work satisfactorily for smaller systems [28]. However, for larger systems and particularly while generating joint density of states, this scheme results in an excessively large number of bins to sample. This can be avoided to a certain extent by using linear interpolation among neighbouring bins [8]. Updating the g-function with a continuous kernel function [29, 51, 52] seems to be consistent with the continuous nature of $g(x)$. Moreover, in the *frontier sampling* method [29], the continuous function, $g(x)$ is updated by two alternate cycles of global and local updates, which force the system towards lower energy regions and prohibit it from visiting the higher energy regions repeatedly. This kind of algorithmic guidance is very essential to simulate systems of reasonable size as the slope of the $g(x)$ becomes progressively steeper as the system size increases,

and the disparity between the relative probabilities of lower and higher energy regions becomes significantly large. In the present study, we have adapted the frontier sampling method [29] and applied it to certain complex liquid crystal systems like confined liquid crystals in various geometries, liquid crystal elastomers, etc, which will be discussed in the subsequent chapters. In the next section, the improved WL algorithm based on *frontier sampling* method is discussed in detail. This is then applied to bulk liquid crystal system and liquid crystals confined to porous media to test the efficiency of the algorithm and to validate the results so obtained by comparing them with earlier known data.

3.5 *Frontier Sampling* based WL algorithm

3.5.1 *Frontier Sampling* method

In the *frontier sampling* method [29], the function $w(x)$ which is equivalent to logarithm of $g(x)$ is updated by a Gaussian kernel function, $k(x) \geq 0$, where $k(x) = exp(-|x|^2)$ as shown below:

$$w(x) \rightarrow w(x) + \gamma k((x - x_0)/\delta) \tag{3.2}$$

where γ and δ are scaling parameters to adjust the height and width of the Gaussian kernel, respectively. According to the above equation, the function $w(x)$ is updated by the Gaussian, whenever random walker arrives in the bin with parameter value, x_0. The acceptance probability is expressed as

$$A = min\,(1, exp[ln\alpha[w(x_i) - w(x_f)]])\,. \tag{3.3}$$

Here, a constant $ln\alpha$ was inserted so that $w(x)$ converges to $log_\alpha g(x)$. Hence, in this method, instead of a single modification factor, f we have a triplet (α, γ, δ) for

updating the function $w(x)$. In [29], the authors have chosen the values of 0.0001 to 0.01 for γ, and 1/200 of energy or magnetization width for δ. During the simulation, δ and α values are not changed. In order to force the random walker to sample the unexplored regions, a global update function is defined. Whenever the values of $w(x) \geq \kappa$ for some value of x in the already explored region, it is updated with a global update function given by:

$$w_T(x) \rightarrow w_T(x) + kexp\left[\frac{-\lambda}{w_T(x) - \kappa}\right]\Theta(w_T(x) - \kappa) \tag{3.4}$$

where, $w_T(x)$ represents the values of $w(x)$ in the region T. From the above equation, we notice that as $w_T(x) \geq \kappa$, the value of $w_T(x)$ is shifted up by an amount k and the exponential function removes the resultant discontinuity. Hence, the simulation is essentially divided into two stages:

1. **Accumulation stage:** Initialise $w(x) = 0$ and perform WL runs with the local updates given by eqn 3.2. As soon as $w(x) \geq \kappa$ for some x, global update is applied eqn 3.4 and accumulation is continued with the local updates eqn 3.2. $w_T(x)$ initially accumulates on the boundary of region T and then extends inside the region T uniformly. Once the uniform growth starts inside this region global update is again applied.

2. **Refining stage:** Once the region T spreads over the entire region of interest, then we continue the simulation with only local updates eqn 3.2 untill uniform growth of $w_T(x)$ is observed in the entire region. The $w(x)$ can be refined further by reducing the value of γ and by following the above two steps at this stage.

The cycle representing the global update and immeadiate local updates at the frontier is as shown in the figure 3.10, [29].

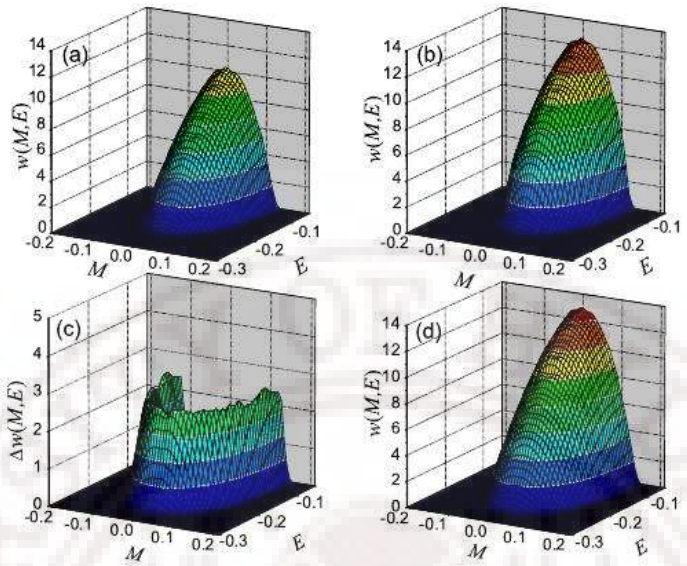

Figure 3.10 Cycle of simulation with global update. (a) original $w_T(x)$, (b) after the global update, (c) the increment at the frontiers at the begining of the accumulation stage and (d) sum of all the above three as seen at the end of the cycle (courtesy: C. Zhou *et. al.,* [29]).

3.5.2 Modifications to the *frontier sampling* method

Our objective now is to adapt the *frontier* sampling method described in the earlier section to study liquid crystal systems, since this shows promise to force the system to span the low energy regions also with an innovative algorithmic guidance scheme. We have modified the algorithm so as to make it work satisfactorily for lattice models of liquid crystals. In [29], the cut-off in the $w_T(x)$ is chosen at a point on the energy axis, where $w_T(x) \geq \kappa$ and all $w(x)$ to the higher energy side (T region) are boosted with a positive value. In the present work, we have chosen the criterion for this frontier depending on the difference in values of $w_T(x)$ accumulated in two successive runs. We made use of the fact that the difference (as a function of x) between values of $w_T(x)$ from two consecutive runs will be nearly uniform if the system has already sampled the T region adequately (thereby making the DoS there nearly accurate).

Extent of such uniform region is a logical basis for defining a frontier, so as to force the system to sample away from the T region in the next iteration in the frontier sampling scheme. Initially, the system will have more tendency to sample the higher entropic regions which in our case is in isotropic phase with energies nearer to zero. So, initially the cutoff is chosen as 95% of the difference in $w_T(x)$ values in the first two runs at the bin with the highest allowed energy value. The corresponding bin number is the so-called frontier. The system is allowed to perform random walk in the usual manner and the difference in the values of $w_T(x)$ is calculated after every two iterations. This difference is compared with the earlier cut-off value. A new frontier (extending to lower energy regions) is defined whenever the above criterion leads to expansion of the T-region. In other words, as more and more higher entropic regions are adequately sampled, the frontier is moved correspondingly to lower energy regions, so as to make the system sample beyond the frontier through the updating procedures described above. This corresponds to boosting all the values of $g(E)$ towards right side of the frontier by a positive value. As the Monte Carlo runs proceed further, the frontier shifts towards lower entropic regions. This procedure is repeated till the entire energy range is sampled. The global update function in our algorithm is given by:

$$w_T(x) \rightarrow w_T(x) + k\Theta(w_T(x) - \kappa) \tag{3.5}$$

The values of γ and δ are not kept constant during the simulation. We find it profitable to reduce these values progressively as the iterations proceed. Once $w_T(x)$ covers the entire energy range, a long smoothening run is performed with very low values of γ and δ to remove discontinuities that would have naturally crept in due to the global update process. Moreover, in our simulation the scale parameters are restricted to two (γ, δ) (eqn 3.2). The acceptance probability is accordingly given by:

$$A = min\,(1, exp[ln[w(x_i) - w(x_f)]]) \tag{3.6}$$

3.5.3 Details of the simulation

We initialise the cubic lattice (size L) of liquid crystal system with random configuration of headless spins. The interactions between the spins is given by Lebwohl-Lasher potential and restricted to nearest neighbours. We performed simulations on lattices of sizes upto L=25. The energy range is divided into N number of bins. On a Woodcrest processor operating at 3.0GHz, the simulation on a $L = 20$ lattice takes about 30 hrs. Orientation of each spin is randomly changed either by choosing spin site randomly, or in a typer-writer fashion. The acceptance probability is given by eqn 3.6. Once a Monte Carlo sweep (MCS) is completed which consists of L^3 Monte Carlo steps, the value of $\xi_i = log(w(i))$ is updated with a Gaussian kernel function:

$$\xi(i) \rightarrow \xi(i) + \gamma exp\left(\frac{|x - x_0|}{\delta}\right)^2. \tag{3.7}$$

We have taken initial values of (γ, δ) as $(1.0, 100)$. After every 100 MCS, the value of γ is reduced $\gamma \rightarrow 0.95\gamma$. This updation of γ is continued until it reaches a preset minimum value (typically 0.001). We call this entire computation as one iteration. After every two successive iterations, we calculate the difference between the updated values of ξ as a function of bin number. Initially, the cut-off bin number is chosen as that corresponding to 95% of the difference, $\xi^k(i) - \xi^{k-1}(i)$, where k is the iteration index, and the bin index, i corresponds to the highest energy of interest, typically zero with LL potential. Once a frontier is defined as the cut-off bin value so defined, the algorithm continues the process of iterations, each time looking for two successive iterations yielding for a lower cut off bin number (i.e., lower energy bin). If a cut-off value is found which is lower than the current one, a new frontier is defined at this latest value and the entire process in search of another new frontier continues. In terms of the algorithm the following steps are followed. We check if there is any other bin j in the lower energy range at which the difference is greater than the

cut-off. If it is so, we reset the cut-off to 95% of $\xi^k(j) - \xi^{k-1}(j)$. This sets the frontier as the bin j above which there is an uniform growth of $\xi_T(x)\ \forall\ x = j, N$. Now we boost the values of $\xi_T(x)$ which are present towards right side of j. This introduces a high entropic barrier for the random walker to enter the higher energy regions. So there is an accumulation of states near the frontier till the height becomes equal to the boosted area. Consequently, the area of the explored region extends towards lower energy region. We perform this simulation untill $\xi_T(x)$ covers the entire energy range. After $\xi_T(x)$ covers the desired energy range, a long smoothening run is performed with initial values of (γ, δ) set to $(0.01, 0.0001)$. The value of γ is progressively reduced during this part of the simulation until it reaches a low value of $\approx 10^{-4}$. This ensures that the discontinuities in DoS introduced artificially during the global updation are eventually minimized, and ξ converges to its asymptotic value.The final ξ is then used to generate a large non-Boltzmann ensemble from which the relevant thermodynamic observables are extracted using unweighting-reweighting techniques, as described earlier. As in our earlier modified version of WL algorithm discussed in section 3.3, we have performed the above simulation also on log-log scale to minimize computational errors. In between the neighbouring bins, linear interpolation is performed to calculate acceptance probabilities.

It is observed that the speed up in the computational time employing this algorithm is about ten times compared to the earlier versions of WL algorithm (without frontier sampling). We now apply the modified *frontier sampling* method to bulk liquid crystal systems and a more realistic liquid crystal system confined to porous medium, and present the results in the subsequent sections. The latter system serves as a bench mark to test the applicability of the modified version of *frontier sampling* method to simulate complex systems with possible rich free-energy landscapes. The subsequent Chapters present the application of this method to other complex systems

like liquid crysal elastomers, liquid crystals in contact with geometrical and chemical patterned sustrates, *etc.*

3.5.4 Application to bulk liquid crystals

We have applied the modified version of *frontier sampling* method to study nematic-isotropic phase transition in bulk liquid crystals. Figure 3.11 shows the logarithm of entropy $\xi(x)$ as a function of energy per particle for a cubic lattice of size, $L = 20$. The figure on the right hand side depicts the energy histogram $H(E)$. We observe that the histogram is not as flat as is expected from simulations on discrete systems. But typically the minimum number of microstates in any of the bins is about 5×10^5 which ensures that any canonical ensemble extracted have at least these many microstates. is reasonably good for bulk liquid crystal systems. We stipulate that sampling of microstates is reasonably good if we obtain similar energy histograms when we repeat the same simulation with different random seeds. One can improve the accuracy of the results by concatenating the microstates obtained from two or more simulations with different random seeds and extracting the thermodynamic observables from this larger concatenated ensemble. Figure 3.12 shows the thermodynamic observables like energy, order parameter, nematic susceptibility, Binder's cumulant and specific heat, in clock-wise order, obtained from the simulation. The transition temperature obtained from the position of specific heat peak is about 1.124 ± 0.001, which is in good agreement with the earlier results.

3.5.5 Application to liquid crystals confined to porous media

Liquid crystals confined to porous media make a very interesting study due to its technological as well as academic importance [54, 55]. A porous medium with a

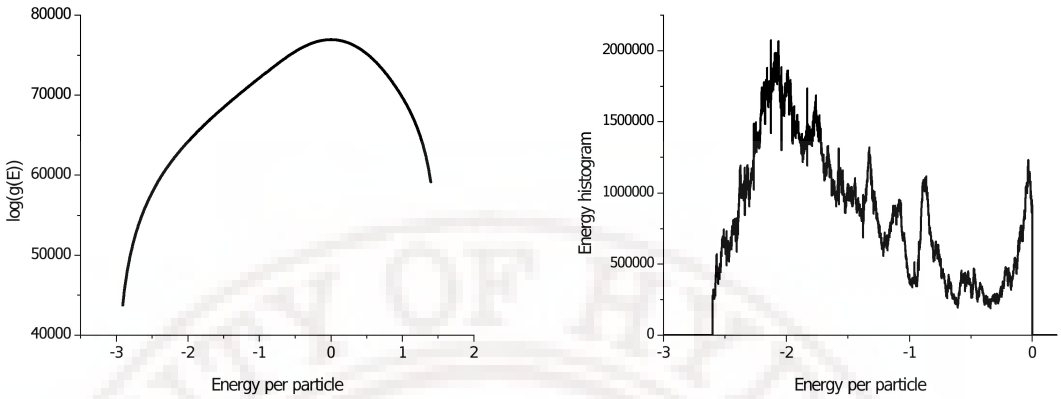

Figure 3.11 Density of States and energy histogram for $L = 20$

random network of interconnected pores of random sizes and shapes provides a simple confining medium. The size of the pores, the geometry and connectivity of the pores influence the nature of the phase transition. Many attempts were made earlier to understand the effect of pore size on the phase transitions of liquid crystals both experimentally and using computer simulations [54–57]. Confinement of any system in a porous matrix can be modelled in one of the following ways:

- construction of an independent pore with different rigid boundary conditions and director configurations [58],
- Potts spin models with the porous medium approximated by the diffusion-limited cluster-cluster aggregate [59],
- random field Ising models [60],
- random anisotropy nematic models [61]
- introduction of quenched random disorder into the system (also called dilution) [62]

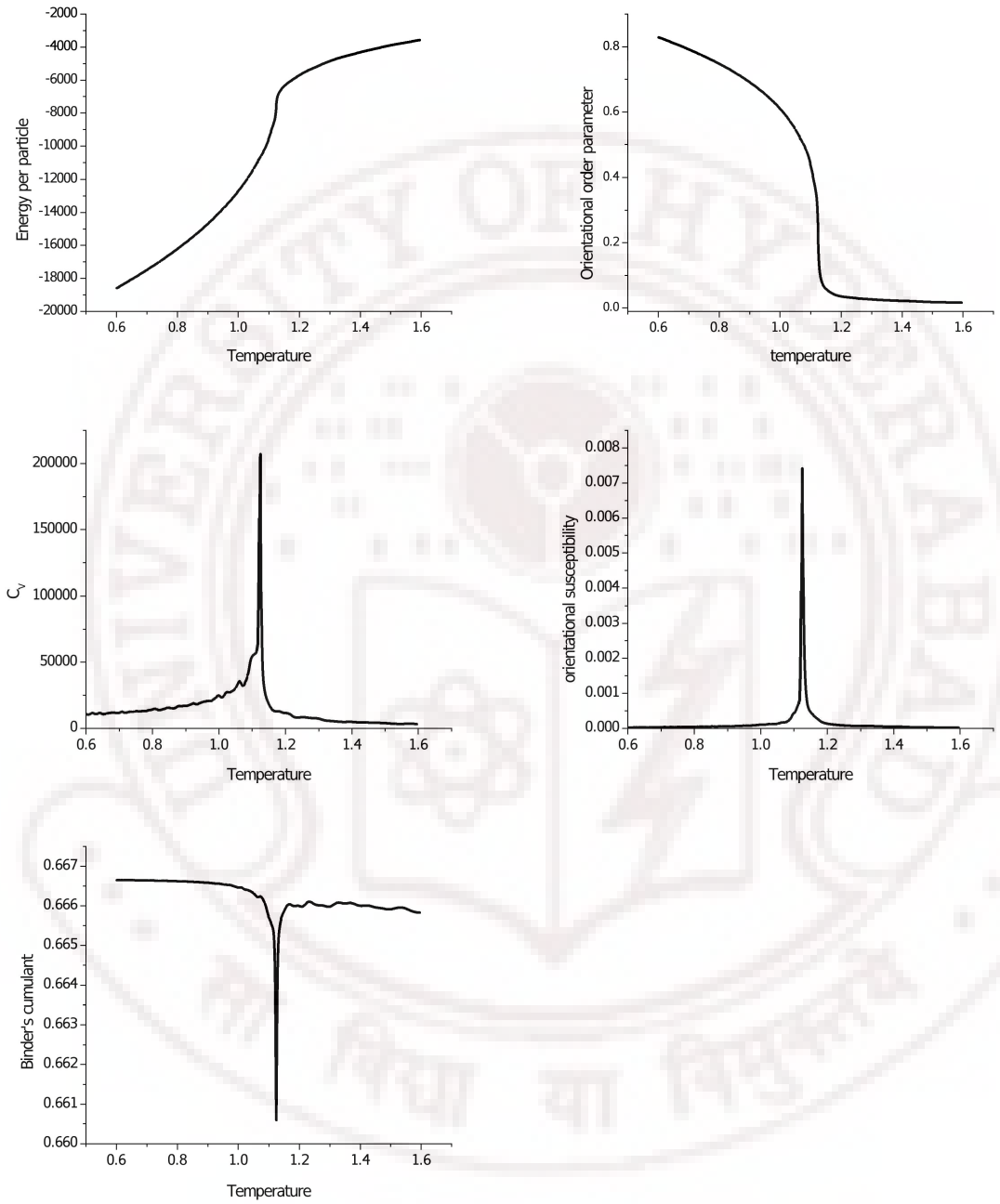

Figure 3.12 Energy, Orientational order parameter, Specific heat, Orientational susceptibility and Binder's fourth cumulant profiles versus temperature for a liquid crystal system of linear size, $L = 20$.

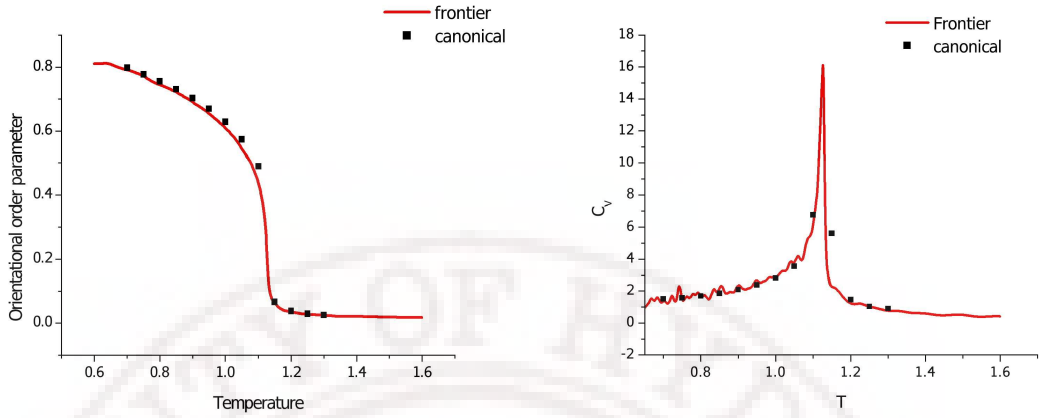

Figure 3.13 Orientational order parameter (left) and Specific heat (right) obtained from *frontier sampling* method (red lines) and canonical simulations (black squares) respectively versus temperature for a liquid crystal system of linear size $L = 20$. Results from *frontier sampling* method tally well with the canonical results.

In the present study, we attempt to investigate the effect of porous medium as modelled by the introduction of quenched random disorder (QRD) on the nature of phase transition using our modified *frontier sampling* method.

Recently a phenomenological model has been proposed to describe the number of quenched random disorders, N_d to be introduced in the liquid crystal system to mimick effectively a system confined in a porous medium. This value N_d is expressed in terms of actual pore size (d), the system size (L) and volume occupied by each liquid crystal molecule (v) [53]. The relation between the pore size and the number of quenched disorders is proposed as:

$$N_d(L, d, v) = \frac{L^3}{d}\left(\frac{v}{36\pi}\right)^{\frac{1}{3}}. \tag{3.8}$$

Based on this prescription, canonical simulations were performed to study the effect of the pore size on the nature of NI transition by introducing appropriate amount of QRD and a lattice model based on Lebwohl-Lasher potential is used. It was observed that the transition temperature, T_{NI} decreases as the pore size is

reduced and the shift in the T_{NI} agrees well with the experimental findings proving the validity of the model. But it is to be appreciated that QRD introduces several minima in the free energy surface of the system, thereby making it in principle difficult for canonical sampling methods to sample the energy landscape comprehensively, more so, when a first order transition occurs in the system. In the present study we have applied the modified *frontier sampling* method to systematically study the effect of QRD on the nematic-isotropic phase transition. We considered a range of pore sizes from $1200A$ to $25A$, and chose a cubic lattice of size, $L = 20$.The variation of orientational order parameter S, orientational susceptibility χ and average energy E with the increasing amount of disorder is shown in the figure 3.14. The figures confirm the earlier observations of the shift in T_{NI} towards lower temperatures with the increase in disorder as observed from the canonical simulations. The transition temperatures T_{NI} obtained from the location of the peaks of C_V and χ profiles are plotted against the pore size d in the figure 3.15. The variation of T_{NI} as obtained from the two response functions are comparable, and agrees well with the predictions from the earlier work [53]. It may be noted in this context that the computational effort needed in the WL procedure is significantly small when compared to canonical methods with similar temperature resolution. The common feature between these two methods in the context of this system is that, as QRD is increased, both the procedures demand correspondingly more effort, owing to the complexity introduced in the free energy profile. This, in entropic sampling procedure translates to a very long learning time for the DoS to converge.

Based on the comparison of results of canonical and entropic sampling methods as shown in figure 3.13, as well as on the satisfactory results obtained on progressively introducing QRD into the system, application of the entropic method to LC system, based on the WL algorithm (aided by frontier sampling technique) thus appears

to stand validated. While being able to handle moderately large sizes, it scores over the canonical sampling procedure, as was noted earlier. We take advantage of these features to investigate LC systems, and report these results in the subsequent chapters.

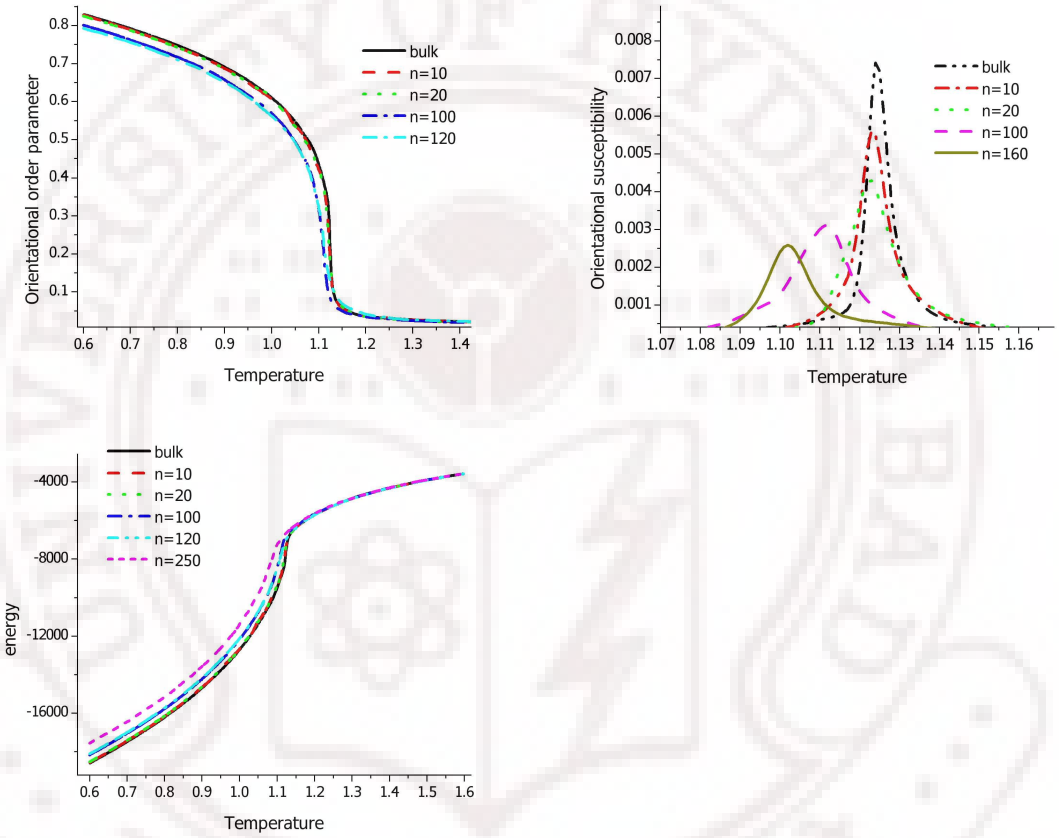

Figure 3.14 Variation of orientational order parameter, susceptibility and energy with temperature for pore sizes $d = 0,\ 10,\ 20,\ 100$ and 160 respectively, for a liquid crystal system of linear size, $L = 20$.

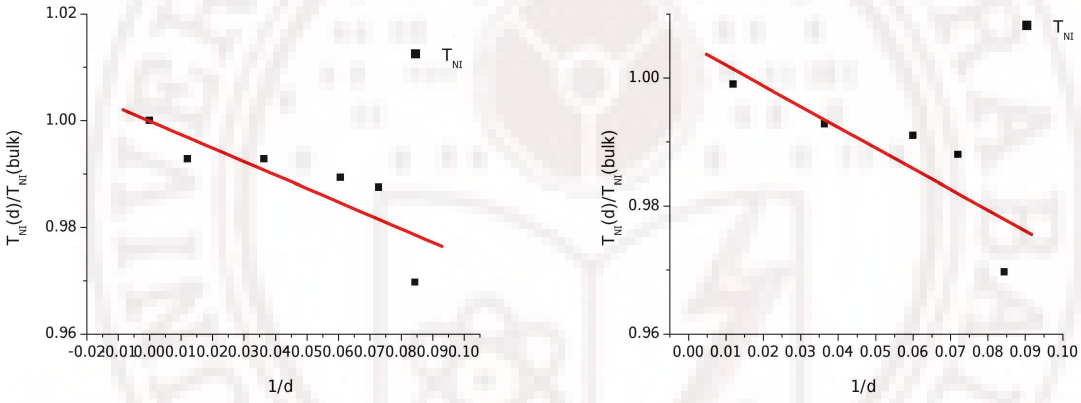

Figure 3.15 Variation of normalized T_{NI} with respect to (inverse) pore size obtained from specific heat peaks (left) and orientational susceptibility peaks (right) respectively, for a liquid crystal system of linear size, $L = 20$. The solid lines are best fit straight lines.

Bibliography

[1] F. Wang, and D. P. Landau, *Phys. Rev. Lett.* **86** 2050 (2001); F. Wang and D. P. Landau, *Phys. Rev. E.* **64** 056101 (2001).

[2] P. A. Lebwohl and G. Lasher, *Phys. Rev. A* **6**, 426 (1972).

[3] N. Rathore and J. J. de Pablo, *J. Chem. Phys* **116** 16, (2002).

[4] N. Rathore, T. A. Knotts IV and J. J. de Pablo, *J. Chem. Phys* **118** 9 (2003); N. Rathore, T. A. Knotts IV and J. J. de Pablo, *Biophysical J* **85** 3963-3968 (2003).

[5] N. Rathore, Q. Yan and J. J. de Pablo, *J. Chem. Phys* **120** , 12 (2004).

[6] C. Junghans and U. H. E. Hansmann, *Int. J. Mod. Phys. C* **17**, 817 (2006).

[7] F. Liang, *J. Chem. Phys* **120**, 14 (2004).

[8] M. S. Shell, P. G. Debenedetti and A. Z. Panagiotopoulos, *Phys. Rev. E.* **66**, 056703 (2002).

[9] Q. Yan, R. Faller and J. J. de Pablo, *J. Chem. Phys.* **116** 20 (2002).

[10] Q. Yan and J. J. de Pablo, *Phys. Rev. Lett.* **90** 035701 (2003).

[11] M. Chopra, M. Muller and J. J. de Pablo, *J. Chem. Phys* **124** 134102 (2006).

[12] M. Chopra and J. J. de Pablo, *J. Chem. Phys* 114102 (2006).

[13] D. T. Seaton, S. J. Mithcell and D. P. Landau, *Braz. J. Phys* **38** 48-53 (2008).

[14] P. Poulain, F. Calvo, *et. al*, *Phys. Rev. E*, **73**, 056704 (2006).

[15] M. Scott Shell, Pablo G. Debenedetti, and Athanassios Z. Panagiotopoulos, *J. Chem. Phys* **119**, 18, 9406-9411 (2003).

[16] T. E. Bogdan and D. J. Wales, *J. Chem. Phys* **120**, 23, 11090-11099 (2004).

[17] F. Calvo and P. Parneix, *J. Chem. Phys* **119**, 1, 256-264 (2003).

[18] G. Ganzenmller and P. J. Camp, *J. Chem. Phys* **127**, 154504 (2007).

[19] J. Kim, J. E. Straub, and T. Keyes, *Phys. Rev. Lett* bf 97, 050601 (2006).

[20] T. J. H. Vlugt, *Mol. Phys* **100**, 17, 2763-2771 (2002).

[21] D. Antypov and J. A. Elliott, *Macromolecules* **41**, 7243-7250 (2008).

[22] V. Varshney and G. A. Carri, *Phys. Rev. Lett* **95**, 168304 (2005).

[23] D. F. Parsons and D. R. M. Williams, *J. Chem. Phys* **124** 221103 (2006).

[24] D. F. Parsons and D. R. M. Williams, *Phys. Rev. E.* **74** 041804 (2006).

[25] E. B. Kim, R. Faller, *et. al J. Chem. Phys* **117**, 16 (2002).

[26] R. Faller and J. J. de Pablo, *J. Chem. Phys* **119**, 8 (2003).

[27] Ethan A. Mastny and Juan J. de Pablo, *J. Chem. Phys* **122**, 124109 (2005).

[28] G. Brown and T. C. Schuthess, *J. Appl. Phys.* **97** 10E303 (2005).

[29] C. Zhou, T. C. Schulthess, S. Torbrugge, and D. P. Landau, *Phys. Rev. Lett.* **96**, 120201 (2006).

[30] S. Sinha and S. K. Roy, *Phys. Lett. A* **373**, 308-314 (2009).

[31] D. Jayasri, 'Wang-Landau Monte Carlo study of nematic-isotropic phase transitions in liquid crystals', *submitted to University of Hyderabad* (2004); D. Jayasri, V. S. S. Sastry and K. P. N. Murthy, *Wang-Landau Monte Carlo simulation of nematic-isotropic transition under confinement*, 22nd International Conference on Statistical Physics, Bangalore, July 4-9, 2004.

[32] D. Jayasri, V. S. S. Sastry and K. P. N. Murthy, *Phys. Rev. E.* **72**, 036702 (2005). P. Poulain, F. Calvo, et. al., *Phys. Rev. E.* **73** 056704 (2006).

[33] M. S. Shell, P. G. Debenedetti and A. Z. Panagiotopoulos, *J. Phys. Chem.* **108**, 19748 (2004).

[34] C. Zhou and R. N. Bhatt, *Phys. Rev. E* **72**, 025701 (R) (2005).

[35] P. Dayal, S. Trebst, S. Wessel, *et. al.*, *Phys. Rev. Lett.* **92**, 097201 (2004).

[36] H. K. Lee, Y. Okabe and D. P. Landau, *Comp. Phys. Comm* **175**, 1, 36-40 (2006).

[37] T. Surungan, Y. Okabe and Y. Tomita, *J. Phys. A: Math Gen.* **37**, 4219-4230 (2004).

[38] T. S. Jain and J. J. de Pablo, *J. Chem. Phys.* **116**, 16, 7238-7243 (2002).

[39] J. V. Selinger and B. R. Ratna, *Phys. Rev. E.* **70**, 041707 (2004).

[40] P. Pasini, G. Skacej and C. Zanoni, *Chem. Phys. Lett.* **413**, 463 (2005).

[41] J. A. Barker and R. O. Watts, *Chem. Phys. Lett.* **3**, 144 (1969).

[42] B. A. Berg, cond-mat/0206333 (unpublished).

[43] U. Fabbri and C. Zannoni, *Mol. Phys.* **58**, 763 (1986).

[44] N. V. Preizjev and R. A. Pelcovits, *Phys. Rev. E* **63**,062702 (2001).

[45] Shan-Ho. Tsai and D. P. Landau, *Am. J. Phys.* **76**, 4 & 5 (2008).

[46] D. P. Landau and F. Wang, *Comp. Phys. Comm.* bf 147, 674-677 (2002).

[47] Shan-Ho. Tsai, F. Wang and D. P. Landau, *Braz. J. Phys.* **38**, 1 (2008).

[48] D. P. Landau, Shan-Ho. Tsai and M. Exler, *Am. J. Phys.* **72**, 10 (2004).

[49] B. J. Schulz, K. Binder, M. Muller and D. P. Landau, *Phys. Rev. E.* **67**, 067102 (2003).

[50] B. J. Schulz, K. Binder and M. Muller, *Int. J. Mod. Phys. C.* **13**, 4, 477-494 (2002).

[51] C. Micheletti, A. Laio and M. Parinello, *Phys. Rev. Lett.* **92**, 170601 (2004).

[52] Y. D. Wu, J. D. Schmitt and R. Car, *J. Chem. Phys.* **121**, 1193 (2004).

[53] K. Venu, V. S. S. Sastry and K. P. N. Murthy, *Europhys. Phys. Lett.* **58**, 646 (2002).

[54] G. P. Crawford and S. Zumer (Editors), *Liquid Crystals in Complex Geometries formed by Polymer and Porous Networks* Taylor and Francis, London (1996).

[55] P. Pasini, C. Chiccoli and C. Zannoni, *Advances in Computer Simulations of Liquid Crystals*, edited by Pasini P. and Zannoni C. (Kluwer Academic Publishers, Dordrecht) 2000, p. 121, and the references cited therein.

[56] L. Wu, B. Zhou, *et. al. Phys. Rev. E*, **51**, 2157 (1995).

[57] A. Golemme, S.Zumer, D. W. Allender and J. W. Doane, *Phys. Rev. Lett.* **61**, 2937 (1988); G. S. Iannachione, G. P. Crawford, S. Zumer, J. W. Doane and D. Finotello, *Phys. Rev. Lett.* **71**, 2595 (1993).

[58] T. Bellini, C. Chiccoli, P. Pasini and C. Zannoni, *Phys. Rev. E* **54**, 2647 (1996); T. Bellini, C. Chiccoli, P. Pasini and C. Zannoni, *Mol. Cryst. Liq. Cryst.* **290**, 226 (1996).

[59] K. Uzelac, A. Hasmy and R. Jullien, *Phys. Rev. Lett.* **74**, 422 (1995).

[60] A. Maritan, M. Cieplak, T. Bellini and J. R. Banavar, *Phys. Rev. Lett.* **72**, 4113 (1994).

[61] M. D. Dadmun and M. Muthukumar, *J. Chem. Phys.* **97**, 578 (1992).

[62] J. Ilnytskyi, S. Sokolowski and O. Pizio, *Phys. Rev. E* **59**, 4161 (1999);R. Folk, Y. Holovatch and T. Yavors'kii, *Phys. Rev. B* **61**, 15114 (2000).

Chapter 4

Wang-Landau Monte Carlo simulation of nematic-isotropic transition in liquid crystal elastomers

4.1 Introduction

Nematic liquid crystals possess long-range orientational order, and hence elasticity associated with the deformations of that order. Rubbers are weakly-crosslinked polymers with very low shear modulus, μ. They can be deformed at practically constant volume and the deformations can be as large as 1000% [1, 2]. Both these materials inhabit the grey area between liquids and solids. In 1975, de Gennes [3] envisaged that the cross-linked polymers made of liquid crystals would lead to very fascinating properties due to the coupling between anisotropic properties of liquid crystals and the elastic properties of the rubbers. It was conjectured that spontaneous alignment

of constituent liquid crystal molecules at NI transition would lead to dramatic effects in stress-strain relation. Due to these extreme thermo-mechanical effects, these materials are considered to be good candidates to function as actuators in applications like artificial muscles, etc., [1, 3].

Fundamentally, irregular cross-links and chemical heterogeneity in a LCE network provide source of quenched random disorder [1, 4] similar to that observed in nematics with sprinkled silica nanoparticles [5, 6] or random anisotropy [7]. Consequently, LCE too, are characterized by a complex free energy landscape leading to glassy ordering ([37] and references therein). While in spin glassy systems quenched disorder can be overcome by a strong enough magnetic field, in LCE this can be achieved mechanically by stretching the sample [8]. LCE can be theoretically described in continuum description, by the neo-classical theory based on anisotropic rubber elasticity [1], by Ginzburg-Landau approaches [9, 15, 27], as well as by 2D modelling [10].

In liquid crystal elastomers, the cross-link density is a crucial parameter since it gives a measure of coupling between the NI transition in orientational parameter space to the elastic degrees of freedom. If the density is more, orientational order is frozen-in since the local mesogenic units are rigidly held at the cross-links. If the density is very less, elastomers behave like melts. The answer to the question as to how many cross-links are sufficient to transform a visco-elastic polymer melt into an elastomer (which is a solid) still remains unanswered [11, 12]. Moreover, as the cross-link density is increased, the transition temperature, T_{NI} increases with gradual smoothening of the order parameter variation from discontinuous to continuous transition, finally tending to a non-singular cross-over from ordered phase to disordered phase. The elastic energy response of the LCE's can be accounted for employing the continuum description which is a simple extension of the elastic theory of polymers. The rubber-elastic response to deformation of any polymer network stems from the entropy change

when the number of conformations allowed for the chains is reduced on stretching their end-to-end distance between the cross-links. According to the classical elastic theory of rubbers, the free energy due to the elongation of the polymer by an amount λ along one of the coordinate axes is given by:

$$F = \frac{1}{2}\mu\left(\lambda^2 + \frac{2}{\lambda}\right) \tag{4.1}$$

where μ is the shear modulus. Here, we have assumed incompressibility of volume of the system, and hence in undeformed state, $\lambda = 1$. In liquid crystal elastomers, the end-to-end distance distribution becomes anisotropic. The uniaxial anisotropy of polymer chains has a principal axis along the nematic director n. The ability of this principal axis to rotate independently under the influence of network strains makes the rubber-elastic response non-symmetric. Thus, we have

$$F_{el} = \frac{1}{2}\mu Tr(\lambda^T \cdot l_\theta^{-1} \cdot \lambda \cdot l_0) + \frac{1}{2}\tilde{B}(Det[\lambda] - 1)^2 \tag{4.2}$$

Here, l is the uniaxial matrix representing chain step length before (l_0) and after (l_θ) the director is rotated by an angle θ. The last term in the above equation 4.2 represents the contribution from bulk modulus $\tilde{B}$ ($(10^{10} - 10^{11} Jm^{-3})$), which is much greater than the shear modulus and independent of the chain conformations. This large energy penalty constrains the system to become physically incompressible. From these equations it is clear that the strain components will now have non-trivial effect on the system, in contrast to the isotropic rubbers. The uniqueness of nematic rubbers stems from the competing microscopic interactions and there exists two levels of characteristic length scales: one is the anisotropy on monomer (small) scale of nematic coherence length, while the strains are defined on a much greater length scale of polymer end-to-end chain length. This length scale seperation calls for the need to carry out multi-scale modelling to understand various underlying phenomena exhibited by liquid crystal elastomers.

4.2 NI transition in liquid crystal elastomers

Experimental observations on liquid crystal elastomers show that both the orientational order parameter and strain vary continuously at the nematic-isotropic transition [17, 18, 21, 22]. The NI transition is neither first-order nor continuous but rather a non-singular crossover from disordered to ordered phase [13–16]. There were several attempts to explain the nature of NI transition and study the effect of relevant factors like cross-link density, history of cross-linking, number of monomers present in between neighbouring crosslinks, monomer-monomer interaction strength, the coupling between the mesogenic units and the elastic degrees of freedom, etc., on the transition. Basically there are two radically different points of view to explain the underlying phenomena. First explanation is based on the effect of aligning stress on the transition. Unless special precautions are taken during the network fabrication, the low temperature phase of nematic elastomers is always an equilibrium polydomain director texture [23, 24]. This is in contrast with a kinetic 'polydomain' texture often referred to as Schilieren texture [25], which is the consequence of nuclueation and growth mismatch in a system undergoing the first-order transition [26]. LCE samples prepared during the Kupfer and Finkelmann's two-step procedure [8] involve imposing an aligning field above the critical value to align the polydomain sample with centres at crosslinks into a monodomain sample. According to the classical theory of phase transitions the behaviour of strain order parameter versus temperature is as shown in the figure 4.1.

There exists a critical stress below which the strain is discontinuous with respect to temperature. As the stress is increased beyond this critical value, the transition becomes continuous and softens gradually to super critical regime, where the strain varies continuously without any singularity as the temperature is varied. This aligning

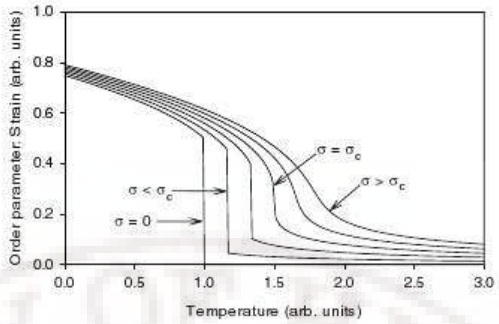

Figure 4.1 Prediction of strain parameter λ versus temperature in a homogeneous elastomer under and aligning stress σ. courtesy [27]

stress can be either due to the external aligning fields as in the Finkelmann's procedure or internal aligning fields due to the cross-links present in the anisotropic nematic medium.

In order to understand the underlying phenomena which causes the LCE systems to exhibit non-singular behaviour, Selinger, *et. al.*, [27] performed experiments and attempted Landau-like free energy expansion as a function of both strain and orientational order parameters to fit the data. They derived Landau's free energy in terms of orientational order parameter, S and elongation e in the presence of aligning stress, σ as shown below:

$$F = \frac{1}{2}\alpha'(T - T_0')S^2 - \frac{1}{3}b'S^3 + \frac{1}{4}c'S^4 - ueS - \sigma e + \frac{1}{2}\mu e^2 \tag{4.3}$$

where T is the temperature and σ is the effective stress which is a combination of applied stress and the internal stress due to anisotropic cross-linking. Averaging over S, we obtain free energy in terms of e alone

$$F = \frac{1}{2}\alpha(T - T_0)e^2 - \frac{1}{3}be^3 + \frac{1}{4}ce^4 - \sigma e. \tag{4.4}$$

The above equation is minimized over e and the resulting predictions are fitted with the experimental data. They found that the fits do not agree well with the experimental data at the transition temperatures, leading to their conclusion that the

experimental observations are not consistent with the super-critical evolution between isotropic and nematic phases. They thus consider, as a consequence, a heterogeneous model for the elastomer.

There can be two ways in which heterogeneties can be introduced in the system. The polymerization process and the crosslinks induce quenched disorder into the system. For example, polydispersity in the chain length gives one type of disorder. This may lead to distribution of regions with different nematic-isotropic transition temperatures. At any given temperature, a sample would have a coexistence of isotropic and nematic domains. As the temperature decreases, it would cross over from mostly isotropic to mostly nematic phase, leading to a smooth evolution in the average orientational order parameter and in the macroscopic strain. This is the so-called random bond disorder. Another scenario is that the cross-links act as sources of random disorder where the director orientations are quenched [4]. As the domain size near each cross-link could be different, this leads to a distribution of internal fields, -the so-called random field disorder. However, recent DNMR studies on LCE's [17, 18] sythesized using Finkelmann's cross-linking procedure showed signatures that supercritical behaviour is predominant with relatively low heterogeneity. As the cross-link density is increased, the nature of the phase transition changes from the first order type (subcritical) to continuous (at the critical point) and then to supercritical. This is also in agreement with the general result that quenched impurities destroy long-range order, first shown by Larkin [19] and then generalized by Imry and Ma [20].

In this context, two coarse grained lattice models were proposed recently [36, 37]. The first model (Model-I) [36], considers both random-bond and random-field disorders in the Hamiltonian, the main aim being study of the effect of such disorders on the NI transition using MC simulations. Here all the interactions including the anisotropic interactions between mesogenic units, energy contribution from elastic

degrees of freedom and the coupling between the two degrees of freedom, are incorporated in the Hamiltonian as energetic terms. The contribution from elastic degrees of freedom is derived from neo-classical rubber elasticity [1] described briefly above. However, in the absence of any heterogeneity and with the particular choice of the strength of coupling interaction, the system is driven towards strong first order and hence contributions from heterogenities (random bond and random field disorders) are found necessary to make contact with the experimental results. The second model (Model-II) [37] however considered the contributions from elastic degrees of freedom and the coupling between the orientational degrees of freedom with the global strain as entropic in nature and hence appear as pseudo Hamiltonian terms. This model, as proposed, has the mechanism to moderate the degree of interaction between the two relevant variables depending on the instantaneous global strain present in the system, and also allows for incorporating other factors (like, cross-link density, nature of polymer formation, etc) through another variable prefactor. The model was studied through canonical MC simulations, and has shown to satisfactorily account for experimental observations.

In Model-I, orientational and strain degrees of freedom are assumed to be strongly coupled, the coupling parameter being fixed at its maximum value of unity. This corresponds to prohibitively large shape anisotropy of the polymer chains. Under these conditions this model predicts, in a homogeneous sample, a strong first order transition. Our interest in this model is to understand the effect of making this coupling more realistic by assuming more practical shape anisotropies for the polymer chain, on the NI transition, and to make the treatment simple we consider a homogeneous system. Such a variable coupling strength can also arise from other factors like cross-link density, nature of polymerization, history of cross-linking, etc. We indeed find that for a typical value of coupling parameter at $\chi = 0.2$, the strain variation with temper-

ature matches well with the experimental results even in a homoeneous system. We also attempted to study the effect of such variable coupling on the strain-orientational order relation for much wider range of temperature bracketing the NI transition with a high temperature resolution. To this end we employed entropic sampling technique as described in Chapter 3 [40], and we modify the algorithm suitably to accomodate the random walk in the two dimensional parameter space. Section 4.3 describes the Model-I; the simulation details and results are discussed in the subsequent sections 4.3.1 and 4.3.2.

Model-II considers the pure elastic and coupling terms in the Hamiltonian as arising from entropic considerations, with a linear temperature dependence. This model was studied by performing canonical MC simulations. The presence of temperature in the Hamiltonian (the so-called pseudo terms) present a challenge in adopting the entropic sampling methods, which basically demands determination of density of states for a given Hamiltonian. Such a concept in the presence of terms of entropic origin needs to be examined closely to devise a methodology which enables us to apply these sampling methods to pseudo-Hamiltonians as well. We propose a procedure to generate a two-dimensional DoS, and hence 2D canonical ensembles, for such models by treating differently the two types of contributions to the Hamiltonian. Model-II is described in section 4.4. The details of the simulation methodology are given in section 4.4.1 and the results are discussed in section 4.5. Finally, we make comparative comment on the two models and discuss our results.

4.3 Lattice model of a liquid crystal elastomer: Model-I

We consider an $L \times L \times L$ cubic lattice. Each lattice site holds a nematic director denoted by a unit vector $|n_i\rangle$. Each nematic director interacts with its six nearest neighbours and the interaction is described by Lebwohl-Lasher potential [43], which has head-tail flip symmetry ($|n_i\rangle$ and $-|n_i\rangle$ are equivalent). Besides, each director is coupled to global elastic degrees of freedom. A model Hamiltonian for such an interaction between local director and global strain has been derived from the neo-classical theory of rubber elasticity [1], see [36]. According to this theory the grand trace formula is given by

$$F_{elastic} = \frac{\mu}{2}\left[Tr(\hat{l_0} \cdot \hat{\lambda^T} \cdot \hat{l^{-1}} \cdot \hat{\lambda}) + ln\left(\frac{Det[l]}{a^3}\right)\right] \tag{4.5}$$

where μ is the shear modulus, $\hat{\lambda}$ is the lattice distortion tensor, $\hat{l}$ is the shape tensor of the polymer chains, $\hat{l_0}$ is the shape tensor of the chains at the time of cross-linking and a is the average step length of the polymer. In a lattice model, the shape tensor l_i at each lattice site in a coordinate system aligned along the director $|n_i\rangle$ is given by,

$$\hat{l_i^{-1}} = \begin{pmatrix} l_\perp^{-1} & 0 & 0 \\ 0 & l_\perp^{-1} & 0 \\ 0 & 0 & l_{||}^{-1} \end{pmatrix} \tag{4.6}$$

where $l_\perp$ and $l_{||}$ are the anisotropic polymer step lengths perpendicular and parallel to the local director n_i, respectively. The lattice distortion tensor, $\hat{\lambda}$ in a coordinate

system aligned along the strain axis, say $\overrightarrow{m}$ is given by

$$\hat{\lambda} = \begin{pmatrix} \lambda^{-1/2} & 0 & 0 \\ 0 & \lambda^{-1/2} & 0 \\ 0 & 0 & \lambda \end{pmatrix} \tag{4.7}$$

It may be noted that the shear deformations are not considered here. The resultant trace term after substituting $\hat{\lambda}$ and the step length tensor $\hat{l}$ is then given by, after certain simplifications [36]

$$F_{elastic}(\mathbf{n}_i, \lambda) = \frac{\mu}{2}\left[(\lambda^2 + 2\lambda^{-1}) - \gamma(\lambda^2 - \lambda^{-1})\left(\frac{3}{2}(\mathbf{m}\cdot\mathbf{n_i})^2 - \frac{1}{2}\right)\right]. \tag{4.8}$$

In the above expression, the first term is classical elastic energy whereas the second term provides the coupling between the elastic strain and the orientational order parameter. γ represents the coupling strength between two degrees of freedom and is given by

$$\gamma = \frac{2l_{\perp}^{-1} - 2l_{||}^{-1}}{2l_{\perp}^{-1} + 2l_{||}^{-1}} \tag{4.9}$$

In the earlier work [36], γ is set at unity, corresponding to extreme anisotropy if the line shape tensor, $l_{||} \gg l_{\perp}$. The final Hamiltonian includes

(i) Lebwohl-Lasher nearest neighbour interaction [43] of the directors, placed on the lattice sites

(ii) the interaction of each local director, $|\mathbf{n}_i\rangle$ with

  (a) the global elastic strain e given by $\lambda = 1 + e$

  (b) a possible inhomogeneous field, $|h_i\rangle$

(iii) an externally imposed global stress, σ

(iv) shear modulus, μ which is held constant in this model.

With this notation, one expresses the lattice Hamiltonian as

$$\begin{aligned} F = & - \sum_{\langle i,j \rangle} J_{i,j} \left(\frac{3}{2} \langle \mathbf{n}_i | \mathbf{n}_j \rangle^2 - \frac{1}{2} \right) \\ & + \sum_{i=1}^{L^3} \left[\frac{\mu}{2} \left(\lambda^2 + \frac{2}{\lambda} \right) - \frac{\mu\gamma}{2} \left(\lambda^2 - \frac{1}{\lambda} \right) \left\{ \frac{3}{2} \langle \mathbf{m} | \mathbf{n}_i \rangle^2 - \frac{1}{2} \right\} \right. \\ & \left. - \sigma\lambda - \langle h_i | \mathbf{n}_i \rangle^2 \right] . \end{aligned} \tag{4.10}$$

In the first term the sum extends over all distinct pairs $\langle i, j \rangle$ of nearest neighbours. $J_{i,j} > 0$ measures the strength of nearest neighbour interaction. Periodic boundary conditions are imposed in all directions.

$\lambda \geq 1$ is a scalar denoting the strain parameter, and $\lambda = 1 + e$, where e is the strain along the distortion axis taken to be along the unit vector $|\mathbf{m}\rangle$. The above Hamiltonian ensures that directors at different lattice sites tend to align along the distortion axis $|\mathbf{m}\rangle$. The above model Hamiltonian has the flexibility to describe the liquid crystal elastomer in the presence of random bond ($\{J_{i,j}\}$) or random field ($\{|h_i\rangle\}$) disorder, as well as under the application of external stress, $\sigma \neq 0$.

Selinger and Ratna [36] considered first a homogeneous elastomer ($J_{i,j} = 1 \; \forall \; \langle i, j \rangle$) in the absence of local fields ($|h_i\rangle = 0 \; \forall \; i$) with maximal coupling ($\gamma = 1$) and no external stress ($\sigma = 0$). Their MC simulations under these circumstances yield a strong first order NI transition, driving a first order strain transition as well. They find that the transition can be smoothened to make contact with experiment by in principle introducing external stress and driving the system into a super critical stress condition. However based on earlier observations and arguments, they rule out the presence of stress as the softening mechanism, and show that heterogeneity in the medium, either in the form of bond-disorder or random local fields can also soften this transition to the required level, by controlling the degree of disorder. Their conclusions were based on, of course, assuming that the coupling between the

orientational and strain degrees of freedom is fixed, and that too at a value which sets the shape anisotropy of the polymer chains at perhaps an inacceptably high value. We argue that this coupling constant itself might have a crucial role in determining the nature of the transition, quite independent of the presence, or otherwise, of external stress or inhomogenities within the sample. It is based on the observations that in reality the shape tensor anisotropy depends on the nature of the polymerization and the constituent mesogenic units, and hence setting $\gamma = 1$ (i.e., $l_| \gg l_\perp$) may be an unrealistic idealization. Secondly, we also expect that crucial properites of the medium like cross-link density should play a role in the effective coupling between the two interacting variables (via their relative length scales of relevance), and hence should affect their coupling. Accordingly, we investigate the effect of this coupling constant γ on the predictions of this model, considering the system to be homogeneous and experiences no stress. We employ entropic sampling method to perform random walk in the configuration space of these two variables, and extract infromation through reweighting procedures. We use the density of states of the system obtained from the WL algorithm to compute free energy profiles of the system and hence to investigate the nature of the transition. The details of this study are given in the next section.

4.3.1 Details of simulation

In the present simulation we apply modified WL algorithm described in detail in Chapter 1 [40]. It may be noted that one exploratory work reported therein, on bulk liquid crystal system as well as liquid crystal confined to a porous media indicated that the modifications introduced into the WL algorithm make the entropic sampling of these systems much more efficient, and reproduce very well the known results on these systems. Our aim here from the simulation point of view is to apply this method to a complex system which involves performing a random walk in a multi-parameter

space: orientational variables and strain parameter.

We consider a homogeneous lattice model of the liquid crystal elastomer eqn 4.10, with no external field and no stress: *i.e.* $J_{i,j} = 1 \; \forall \; \langle i, j \rangle$ and $|h_i\rangle = 0 \; \forall \; i$, $\sigma = 0$ and $\mu = 1$. Because of the complexity involved in performing random walk with uniform distribution with respect to energy, which itself is dependent on two MC variables, we restrict the size of the lattice, to a linear size L=6. We subsequently extended the study to L=8, just to check for the consistency of these results. We take the initial microstate with $\{|\mathbf{n}_i\rangle\}$ chosen randomly on each lattice site and $\lambda = \lambda_0 = 1$. Let C_0 denote the initial microstate and E_0 be its energy. We probe the system in an energy range -500 to 50 expressed in units of J_i. This energy range is divided into 8000 bins of equal width. Let ν denote the energy bin index of the initial microstate. We set $g_i = 1 \; \forall \; i$. In each Monte Carlo step a director is chosen at random and its orientation is changed to a trial orientation employing Barker's method [44]. A trial strain parameter, λ_t is obtained from the current strain parameter λ_0 randomly following the prescription $\lambda_t = \lambda_0 + 0.01 \times (\xi - 0.5)$ where ξ is sampled from a uniform distribution $[0, 1]$. These two operations correspond to taking random step involving both MC variables, and producing a new trial microstate C_t of the lattice elastomer. The acceptance of the trial microstate is based on entropic sampling criterion described earlier. Once a microstate is accepted we update g as per Wang-Landau algorithm, as before. We carry out in this fashion one Wang-Landau run; the g function at the end of a Wang-Landau run is taken as the input for the next run. The procedure is exactly as described in the earlier Chapter, and finally we get a converged density of states which can then be used to produce an entropic ensemble of microstates spanning the space of both the degrees of freedom. This is achieved by carrying out a long production run based on the DoS obtained, and let us denote this as g-ensemble. From this g ensemble, we calculate the desired macroscopic properites

of the liquid crystal elastomer system, with a high temperature resolution, through the re-weighting scheme described in Chapter 2. For the system of size $6 \times 6 \times 6$, the time taken to generate DoS , involving MC steps in the two variable spaces on a Pentium IV (Intel based) computer (at 2..0GHz) is about 10 days, while it extends beyond 20 days for a system of size $8 \times 8 \times 8$.

4.3.2 Results and Discussions

Figure (4.2) depicts orientational order S as a function of temperature T, while finite size effects do effect the computed results, one interest is in the differences in the relative variation of parameters as the coupling is varied. for various values of coupling parameter $\gamma = 1,\ 0.8,\ 0.6,\ 0.4,$ and 0 on a system of size $6 \times 6 \times 6$. For $\gamma = 1$ we find that order parameter drops sharply when temperature increases. For smaller γ, the transition becomes less sharp and occurs at lower temperature. Figure (4.3) depicts the strain parameter λ as a function of temperature for various values of γ. At high temperature the system is isotropic and hence irrespective of the coupling strength, the strain is zero *i.e* $\lambda = 1$ for all temperatures. When the temperature is lowered, say below T_t, strain develops, see Fig. (4.3). The value of T_t is higher for larger γ. For $\gamma = 1$ the strain rises rather steeply with lowering of temperature. For lower values of γ the increase of strain with decrease of temperature for $T < T_t$, is progressively smaller. For $\gamma = 0$ the orientational and elastic degrees of freedom are completely decoupled and hence $\lambda = 1$ for all temperatures, *i.e.* no strain develops even when nematic order sets in on lowering the temperature. These results are consistent with experimental observations. For $\gamma = 0.2$, the elongation at lower temperatures in the nematic regime is about 14% of the original sample size, which seems to be a bench mark value typically expected in an experiment. Thus it seems equally plausible, in principle, to soften the transition and tune the model to correspond to expected

results, without invoking the presence of stress or heterogeneity. The variable nature of γ can be attributed to many contributing factors like cross-link density, nature of polymerization, etc. But the tuning of this model Hamiltonian to make contact with an experiment may encompass contributions from all possible factors, including deviation of γ from unity.

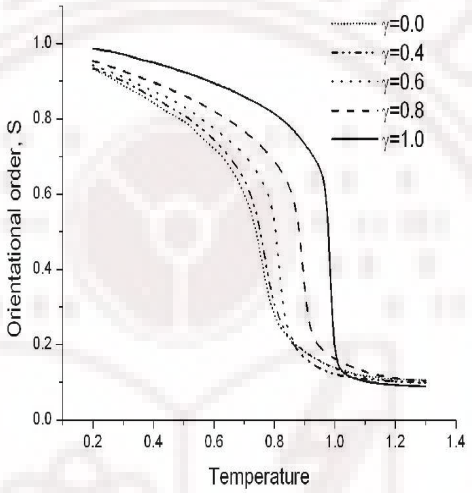

Figure 4.2 Orientational order parameter S versus temperature for various values of the the coupling parameter γ.

Figure (4.4) depicts specific heat, calculated from the fluctuations of energy, as a function of temperature for various values of γ. For $\gamma = 1$, we find that the specific heat shows a sharp maximum at the transition temperature. For lower values of γ the transition occurs at lower temperature and C_V peak broadens. This is in agreement with the mean-field arguments Uchida [47];

Figure (4.5) depicts the transition temperature as a function of γ. The transition temperature is taken as the value of T at which the specific heat shows a maximum. As γ increases the transition temperature increases slowly initially; when γ increases beyond 0.6 the transition temperature increases rather steeply.

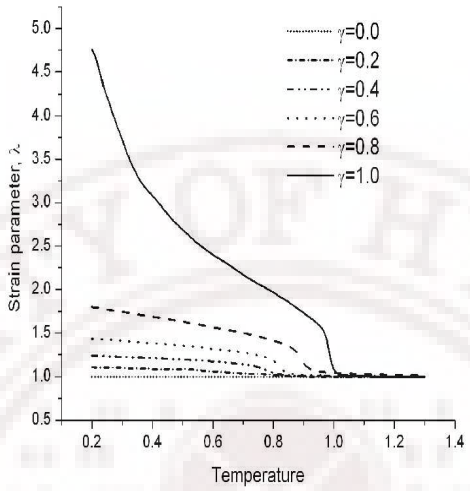

Figure 4.3 Strain parameter λ versus temperature for various values of the the coupling parameter γ.

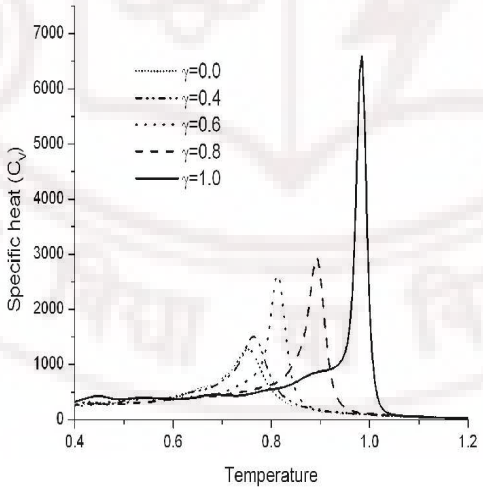

Figure 4.4 Specific heat C_V versus temperature for various values of the coupling parameter γ; C_V has been obtained from the energy fluctuations.

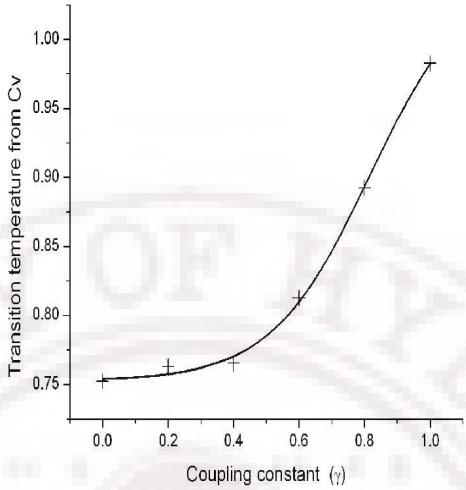

Figure 4.5 Transition temperature versus the coupling parameter γ; the temperature at which the specific heat exhibits peak is taken as the transition point.

As seen from figures. (4.2) and (4.3), both S and λ increase with decrease of temperature. To see the nature of their correlation we have plotted in figure (4.6), λ versus S for various values of γ. For $\gamma = 0$ the strain is zero ($\lambda = 1$) and is independent of S as expected. For small values of γ the strain parameter λ scales linearly with S over the full range of temperature. For $\gamma = 1$, the scaling is linear for $S \leq 0.6$ and $\lambda \leq 1.25$, which correspond to temperatures greater than about 0.8. This is consistent with the results of earlier simulations [36] performed for $T \geq 0.8$, showing linear scaling between λ and S. However, we find that for lower temperatures the scaling of λ with S is nonlinear. The strain increases steeply to fairly large values as the orientational order increases and attains its maximum value of unity. Fig. (4.7) depicts g function and the corresponding energy histogram. The energy histogram is fairly flat indicating the reasonable convergence of DoS to its true value. From the g function we can calculate the microcanonical entropy and free energy up to an additive constant. Note that entropy or free energy calculations are very difficult if

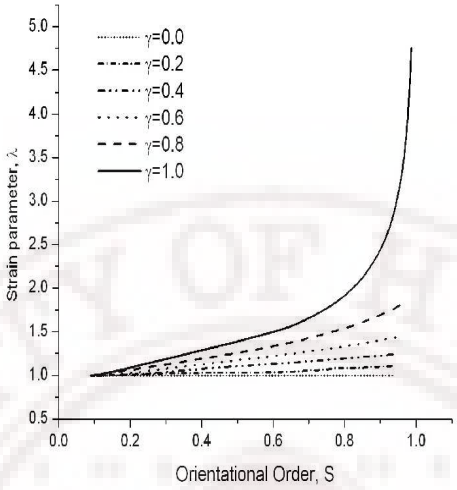

Figure 4.6 Variation of strain (λ) with orientational order (S)

not impossible from conventional canonical simulations.

We show in figure (4.8) the variation of (representative) free energy with energy for $\gamma = 1$ at three temperatures bracketing the transition point. We can see clearly that the transition is first order and strong. Figure (4.9) depicts free energy versus E for $\gamma = 0.8$.The transition is still first order but is relatively weak, as seen by the decreased barrier height relative to $\gamma = 1$ (for the same system size).For smaller values of γ the transition weakens further. For γ less than 0.4 or so, the micro-canonical free energy barrier is not discernible.

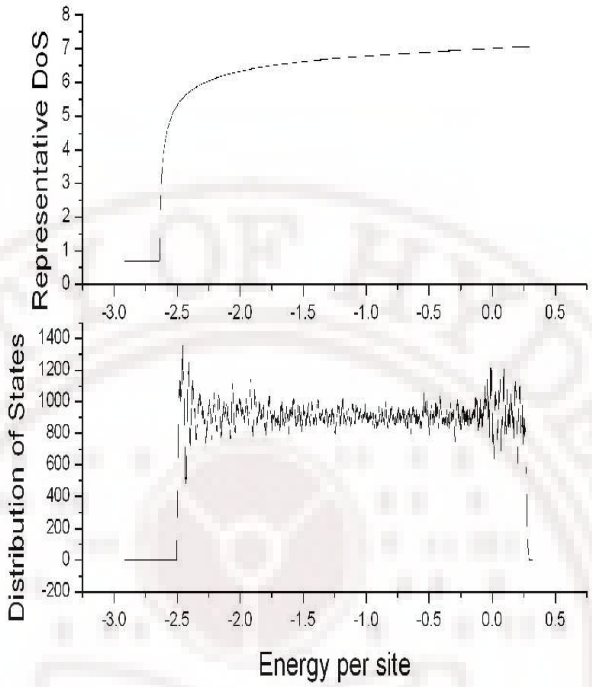

Figure 4.7 (Top) Logarithm of entropy as a function of energy. (Bottom) Histogram of energy of mictrostates.

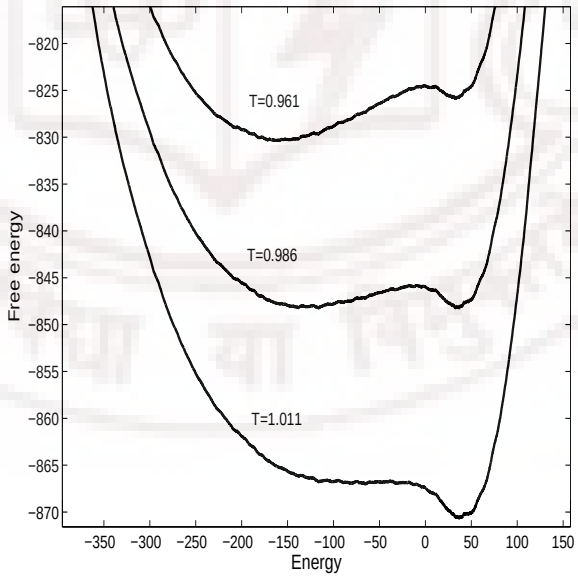

Figure 4.8 Free energy versus energy for temperatures above, below and at the transition point (with equal minima) for the system with $\gamma = 1.0$.

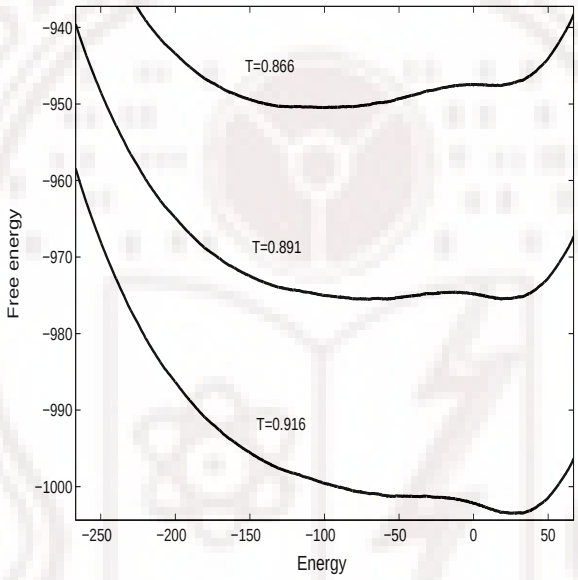

Figure 4.9 Free energy versus energy for temperatures above, below and at the transition point for the system with $\gamma = 0.8$. The barrier height is small; the transition is still first order though weak.

4.4 Lattice model of a liquid crystal elastomer: Model-II

Recently, Pasini, et. al., [37] suggested another coarse-grained lattice model to describe the features of NI transition in LCE's. While retaining the pure energetic nature of the contributions from interactions among orientational degrees (like Model -I), they introduce the entropic nature of the contribution from elastic degrees by presenting their explicit (linear) temperature dependence in the Hamiltonian. Consequently, the Hamiltonian has two pseudo terms. In this model, cross-links are taken to coincide with the lattice sites in a three dimensional cubic lattice. Let us consider that there are M monomers of length b each present in each polymer chain. The pseudo-Hamiltonian to mimic the entropic effect of uniform stretching of the lattice λ is given by:

$$H_e = NK_BT\alpha\left(\lambda^2 + \frac{2}{\lambda}\right) \tag{4.11}$$

where N is the number of lattice points. α is the cross-link density which depends on the characteristics of the polymer chain as $\alpha = 3a^2/2Mb^2$, where a is the distance between two lattice points. The interaction between two mesogenic units (i, j) whose average orientations are represented by directors,($\mathbf{n}_i$,$\mathbf{n}_j$) is given by Lebwohl-Lasher potential:

$$H_n = -\sum_{\langle i<j\rangle} \epsilon_{ij} P_2(\mathbf{n}_i \cdot \mathbf{n}_j) \tag{4.12}$$

Here, ϵ_{ij} represents the nearest neighbor cell-cell interaction strength. In a homogeneous system that is under consideration all the coupling coefficients, ϵ_{ij} are equal, say ϵ. The coupling between the elastic strain and mesogenic alignment is given by

$$H_c = -k_BT\chi Q(\lambda)\sum_{i=1}^{N} P_2(\mathbf{n}_i \cdot \mathbf{z}) \tag{4.13}$$

where χ is the coupling constant and the value $Q(\lambda)$ is the measure of anisotropy of polymer chain end-to-end tensor distribution when the sample is deformed to a value λ along the z-axis, preserving the volume. It is defined as

$$Q(\lambda) = (4\pi)^{-1} \int_{\epsilon} P_2(cos\theta) d\Omega = (3\lambda^3/2)\mathcal{L}(\lambda^3 - 1) - 1/2 \tag{4.14}$$

where

$$\mathcal{L}(\zeta) = \begin{cases} (\text{arctanh}\sqrt{-\zeta} - \sqrt{-\zeta})/\sqrt{-\zeta^3}, & -1 < \zeta < 0, \\ 1/3, & \zeta = 0 \\ (\sqrt{\zeta} - \arctan\sqrt{\zeta})/\sqrt{\zeta^3}, & \zeta > 0; \end{cases} \tag{4.15}$$

The volume of integration as indicated in the equation 4.14 corresponds to a uniaxial ellipsoid obtained from an isovolume deformation of a unit sphere by a factor of λ along the z-axis. In an undistorted sample, $\lambda = 1$ and hence $Q(\lambda) = 0$. On stretching along or perpendicular to the z-axis, $Q(\lambda)$ becomes either positive or negative, respectively. The important point to be noted here is that $Q(\lambda \to \infty) \to 1$, hence it is finite even for very large deformations bounded between -0.5 and 1.0. In contrast, the λ-dependent contribution in the coupling interaction of Model-I diverges for extreme deformations. The total Hamiltonian of Model-II is given by:

$$\begin{aligned} H = & - \sum_{\langle i,j \rangle} \epsilon_{i,j} P_2(\mathbf{n}_i.\mathbf{n}_j) + N\ k_B\ T\ \alpha \left(\lambda^2 + \frac{1}{\lambda}\right) \\ & - k_B\ T\ \chi\ Q(\lambda) \sum_{i=1}^{N} P_2(\mathbf{n}_i \cdot \mathbf{z}) \end{aligned} \tag{4.16}$$

This model was investigated based on canonical MC simulations [37] to compare the predicted macroscopic behaviour of the system with experimental observations. These should also include the effects of heterogeniety and stress. These investigations indicate that proposed Hamiltonian model satisfactorily accounts for the observed thermal behavioiur of the LCE. In this context, the objectives of the current effort

is to look for ways of implementing entropic sampling algorithm on a Hamiltonian which itself contains parametric dependence on temperature. Estimation of DoS, construction of canonical ensembles and extraction of physical properties out of such a model is new, and is the aim of the next section.

4.4.1 Details of the simulation

We use the scheme of frontier sampling discussed in the earlier chapter along with Gaussian update protocol [51] to investigate this model. In brief, the key steps in the procedure are:

- When the random walker arrives at the microstate x_0 whose energy is say E_0 the logarithm of density of states $\omega(E_0)$ is not updated locally as $\omega(E_0) \rightarrow \omega(E_0) + f$, but a Gaussian kernel $k(E)$ is placed using the updating scheme: $\omega(E) -> \omega(E) + \gamma * k((E - E_0)/\delta)$ where $k(x) = exp(-|x|^2)$ [51].

  In each WL iteration we start with a certain γ value (say 0.1) and perform 1000 or more MC sweeps (one WL run). Such WL runs are repeated by gradually decreasing γ till it reaches atleast 0.001. The value of δ is kept fixed during this simulation.

- Each frontier run consists of a learning run followed by a reference run.

  - **Learning run**: A cut-off point in the energy range is identified by examining the the constancy of the difference between $\omega(E)$ values within a chosen tolerance corresponding to two consecutive WL iterations, and $\omega(E)$ is preferentially updated inside the frontier defined by the cut-off point, to force the system to low probable regions.

  - **Reference run**: WL iteration is performed to smoothen the DoS generated from the learning run. The difference in $\omega(E)$ from reference run and

the earlier learning run is used to find a possible new (lower) cut-off in the next learning run. Otherwise, this step is repeated until a new frontier at a lower energy could be found.

- After the desired energy range is spanned, a long smoothening run is performed.
- Linear interpolation method among energy bins is employed while calculating the acceptance ratios to avoid the possibility of the system getting sometimes trapped in the same energy bin for too long. Indeed this trick has speeded up the upgrade process considerably.

Entropic sampling procedure is intuitively clear while dealing with usual Hamiltonians with pure energetic contributions. Such a Hamiltonian once defined, has a set DoS. Canonical sampling based on a temperature dependent probability distribution merely corresponds to moderation of the natural tendency of the system with a given Hamiltonian to exist with different probabilities in different energy regions, with a statistical necessity of complying with the given probability prescription, owing to the energy exchanges under canonical external conditions. This somewhat clearer role of DoS, well defined and temperature independent for a given Hamiltonian, needs a re-examination if the Hamiltonian also contains entropic contributions with explicit temperature dependencies. In such a case, the above picture implies temperature dependent DoS, as the variation of temperature in effect corresponds to changing the relative strength of the terms involved, with respect to the chosen energy scales. Then it is not possible to directly proceed with the above procedure for Model-II. For convenience of discussion, we write the Hamiltonian as consisting of two parts:

$$\mathcal{H} = \mathcal{H}_{energy} - T\mathcal{H}_{entropy} \tag{4.17}$$

$$\mathcal{H}_{energy} = -\sum_{\langle i<j \rangle} \epsilon_{ij} P_2(\mathbf{n}_i \cdot \mathbf{n}_j) \tag{4.18}$$

$$\mathcal{H}_{entropy} = -N\ k_B\alpha \left(\lambda^2 + \frac{1}{\lambda}\right) + k_B\chi\ Q(\lambda) \sum_{i=1}^{N} P_2(\mathbf{n}_i \cdot z) \tag{4.19}$$

Because of the different procedures we adopted to compute the DoS of this system, it has been possible to carry out simulations on a bigger lattice (relative to Model-I), with a linear size $L = 20$. We initialize the orientations of spins representing the local directors on a cubic lattice of size $20 \times 20 \times 20$. The desired energy range corresponding to interactions purely among the orientational degrees (the H_{energy} term), say along the E axis is divided into 16000 bins, whereas λ axis is divided into 100 bins over the range [1,1.5]. Before presenting the results of these simulations the generic procedure for computing the DoS and construction of entropic ensemble is presented first. The total DoS of the system is to be defined over the two dimensional grid (16000×100) specified by the (spin) energy bins and the λ bins. The choice of the number of bins is constrained by the limitations on the memory available for storage and the computational time required, (compuations being carried out on a single processor). Recognizing the fact that this Hamiltonian assigns entropic origin to all interactions involving the strain variable, we split the process of computing the DoS of the total Hamiltonian into two steps. We first compute the DoS arising entirely from H_{energy}, using the normal entropic sampling procedure; and this corresponds to, as far as, orientational variables are concerned, computing the DoS of the total Hamiltonian at $\lambda = 1$ (the third interacting term is set to zero via the factor $Q(\lambda)$). Next, we note that minimization of free energy of a system with a purely energetic Hamiltonian by a random walk in the appropriate configurational space guided by a Markov chain Monte Carlo dynamics can be mapped to the present system by simply realizing that $H_{entropy}$ is in effect the entropy of the system defined on the

two-dimensional space of (λ,E). Ofcourse, E is determined by the amount of orientational order of the specific microstates, and hence influences the contribution to the coupling term through the local director distribution. Thus, the construction of a 2D DoS spanning (λ,E) space, or equivalently (λ,S) space (S is the scalar orientational order parameter), simplifies to the evaluation of the contribution of $H_{entropy}$ term over a chosen range of λ, for a given state of orientational order (i.e., S, and hence E), as the entropy contribution arising from λ-dependent part of the Hamiltonian.Thus, for every energy value of E in the range of interest, or more practically for every bin value of E, the extension of DoS along the λ-axis can be computed using the information on the instantaneous distribution of entropy along the λ-axis. The 2D DoS in (λ,E) space is thus constructed. In the absence of coupling between the two variables, a bell-shaped distribution function located at each E bin value, extending over the λ-axis and peaked at $\lambda = 1$, would result. The effect of the interaction to modify this function, changing its shape as well as the location of its peak along the λ-axis. The thermally driven orientational order thus modifies the DoS of the system so as to yield different (canonical) averages of λ for different degrees of orientational order.

After checking for its convergence, the DoS is used to generate entropic ensemble of microstates in (λ,E) space by sampling both the variables (over their respective ranges) during a long production run, the acceptance criterion being stipulated by the DoS, as usual. The quality of the entropic ensemble can be checked by plotting the distribution of these states over the (λ,E) plane as a histogram over the 2D bin structure. Knowledge of 2D DoS, along with the entropic ensemble of microstates spanning the desired range of the parameters is sufficient to extract a 2D canonical ensemble at the chosen temperature by the reweighting procedure. Computation

of averages of different properties of the system over the corresponding canonical ensemble, then follows. The above procedure is adopted to apply entropic sampling to the Model-II Hamiltonian, and we examined the outcome of reweighting from the grand ensemble of microstates, comparing it with the canonical MC data reported earlier [37].

4.5 Results and discussion:

The energy scale is set by choosing $\epsilon = 1$ in eqn 4.12. The cross-link density α is initially chosen to be 0.3, and the coupling constant χ at 0.5. The DoS corresponding to H_{energy} is computed by choosing the initial and final avlues of γ during a WL iteration to be 30 and 0.0001, respectively. The value of δ is kept at 35 throughout the simulation. The ranges of these values are determined by carrying out a few exploratory runs on the chosen system size ($L = 20$) to obtain a reasonably well convergent DoS along the E-axis ($\lambda = 1$), as verified by the flatness of the corresponding energy histogram. The DoS is thus available at 16000 distinct energy values (bins). Corresponding to each such energy bin value (or, equivalently order parameter value), a large number of microstates (corresponding to simple LL potential, since λ is set to 1) are available representing different orientational organization consistent with the bin value. The DoS at each of the E-bins is now extended along λ-axis by the following procedure. For each microstate within a given bin, the contribution to DoS from $H_{entropy}$ as a function of λ (over the range 0.8 to 1.2) is computed eqn 4.11. All such distributions along λ arising from each of the microstates associated with the bin are now averaged to yield the coarse grained extension of the DoS of that bin along λ (λ being spread over 100 bins). This has been carried out over all the E bins to finally compute the 2D DoS of the system. Figure 4.10 depicts the corresponding

entropy in the (λ,E) space. A long production run is performed in the (λ,E) space assisted by the 2D DoS, and histogram of microstates is collected as shown in figure 4.11.

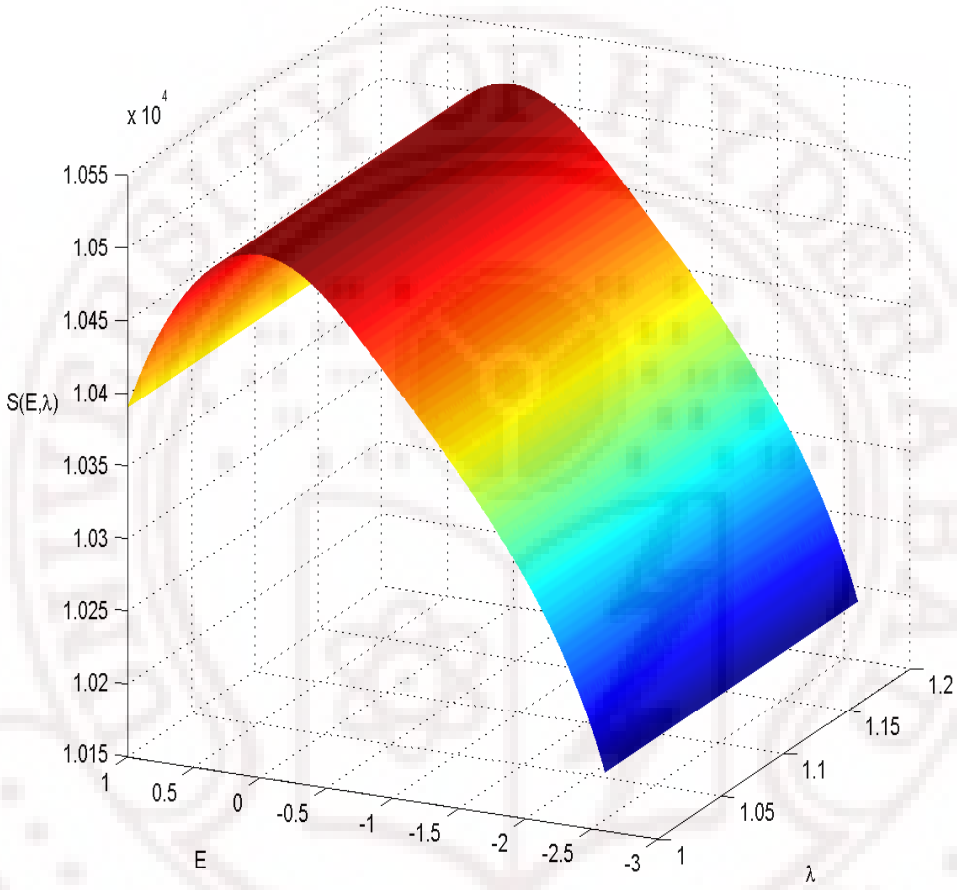

Figure 4.10 Two-dimensional entropy, $S(E, \lambda)$

The reweighting of the microstates in the entropic ensemble appropriate to a chosen temperature is carried out in two steps. First, the canonical ensmeble corresponding to H_{energy} part of the Hamiltonian is extracted by reweighting the microstates associated with the cross section of the DoS at $\lambda = 1$. This yields a set of equilibrium states corresponding to LL potential at that temperature. Let this

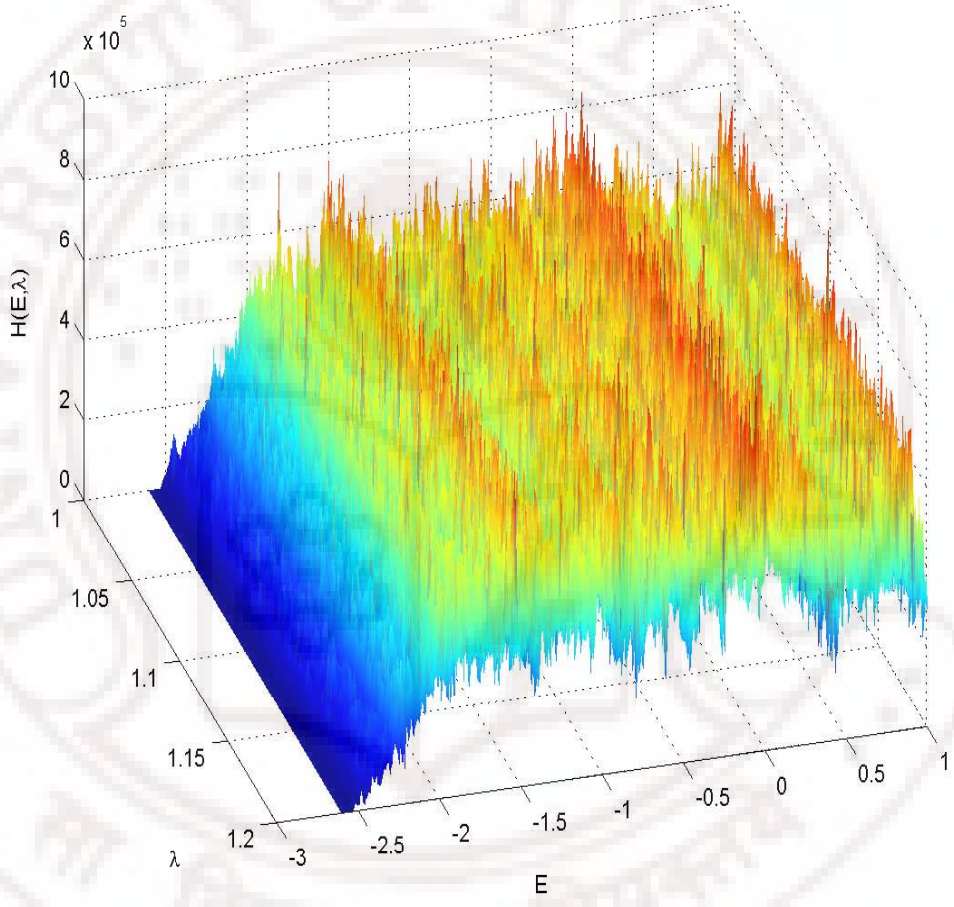

Figure 4.11 Two-dimensional multicanonical histogram,$H(E, \lambda)$

distribution be represented by $N(E;\lambda = 1)$. Now we performed reweighting on all the states collected in the grand entropic ensemble (in the (λ,E) plane), with variable weight factors at each E-bin set by the canonical distribution $N(E;\lambda = 1)$. This results in 2D canonical ensemble of states distributed over E and λ axes, appropriate to that temperature. Figure 4.12 shows these distributions $N(E,\lambda)$ in different temperature regions bracketing the NI transition. The physical properties of interest are now averaged over $N(E,\lambda)$.

To illustrate the effect of temperature on the distribution of microstates along the λ-axis, the E-bin corresponding to the maximum in $N(E,\lambda = 1)$ at a given temperature is chosen, and the corresponding variation of distribution at that E-bin along λ-axis is extracted. This is repeated at different temperatures covering the phase transition region, yielding probability distributions along λ-axis as a function of temperature at the corresponding most probable orientationally ordered states. Figure 4.13 shows changes in the λ probability distribution, say $P(S,\lambda)$, as the transition temperature is crossed. The development of strain across the transition is clearly seen from this cross sectional distribution, and the locations of the maxima of the peaks practically coincide with the canonical λ averages reported above. Figures 4.14 and 4.15 show the variation of different parameters (like energy, orientational order, strain, specific heat and nematic susceptibility) computed as a function of temperature (with a resolution of 0.001) from the canonical ensembles generated as described above. These compare very well with the corresponding variations reported based on canonical sampling method on Model-II Hamiltonian [37]. The additional computation is of course the density of states of this complete system, and the higher resolution in temperature.

This model is further investigated with this procedure to look for the effect of other parameters on the strain transition, namely the cross-link density α and the coupling

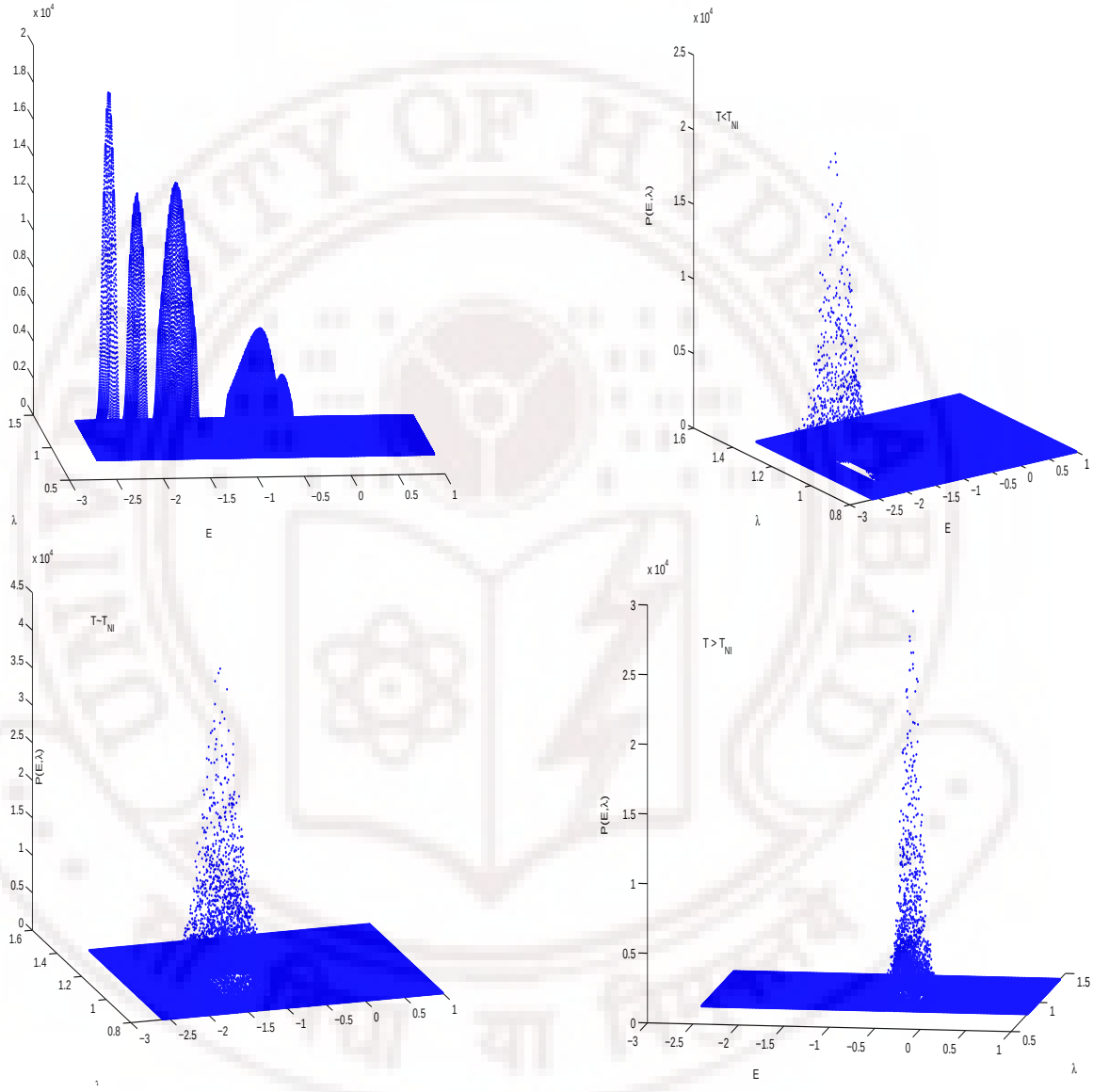

Figure 4.12 Canonical ensembles at different temperatures. Canonical ensembles at $T < T_{NI}$, $T \approx T_{NI}$ and $T > T_{NI}$

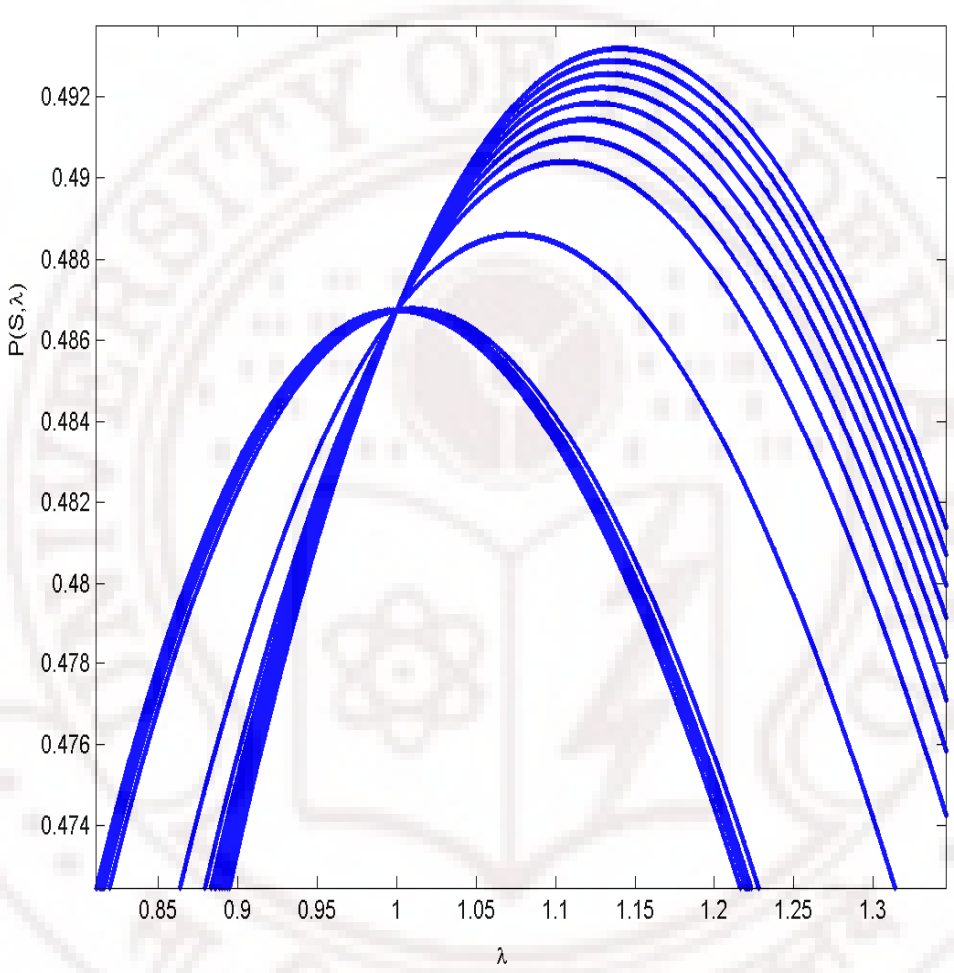

Figure 4.13 Probability distribution function, $(N(E,\lambda))$ calculated using method-II as a function of λ at various temperatures. As the temperature decreases, the maximum value of $N(E,\lambda)$ shifts towards larger values of λ.

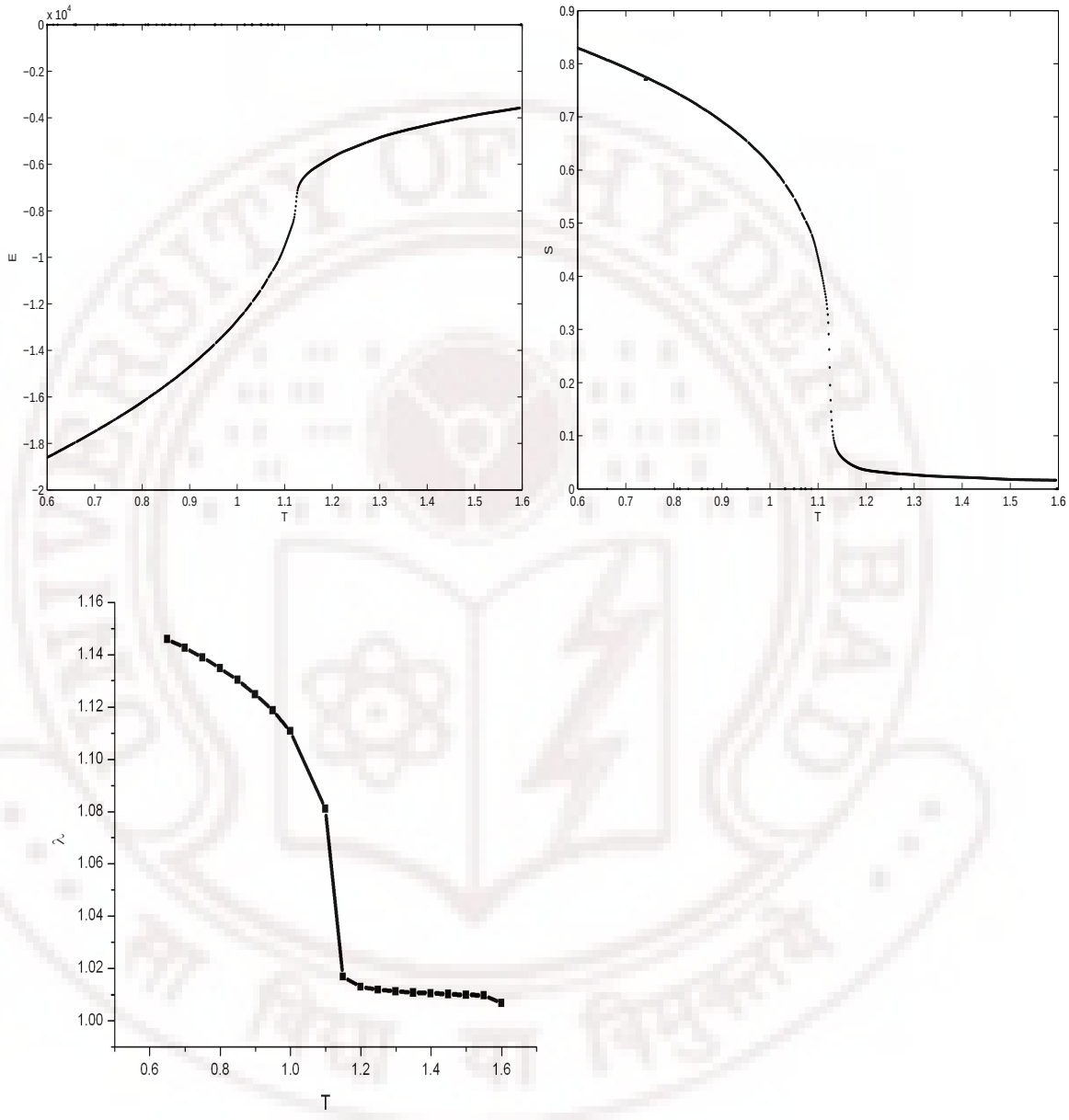

Figure 4.14 Variation of energy, order parameter and strain with temperature

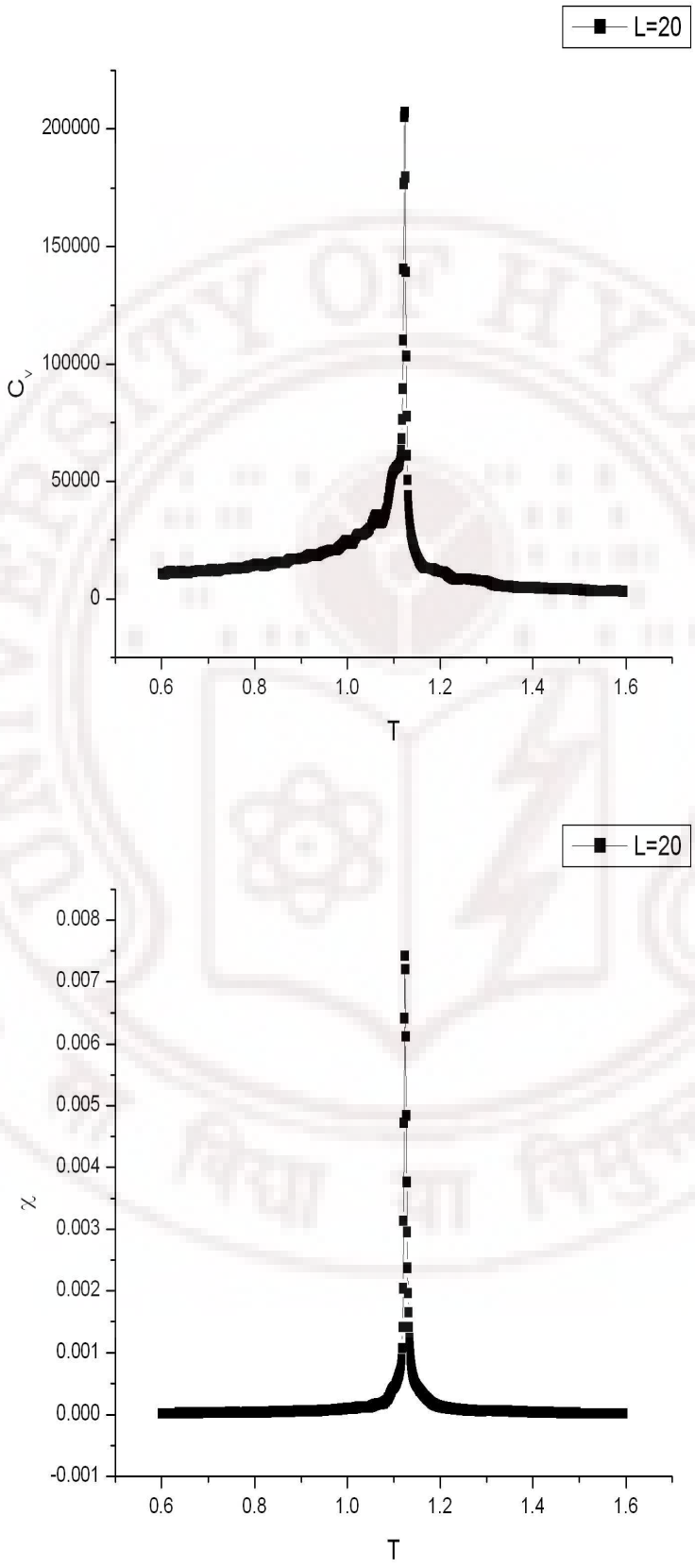

Figure 4.15 Variation of specific heat, C_v and susceptibility, χ_S with temperature

strength χ (eqn 4.16). Variation of α will directly affect the degree of elasticity exhibited by the elastomer, and increase in this vaue should resist more the influence of the (spontaneous) orientational order on the consequent onset of the strain. Figure 4.16 shows the thermal behaviour of strain at these values of α: 0.3. 0.5 and 1.0. The percentage of strain induced due to the formation of nematic order has reduced from about 15% to about 4.5%, correspondingly. Effect of χ, on the other hand, is a measure of the coupling between orinetational order and global strain, and variation of χ also brings about changes in the thermal behaviour. To make a comparison with the earlier figure (depicting the effect of α), we decrease χ and compute the profile of the strain transition at these values: 0.5, 0.3 and 0.1. Figure 4.17 shows the corresponding changes in strain; in this case the strain induced reduces from about 15% to about 4% at the same low temperature (in reduced units) as in figure 4.16. Arguing that variation in χ could be viewed, besides other contributing factors, as an indication of changes in the relative length scales of the two variables, it appears plausible that variation of cross-link density (which directly affects the primary elastic property of the material) could indirectly influence the coupling strength as well. In the present simulations we however consider them to be independent, as per the original prescription of this Hamiltonian.

Finally, we present the basic results of our simulations on both the models as shown in figure 4.19. For convenience of comparison, we set the value of χ to be unity in Model-II (comparable to that of γ in eqn 4.10) in computing these variables. As may be seen, there is a difference in the variation of orientational order itself between the two models. It may be noted in this context that simulation on Model-I proceed with the assumptions that all the Hamiltonian terms are energetic in nature. Correspondingly, the DoS of the system, in particular concerning the orientational degrees is determined by the coupling term as well. In contrast, the DoS as far as

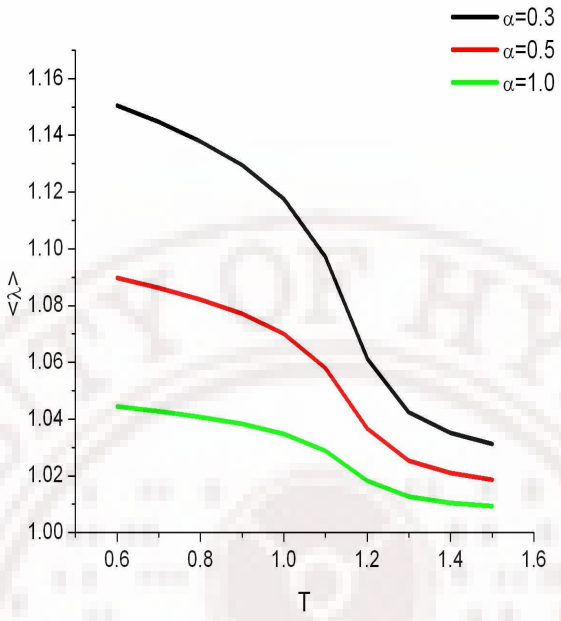

Figure 4.16 Effect of cross-link density, α on the variation of strain with temperature

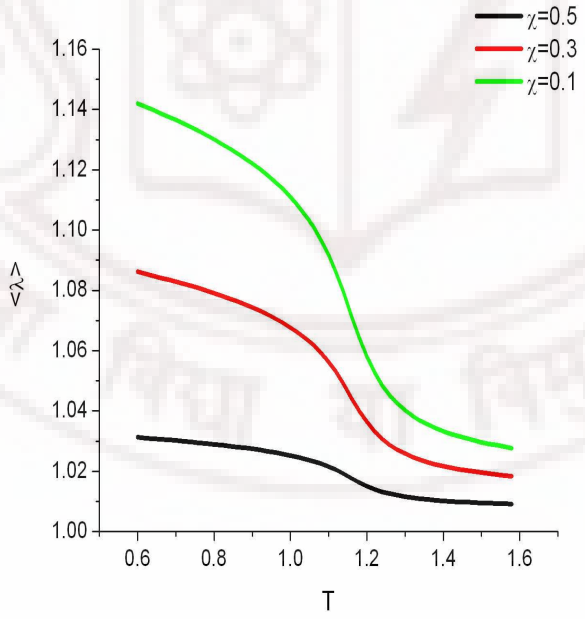

Figure 4.17 Effect of coupling parameter, χ on the variation of strain with temperature

orientational degrees are concerned are primarily determined by the energetic part of the Hamiltonian (H_{energy}) and seem to be only marginally affected by the other terms. But, the more dramatic difference is seen in the variation of strain. While Model-II predicts even at $\chi = 1$ a change in strain of $\lambda = 1.28$, Model-I yields at a comparable temperature ($(T - T_C) \sim -0.5$ in figure 4.19) a change in λ of about 2.75. Also the nonlinear variation of λ with orientational order from Model-I is in contrast to the corresponding variation expected from Model-II.

The above differences in the predictions of the two models can be readily appreciated by referring to the figure 4.18. Here we plot the contributions coming from the second and third terms of the respective Hamiltonians, representing the contribution to the λ-dependent energy. The functional dependence of elastic energy on λ due to pure strain variation (second terms in the two Hamiltonians) is the same, but for an adjustable prefactor. For comparison we make them look identical and plot them, as in figure 4.18. In order to evaluate the contribution from the coupling terms, we consider the case of perfectly aligned nematic for convenience in calculation. This contribution diverges, in Model-I, in the two opposite directions as λ is varied over the range. The equilibrium strain is determined by the location of the minimum of energy contributions from the last two (λ-dependent) terms. Thus in this model the orientation induced contribution to the elastic energy drives the resultant minimum asymptotically to very large values of λ, as the orientational order builds up. In Model-II a limiting function in the form of $Q(\lambda)$ is introduced which bounds the variation of the orientation dependent elastic contributions, resulting in asymptotically limiting variation of strain as orientational order in the system increases. In figure 4.18 the total elastic energy contribution arising from Model-II in a completely aligned nematic is shown to indicate the shift in the minimum on introduction of coupling with a maximal orientational order.

In this Chapter, we reported the extension of entropic sampling technique to LCE with two ordering parameters, requiring a more elaborate walk in higher dimensional space. The second issue dealt with is the extension of this methodology to Hamiltonians with temperature dependent terms. We applied these sampling procedures to the two lattice Hamiltonians recently proposed to capture the features of these systems, by certain coarse-graining at the microscopic level. We present the results on these systems and compare their predictions. This work has been reported recently [53, 54].

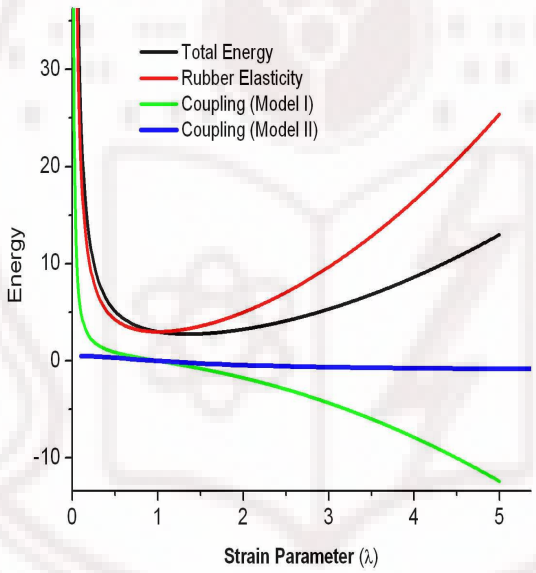

Figure 4.18 Energy contributions of coupling terms of both the models (Model-I(red) and Model-II(blue)) compared to purely elastic energy (green) and total energy term (black) as a function of strain (λ) in completely aligned nematic state.

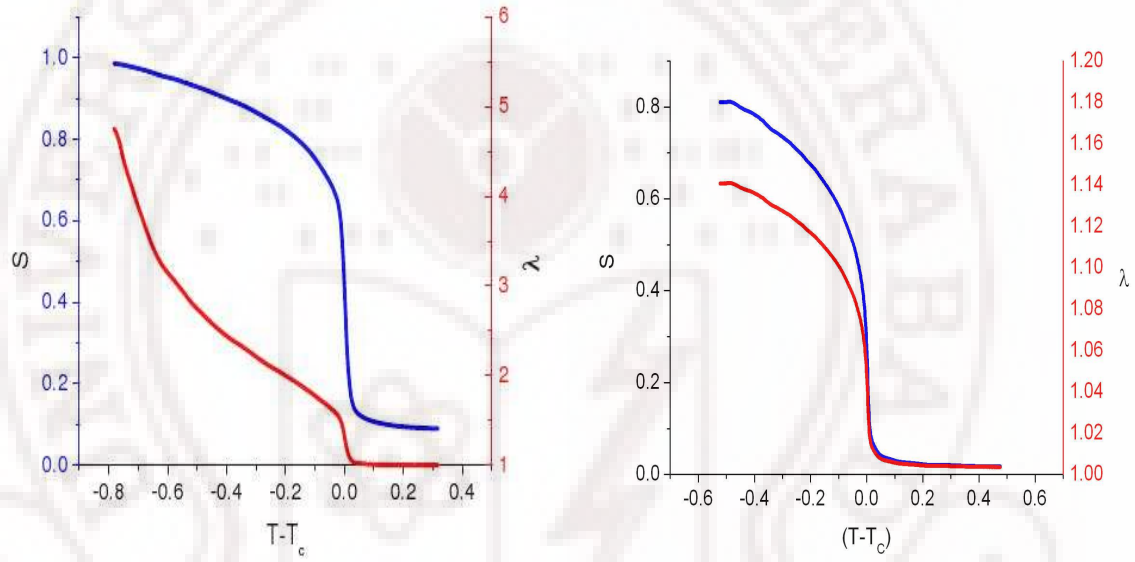

Figure 4.19 Variation of orientational (blue) and strain order parameter (red) as a function of temperature for Model-I (left) and Model-II (right), respectively

Bibliography

[1] M. Warner and E. M. Terentjev, *Liquid Crystal Elastomers*, Clarenden Press, Oxford (2003); M. Warner and E. M. Terentjev, *Prog. Polym. Sci.* **21**, 853 (1996); E. M. Terentjev, J. Phys. : Condens. Matter **11**, R239 (1999).

[2] Y. Mao and M. Warner, *Phys. Rev. Lett.* **84**, 5335 (2000); M. Warner, E. M. Terentjev, R. B. Meyer and Y. Mao, *Phys. Rev. lett.* **85**, 2320 (2000); S. M. Clarke, A. R. Tajbakhsh, E. M. Terentjev and M. Warner, *Phys. Rev. Lett.* **86**, 4044 (2001); Y. Mao and M. Warner, *Phys. Rev. Lett.* **86**, 5309 (2001); P. Pasini, G. Skacej and C. Zannoni, *Chem. Phys. Lett.* **413**, 463 (2005); O. Stenull and T. C. Lubensky, *Phys. Rev. E.* **73**, 030701(R) (2006).

[3] P. G. de Gennes, Polymer liquid crystals, edited by A. Ciferri, W. R. Krigbaum and R. B. Meyer (Academic, New york, 1982); *C. R. Acad. Sci. Ser B*, 281, 101 (1975).

[4] L. Petridis and E. M. Terentjev, *Phys. Rev. E***74**, 051707 (2006).

[5] T. Bellini, M. Buscaglia, C. Chiccoli, F. Mantegazza, P.Pasini, C. Zannoni, *Phys. Rev. Lett***85**, 1008 (2000).

[6] T. Bellini, M. Buscaglia, C. Chiccoli, F. Mantegazza, P.Pasini, C. Zannoni, *Phys. Rev. Lett***88**, 245506 (2002).

[7] R. Harris, M. Plischke, M. J. Zuckermann, *Phys. Rev. Lett* **31**, 160 (1973).

[8] J. Kupfer, H. Finkelmann, *Macromol. Chem. Rapid Commun.* **12**, 717 (1991).

[9] N. Uchida, A. Onuki, *Europhys. Lett.* **45**, 341 (1999);

[10] Y. K. Yu, P. L. Taylor and E. M. Terentjev, *Phys. Rev. Lett.***81**, 128 (1998).

[11] D. Stauffer, *Introduction to Percolation theory*, Taylor and Francis, London (1985).

[12] S. Borderix, P. M. Goldbart and A. Zippelius, *Phys. Rev. Lett* **79**, 3688 (1997).

[13] D. L. Thomsen *et al.*, *Macromolecules* **34**, 5868 (2001).

[14] J. Schatzle, W. Kaufhold and H. Finkelmann, *Makromol. Chem.* bf 190, 3269 (1989).

[15] W. Kaufhold, H. Finkelmann and H. R. Brand, *Makromol. Chem.* **192**, 2555 (1991).

[16] S. Disch, C. Schmidt and H. Finkelmann, *Macromol. Rapid Commun.* **15**, 303 (1994).

[17] A. Lebar, Z. Kutnjak, S. Zumer, H. Finkelmann, A. Sanchez-Ferer and B. Zalar, *Phys. Rev. Lett.* **94**, 197801 (2005).

[18] G. Cordoyiannis, A. Lebar, B. Rozic, B. Zalar, Z. Kutnjak and S. Zumer, *Macromolecules* **42**, 2069 (2009).

[19] A. I. Larkin, *Sov. Phys-jetp. Engl. Trans.* **31**, 784 (1970).

[20] Y. Imry and S. Ma, *Phys. Rev. Lett.* **35**, 1399 (1975).

[21] H. Finkelmann, A. Greve and M. Warner, *Eur. Phys. J. E* **5**, 281 (2001).

[22] S. M. Clarke, A. Hotta, A. R. Tajbakhsh and E. M. Terentjev, *Phys. Rev. E* **6406**, (2001).

[23] S. M. Clarke, E. M. Terentejev, I. Kndler and H. Finkelmann, *Macromolecules* **31**, 4862 (1998).

[24] S. M. Clarke, F. Elias, R. Pech and E. M. Terentjev, *Eur. Phys. Lett* **47**, 442 (1999).

[25] P. G. deGennes and J. Prost, *The physics of liquid crystals* (Oxford Science Publications) (1995).

[26] I. Chuang, N. Turok and B. Yurke, *Phys. Rev. Lett* **66**, 2472 (1991).

[27] J.V. Selinger, H.G. Jeon, and B.R. Ratna, *Phys. Rev. Lett.* **89**, 225701 (2002)

[28] H. Finkelmann, E. Nishikawa, G. G. Pereira and M. Warner, *Phys. Rev. Lett.* **87**, 015501 (2001).

[29] J. Küpfer, and H. Finkelmann, *Macromol. Chem. Phys.* **195**, 1353 (1994); H. Finkelmann and H. Wermter, *Polym. Mater. Sci. Eng.* **82**, 319 (2000).

[30] P. G. de Gennes, . *R. Acad. Sci. Paris* **281**, 101 (1975); P. G. de Gennes, M. Hubert, and R. Kant, *Macromol. Symp.* **113**, 39 (1997); I. Kuñdler, H. Finkelmann, *Macromol. Chem. Phys.* **199**, 677 (1998); W. Lehmann, H. Skupin, C. Tolskdorf, E. Gebhard, R. Zentel, P. Kruger, M. Losche and F. Kremer, *Nature* **410**, 447 (2001); Y. Yusuf, Y. Ono, Y. Sumisaki, P. E. Cladis, H. R. Brand, H. Finkelmann and S. Kai, *Phys. Rev. E* **69**, 021710 (2004); Y. Yusuf, P. E. Cladis, H. R. Brand, H. Finkelmann and S. Kai, *Chem. Phys. Lett.* **389**, 443 (2004); A. Arcioni, C. Bacchiocchi, I. Vecchi, G. Venditti and C. Zannoni, *Chem. Phys. Lett.* **396**, 433

(2004): D. K.Cho, Y. Yusuf, P. E. Cladis, H. R. Brand, H. Finkelmann and S. Kai, *Chem. Phys. Lett.* **418**, 217 (2006).

[31] D. L. Thomsen III, P. Keller, J. Naciri, R. Pink, H. Jeon, D. Shenoy, and B.R. Ratna, *Macromolecules*, **34**, 5868 (2001).

[32] C. -C. Chang, L. -C. Chien and R. B. Meyer, *Phys. Rev. E* **56**, 595 (1997).

[33] A. R. Tajbaksh and E. M. Terentjev,*Euro. Phys. J E* **6**, 181 (2001).

[34] D. K. Shenoy, D. L. Thomsen III, A. Srinivasan, P. Keller and B. R. Ratna, Sens. *Actuators A* **96**, 184 (2002); J. Naciri, A. Srinivasan, H. Jeon, N. Nikolov, P. Keller, and B. R. Ratna, *Macromolecules* **36**, 8499 (2003).

[35] S. Chandrasekhar, *Liquid Crystals*, Cambridge University Press, Cambridge (1972); G. R. Luckhurst and G. W. Gray (Eds.), *The Molecular Physics of Liquid Crystals*, Academic Press, New York (1979).

[36] J. V. Selinger and B. R. Ratna, *Phys. Rev. E* **70**, 041707 (2004).

[37] P. Pasini, G. Skacej and C. Zanoni, *Chem. Phys. Lett.* **413**, 463 (2005).

[38] Z. Zhang, O. G. Mouritsen, M. J. Zuckermann, *Phys. Rev. Lett.* **69**, 2803 (1992).

[39] J. Schätzle, W. Kaufhold and H. Finkelmann, *Makromol. Chem.* **190**, 3269 (1989); W. Kaufhold H. Finkelmann and H. R. Brand, *Makromol. Chem.* **192**, 2555 (1991); S. Dishch, C. Schmidt and H. Finkelmann, *Macromol. Rapid Commun.* **15**, 303 (1994).

[40] D. Jayasri, V. S. S. Sastry and K. P. N. Murthy, *Phys. Rev. E.* **72**, 036702 (2005).

[41] F. Wang, and D. P. Landau, *Phys. Rev. Lett.* **86** 2050 (2001); F. Wang and D. P. Landau, *Phys. Rev. E.* **64** 056101 (2001).

[42] B. A. Berg and T. Neuhaus, *Phys. Lett. B* **267**, 249 (1991); B. A. Berg and T. Neuhaus, *Phys. Rev. Lett.* **68**, 9 (1992); J. Lee, *Phys. Rev. Lett.* **71** 211 (1993); Erratum: **71** 2353 (1993)

[43] P. A. Lebwohl and G. Lasher, *Phys. Rev. A* **6**, 426 (1972).

[44] J. A. Barker and R. O. Watts, *Chem. Phys. Lett.* **3** 144 (1969)

[45] N. Metropolis, A. W. Rosenbluth, M. N. Rosenbluth, A. H. Teller and E. Teller, *J. Chem. Phys.* **21**, 1087 (1953).

[46] M. Creutz, *Phys. Rev. Lett.* **43**, 553 (1979); R. J. Glauber, *J. Math. Phys.* **4**, 294 (1979); K. Kawasaki, in *Phase Transition and Critical Phenomena*, Vol. 2, edited by C. Domb and M. S. Green, Academic, London (1972)

[47] N. Uchida, *Phys. Rev. E* **62**, 5119 (2001).

[48] P. G. de Gennes, *C. R. Acad. Sci. Ser. B* **281**, 101 (1975).

[49] E.M. Terentjev, *J. Phys.: Condens. Matter 11*, R239-R257 (1999)

[50] M. S. Shell, P G. Debenedetti and A. Z. Panagiotopoulos, *Phys. Rev. E* **66** 056703 (2002); C. Zhou and R. N. Bhatt, *Phys. Rev. E* **72** 025701 (2005); D. Jayasri, V. S. S. Sastry and K. P. N. Murthy, *Phys. Rev. E* **72**, 036702 (2005); P. Poulain, F. Calvo, et. al., *Phys Rev E* **73** 056704 (2006).

[51] C. Zhou, T. C. Schulthess, S. Torbrugge, and D. P. Landau, *Phys. Rev. Lett.* **96**, 120201 (2006).

[52] H. Tanaka, *J. Chem. Phys.* **111**, 3163 (1999); F. Mercuri, S. Paolone, U. Zammit and M. Marinelli, *Phys. Rev. Lett.* **94**, 247801 (2005); M. Marinelli, F. Mercuri, S. Paoloni and U. Zammit, *Phys. Rev. Lett.* **95**, 237801 (2005).

[53] D. Jayasri, N. Satyavathi, V. S. S. Sastry and K. P. N. Murthy, *Physica A: Statistical Mechanics and its Applications*, **388**, 4 (2009).

[54] D. Jayasri, V. S. S. Sastry and K. P. N. Murthy, *J. comp. mat. sci*, **44**, 185-189 (2008).

Chapter 5

Liquid crystals confined to complex geometries

Nematic liquid crystals (NLC) in contact with patterned substrates have been receiving considerable attention recently because of the potential they exhibit for applications as evidenced by experimental studies, as also due to many fascinating challenges one encounters in dealing wth them theoretically. It is known that surface inhomogeneities like surface roughness or varying degrees of surface composition do influence the anchoring of NLC. These features normally are restricted to nanometer range in a flat substrate, and the NLC films are treated as macroscopically homogeneous. This is because the extent of inhomogeneities in the director field due to perturbations at the rough surface extends typically only to a distance comparable to the length scale associated with the roughness. In the recent past, the focus has shifted to specifically patterned surfaces, with possibly variable anchoring conditions within a period, on a length scale of micrometers, as has been reviewed in the next section. Preperation of such surface structures with specific anchoring properties is an experimental challenge, and is largely driven by the promise they hold out for rich director structures,

relatively easily susceptible to external stimuli. Varying anchoring conditions induce elastic distortions and flexoelectric polarizations within the contacting NLC. Drawing on the information obtained on the phase behaviour of such systems in contact with either geometrically structured substrates or chemically patterned substrates, investigations now continue on more complex confining substrates treated for both types (chemical and geometrical) of perturbation. The result is the new predictions of recent theoretical investigations on nematic cells suggesting the possibility of zenithally bistable nematic devices. These generally consists of a flat substrate with a desired anchoring angle (measured with respect to the normal to the surface), and a grating surface comprising of a chosen chemically and geometrically structured substrate.

The theoretical treatments make use of the presumed translational symmetry in the direction parallel to the gratings, and thus reduce the problem to one of minimising the free energy of a two dimensional NLC layer, subject to the boundary conditions imposed at the two bounding surfaces. In continuum approximation, the free energy is decomposed into two parts: the distortion energy from the NLC medium (Frank-Oseen formulation) and the contribution from the surface (Rapini-Papoular interaction). Reasonably reliable predictions seem to emerge by extremizing this free energy (in 2-dimension) either numerically, or reducing the problem to a single dimension (by a suitable transformation of the coordinates) or by introducing an effective free energy which on one hand replaces the geometrical pattern and on the other does not pay attention to the actual transient director structure near the surface within a typical length scale determined by the geometric pattern in the real system. It is now conjectured, based on such theoretical investigations, that there are possibilities of zenithal bistability of these films (meaning that there are atleast two distinct (stable) director configurations lying within the two dimensional plane perpendicular to the

direction of the stripes on the grating surface) which can be exploited.

In this context of the above developments, the objective of the work reported in this Chapter is three fold: To try the extremization of the free energy of the system through the numerical procedure offered by Monte Carlo simulation, mimicking the elastic and surface effects through the known introduction of equivalent lattice-based interactions (in 3-dimension) among mesogenic units and of surface anchoring; to investigate the variation in the director structures as variation of averages over corresponding canonical ensembles covering a range of temperatures for a given set of boundary conditions; and finally to compute free energy profiles of this simplified model using entropic sampling techniques. We present a brief overview of recent work on these fascinating confined structures in the next section, before presenting the results of our simulations.

With these objectives, two such systems are studied. The first system comprises of a nematic LC cell confined between a flat substrate (with variable anchoring direction) and a grating surface with a sinusoidal groove (defining its geometric structure) and alternating regions of locally homeotropic and planar anchoring conditions on the sinusoidal surface. The period of the chemical pattern is half of that of the geometrical structure. We investigate this model also for the effect of relative phase shift between the physical and chemical patterns. We compare the results of these simulations with predictions from analysis based on continuum model. The second system is a liquid crystal film pasted over a spherial substrate. The NLC film experiences a radial anchoring condition at the substrate with variable strength, while the outer layer of the film experiences free boundary conditions. The interest in this system arises from the variation in the director configuration as studied as a function

of temperature and the radial anchoring strengths.

5.1 Nematic liquid crystals confined to geometrically and chemically patterned substrates

Nematic liquid crystals in contact with solid substrates are extensively used in display devices, like the twisted nematic configurations between flat substrate surfaces. The application of small external field is sufficient to change qualtatively the equilibrium director configurations dictated by the substrates, and thus leading to dramatic changes in the optical properties of the nematic cell. But several inhomogenities do occur naturally as a result of surface treatments like rubbing, needed to induce necessary boundary conditions. In most of the cases such inhomogenities do not reflect in the bulk properties of the nematic cell as the length scales of such patterns are very small compared to the thickness of the cell and also to the wavelength of the visible light. More recent developments however have demonstrated that surfaces patterned with large periodicity are of considerable interest from technological point of view like, for example, in flat panel displays with wide viewing angles ([6] and references therein). In view of their potential technological importance, it is essential, from the basic science point of view to understand the anchoring effects in detail, and also investigate possible phase transitions between various nematic textures induced by non-uniform surface interactions. Moreover, these systems could prove to be more curious if they are found to exhibit bistable nematic states with two different director orientations possible at same energy [7–11]. Whereas many experimental and theoretical studies have concentrated on either geometrically [12–18] or chemically patterned surfaces [19–24], nematic liquid crystals confined to both geometrically

structured and chemically patterned substrates have been objects of investigation only recently [22, 26–28]. For example, studies based on the continuum theory of nematic liquid crystals in contact with certain specific geometrically and chemically patterned substrates predicted possible transition between two nematic textures, the so-called H and HAN phases, on varying the thickness of the cell or changing the anchoring angle, θ_D at the top substrate as depicted in figure 5.1 [22, 26, 28]. In such studies, the interaction of the nematic liquid crystal system in contact with sinusoidal grating with alternating patterns of homeotropic and planar anchoring is accounted for, based on Frank-Oseen model for distortion free energy [29, 30], while the surface energy function is written in terms of Rapini-Papoular expression [31]. A brief description of these aspects is already given in Chapter 1.

The theoretical treatments normally proceed by reducing the dimensionality of the system for convenience of analysis by including translational periodicity along one of the directions, and sometimes by performing a conformal mapping appropriately to eliminate one more dimension. A recent innovation in this direction has been the proposal to eliminate the geometrical structure in preference to a planar surface, but modifying the surface interaction suitably to mimic the real system as closely as possible. The underlying argument relies on the observation that the effect of the patterned surface do not extend into the film beyond the length scale of the geometric structure and hence can be replaced by an effective free energy expansion. In all the cases the equilibrium configurations under different distorting conditions are obtained as corresponding to the minimum values of the effective free energy so proposed. One of the reason for attempting these simplifications has been the prohibitive effort involved in numerically tackling the problem within continuum approximation. This extremization procedure within this limit inter alia does not allow for possible ther-

mal effects which could be important in principle in real nematic samples. It could be also interesting from the point of our understanding the thermal effects on these systems to follow the formation of films as the system is cooled gradually from the isotropic phase.

Keeping these curiosities in view, we propose a lattice model to investigate the formation of such director structures and report their low temperature configurations. We invoke the Lebwohl-Lasher interaction between nearest neighbours, as usual, and impose the boundary conditions through ghost layers. Keeping in view the suggestions in the earlier work that determining free energy barriers and detecting metastable states are crucial to investigate such nematic devices (which are not possble to obtain via canonical sampling MC methods) [32], we apply here entropic sampling methods [34, 37, 38] in our work.

Our main interest here is to investigate the effect of such a confinement of nematic liquid crystal in a periodically patterned substrate on NI transition by applying modified *frontier sampling* method discussed in Chapter 3. We choose a specific geometerical and chemical pattern which has been recently analysed analytically via free energy mimization procedure, and study the effect of different control parameters on the formation of the film as the temperature is cooled, and investigate the stable structures at very low temperatures. We compute the development of free energy surfaces and correlate it with the distribution of different microstates of different types of order but with the same energy, collected in the entropic ensemble.

5.1.1 Model and Simulation Methodology

As the first system of study, we choose the nematic liquid crystal embedded between two substrates, schematically shown in figure 5.1. This system was investigated earlier based on the minimization of the relevant free-energy [26, 28]. It was concluded that there exist two distinct director configurations depending on the tilt angle introduced by the top layer θ_D (strong anchoring). For $\theta_D = 0$ it is predicted that the film will be essentially in the homeotropic (H) configuration but for a small thickness near the bottom layer, wherein the configurations change to match the boundary conditions. For a value of $\theta_D \neq 0$, and beyond a threshold value, the configuration is expected to undergo a transtion to a second structure, called hybrid aligned nematic (HAN) as is illustrated in the figure 5.1.

We use Lebwohl-Lasher potential [35] to describe the interaction between two nearest neighbouring mesogenic units placed on such a cubic lattice. The Hamiltonian is given by:

$$H = -\sum_{\langle i,j \rangle} \epsilon_{ij} P_2(cos\theta_{ij}) \tag{5.1}$$

Here $\epsilon_{ij} = \epsilon$ if two liquid crystal molecules are the nearest neighbours, and 0 otherwise; $\epsilon_{ij} = \omega$, the anchoring strength, if one of the nearest neighbours is a substrate molecule. ω varies between 0 and 1. The top layer is a solid substrate inducing strong anchoring ($\omega = 1$) at an angle, θ_D as shown in the schematic figure 5.1 ([22, 26, 28]). A sinusoidal pattern referred to above is carved out of the bottom layers (say, with amplitude, A) along the x-axis. The thickness of the cell, D along the z-direction is taken to be large compared to the amplitude of the sinusoidal pattern. The surface induced interaction is invariant along the y-direction.

These results are obtained under the simplifying condition that the cell thickness is much larger than the period of the sinusoidal grating at the bottom surface. Fur-

ther, the amplitude of the sinusoidal geometric structure is supposed to be a very small fraction of its wavelength. Now, in order to mimic this scenario on a lattice model, we choose a cubic lattice of size $16 \times 4 \times 66$, in the notation of x, y and z dimensions shown in the figure 5.1. We introduce a sine wave extending over 16 lattice points in the x-dimension, and a film thickness (z-direction) of 66 units. While the y-dimension was argued to be unimportant since the problem under simplifying assumptions is reducible to x-z plane, we extend the lattice along y-direction also over 4 units, in order to facilitate the interactions among different mesogenic units to take place in 3-dimensional space. Periodic boundary conditions are applied along x and y directions. The amplitude of the sinusoidal grating was initially chosen to be 2 units. While such a choice does not implement the geometrical constraints implied in figure 5.1 accurately due to the limitations introduced by the discretization of space into lattice points, it does capture essential features of the underlying model, the assumption in the continuum treatment being that any arbitrary distribution over the grating period can always be effectively taken into account by introducing an effective tilt angle (say, θ_D) for purposes of predicting the bulk behaviour of the film. The focus of this simulation is thus more on the process of formation of the director structures as nematic phase forms, and on the realizability of H and HAN structures at low enough temperatures, as were predicted by continuum models.

We consider two model systems in the present work according to the phase shift introduced between the chemical and geometrical patterns on the bottom substrate, see figure 5.2. In Model A, the chemical pattern is in certain phase with respect to the geometrical pattern. Homeotropic alignment is induced at crests and troughs of the sinusoidal wave each for a period of one fourth of the period, while in the other regions locally planar alignment is imposed. In Model B, the chemical pattern is shifted by

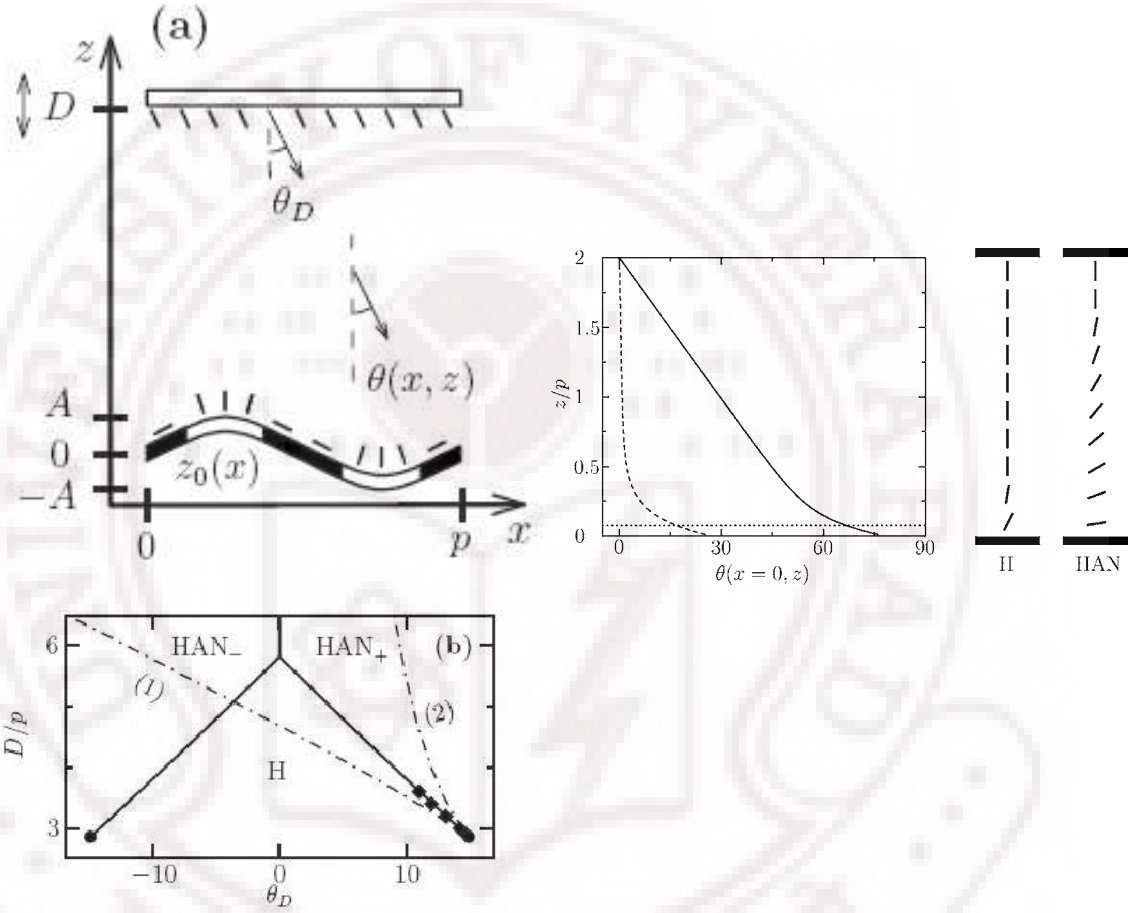

Figure 5.1 Nematic liquid crystal cell confined to a sinusoidal substrate with chemical pattern on it (left) [28] and nematic director structures obtained by changing the angle,θ_D (right) [26]. The phase diagram predicted by continuum theory showing phase transitions between H and HAN phases (bottom)

one-eighth of the wavelength with the geometrical pattern relative to Model A. The anchoring directions in the two models are shown in the figure 5.2.

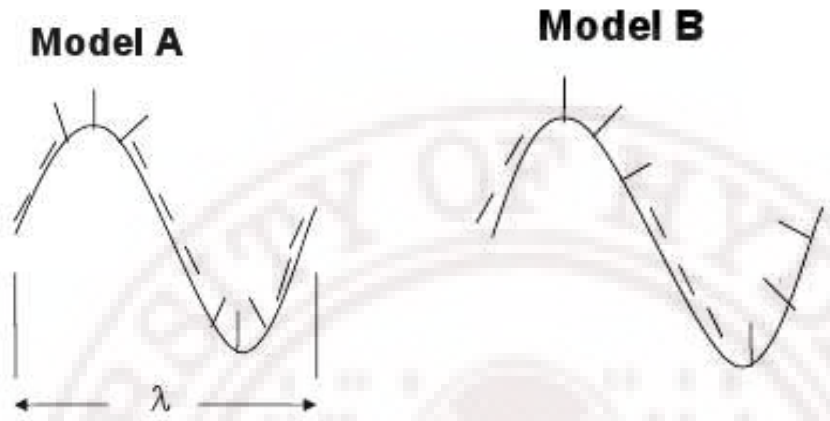

Figure 5.2 Model A(left): Chemical pattern is in phase with the geometrical pattern; Model B (right): chemical pattern is shifted by $\lambda/8$ with respect to geometrical pattern

We employ the *frontier sampling* method as described in Chapter 3 [33, 34, 36] to study the system for different angles, θ_D (between 0^0 and 45^0) in the nematic region. We compute the density of states and hence free energy profiles of the two systems. From the entropic ensemble of states, we obtain as usual the canonical ensemble of states at different temperatures. Thus for each value of θ_D, we compute equilibrium averages of different relevant physcial observables as a function of temperature. We also examine the distribution of different regions of energy and look for correlations of these features with corresponding regions in the free energy profiles.

5.1.2 Results and Discussion

In the present work, we have simulated a film of size $16 \times 4 \times 66$ lattice units along x-, y- and z- directions, respectively. The substrates are introduced at $z = 1$ and $z = 66$ layers by considering an additional layer of lattice points on either sides.

The orientation of mesogenic units on these substrate layers are held fixed as per the prescribed orientations, and are not involved in the MC steps. At the top substrate, i.e., at $z = D$, anchoring strength ω is set to unity and the anchoring angle θ_D is chosen at the values (0^0, 10^0, 20^0, 30^0 & 45^0) for carrying out simulations. We keep the groove depth, A to be 1 lattice unit at $z = 0$. We try to adhere to the prescribed inequalities among different scales, as were found necessary in the analysis of the model as per the continuum theory. The relevant physical properties that describe adequately the symmetry of the director field arising from orientational alignment of uniaxial molecules are the extent of uniaxial order and the possible loss of cylindrical symmetry around the principal director represented by the phase biaxiality parameter. The corresponding variance representing different nematic susceptibilites, and the energy fluctuations (specific heat) are the other important indicators that can be computed from equilibrium ensembles derived from these simulations.

Figure 5.4 represents the logarithm of DoS ($\alpha(E)$) and energy histogram ($H(E)$) obtained from the modified *frontier sampling* method discussed in Chapter 3 for Model A (top) and Model B (bottom) respectively, when $\theta_D = 0$. The energy histogram $H(E)$ is reasonably flat over the desired range of energy.

We depict the thermal behaviour of the two types of confined liquid crystal systems (models A & B), by plotting C_V versus temperature in each of the cases, for different tilt angles θ_D at the top flat surface. These are obtained by constructing canonical ensembles of the corresponding systems at different temperatures (with a temperature resolution of 0.001), and derived from energy fluctuations. Both the samples indicate a well defined IN transition, and the transition temperatures are very weakly, though measurably, depending on the tilt angle θ_D. In Model A, where a specific phase shift between the chemical and geometrical patterns has been chosen (with the hills and troughs of the sine wave located at the centres of homeotropic an-

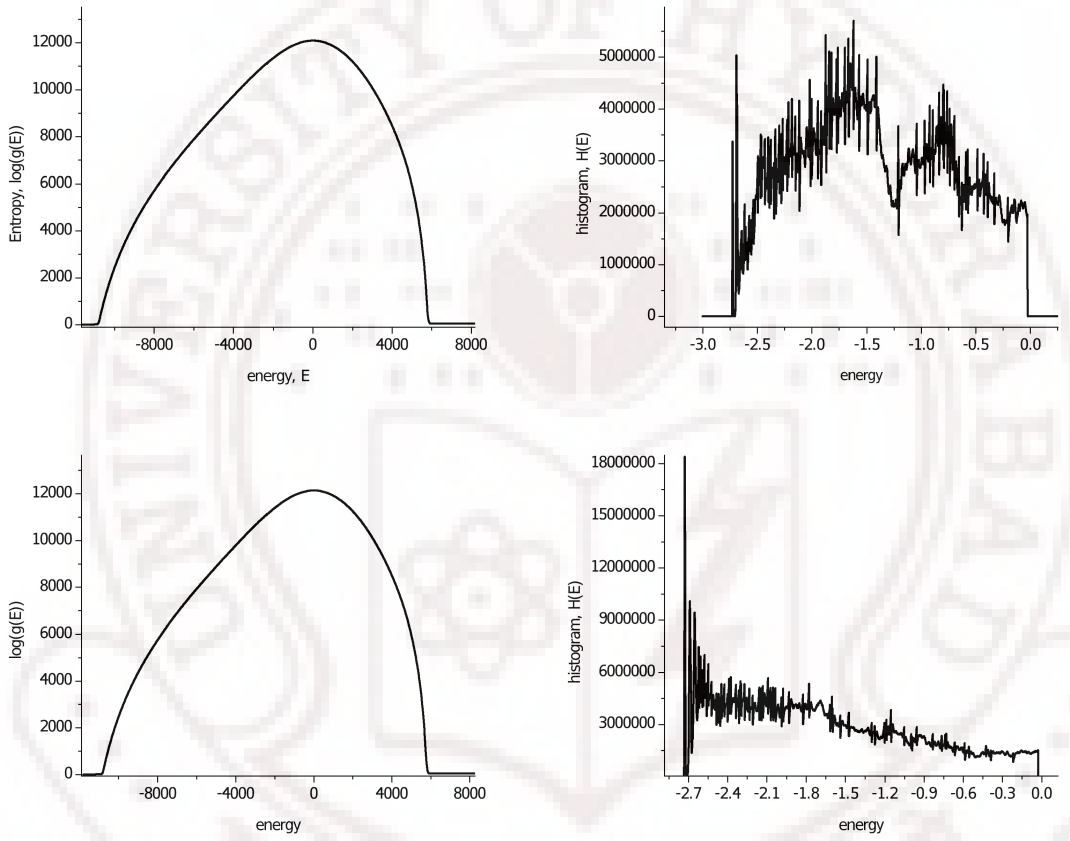

Figure 5.3 Logarithm of density of states, $\alpha(E)$ (left) and histogram of energy collected during the simulation $H(E)$ (right) as a function of energy E of the sample for a cubic lattice of size $16 \times 4 \times 66$ of Model-A (top) and Model-B (bottom), respectively, with $\theta_D = 0^0$.

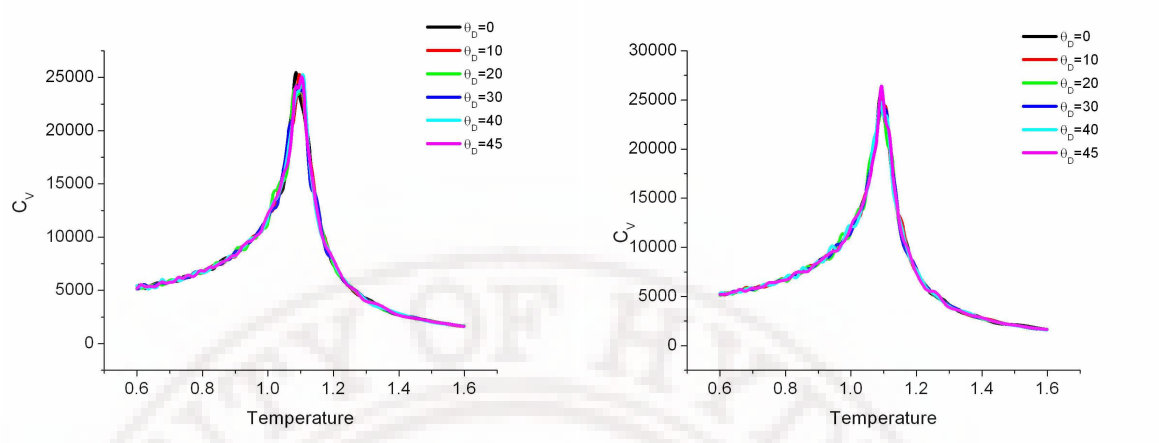

Figure 5.4 Variation of specific heat profiles as a function of temperature as we increase the angle θ_D from 0^0 to 45^0 for Model A (left) and Model B (right).

choring, fig 5.2), the general trend due to variation of θ_D away from 0 (i.e., away from homeotropic condition) is to slightly increase the transition temperature by about 0.02. Interestingly, the corresponding change in the transition temperature in Model B is in the opposite direction, i.e., the transition occurs at lower temperatures with increase in the tilt angle.

Figure 5.5 shows the uniaxial and biaxial order parameters as a function of temperature for four values of θ_D (0^0, 10^0, 20^0, 30^0 & 45^0) for Model A. As the anchoring angle of the top substrate θ_D increases from 0^0 to 45^0 (i.e., as the anchoring deviates gradually away from homeotropic condition), the uniaxial order parameter softens gradually, though slightly. For all θ_D values, the phase biaxiality in Model A increases slightly near the NI transition, to about 0.12, but does not persist at much lower temperatures except near, $\theta_D = 45^0$. In Model B (which results from a shift of chemical pattern with respect to the geometrical structure, relative to Model A, figure 5.2, the biaxiality is found to persist till lower temperatures for all values of

θ_D including zero, see figure 5.6; i.e., even when the anchoring at the top substrate is homeotropic, biaxiality persists in the system (see, figure 5.7). The amount of biaxiality in this system (Model B) increases as the θ_D increases further to 45^0 (from 0.05 to 0.14). The uniaxial order parameter changes from about 0.73 to 0.68 during this variation of θ_D, for Model B.

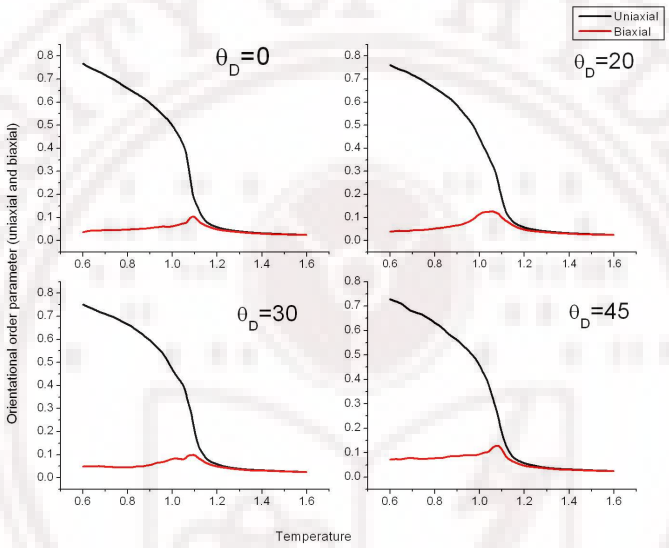

Figure 5.5 Uniaxial (black) and biaxial (red) order parameters as a function of temperature for $\theta_D = 0^0$, 20^0, 30^0, 45^0, respectively for Model A.

Figure 5.8 depicts the temperature variation of fluctuations in the uniaxial order parameter for Model A (left) and Model B (right), for θ_D values ranging from 0^0 to 45^0. Figure 5.9 shows correspondig fluctuations in phase biaxiality parameter. In general the effect of increasing θ_D is to make the fluctuations more dominant, and persistent till lower temperatures in both the models. However, Model B seem to be qualitatively different. In this case fluctuations in both the parameters increase considerably with θ_D, and persist very significantly at lower temperatures (see figure 5.8 and 5.9 for comparison). It may also be noted that these fluctuations are abnormally high for two particular values of θ_D (20^0 and 40^0) in both the models.

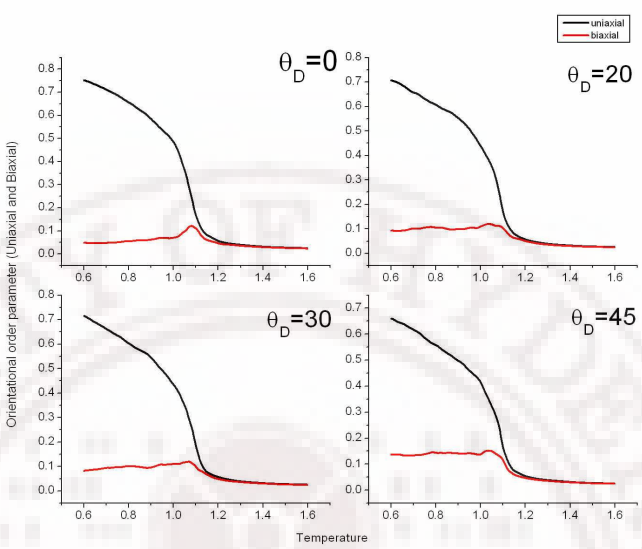

Figure 5.6 Uniaxial (black) and biaxial (red) order parameters as a function of temperature for $\theta_D = 0^0$, 20^0, 30^0, 45^0, respectively for Model B.

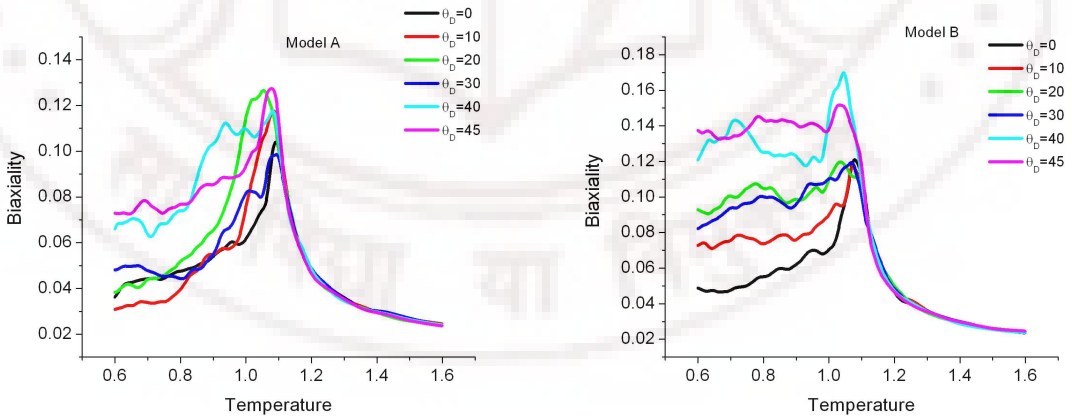

Figure 5.7 Biaxiality parameters obtained for different angles, $\theta_D(0^0$ to $45^0)$ at the top substrate for Model A (left) and Model B (right) respectively

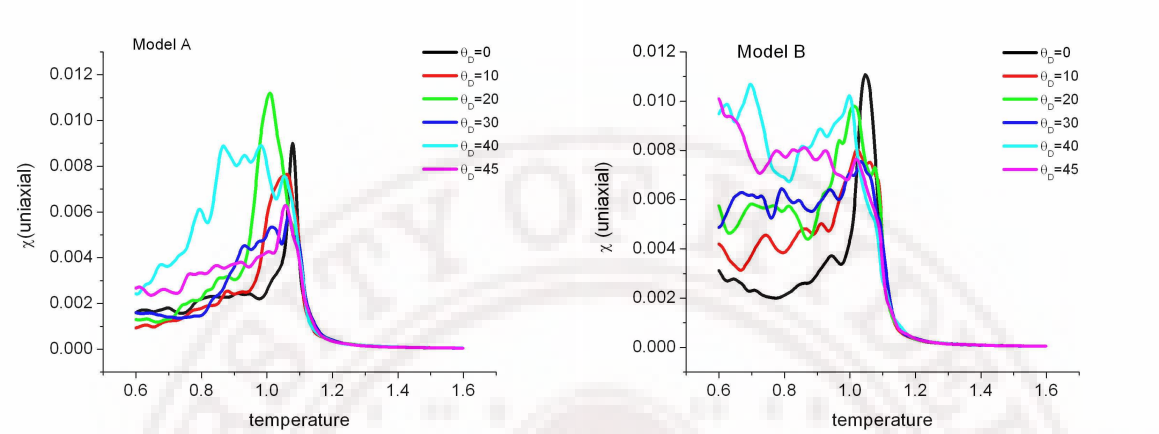

Figure 5.8 Fluctuations in the uniaxial order parameter for various values of $\theta_D(0^0$ to $45^0)$ for Model A (left) and Model B (right), respectively.

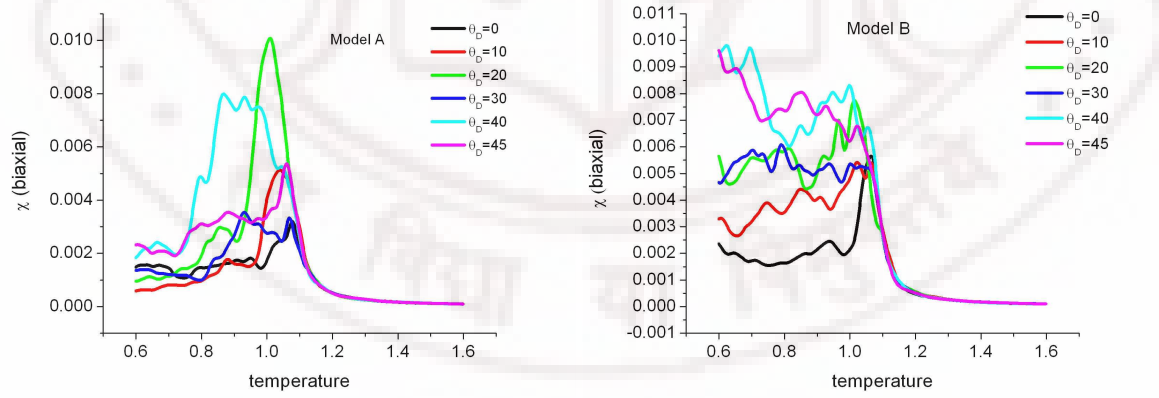

Figure 5.9 Fluctuations in the phase biaxial order parameter for various values of $\theta_D(0^0$ to $45^0)$ for Model A (left) and Model B (right), respectively.

The average of layer-wise director orientations corresponding to each x-y plane in the system is calculated, and its angle with respect to the z-axis is plotted against the layer number as a function of θ_D. For clarity the variation of this angle for only alternate layers is presented in figures 5.10 and 5.11 for Model A and Model B, respectively. These values are computed by reweighting the data at $T = 0.6$ to construct the corresponding canonical ensemble. According to the predictions of the continuum theory, the director structures at $\theta_D = 0$ should exhibit H phase, wherein the homeotropic alignment of the director percolates throughout the cell except, for a few layers in the immediate vicinity of the bottom substrate at $z = 0$. But we find that, even at the fairly low temperatures Model A, for example, deviates from the H phase. For example for the case of $\theta_D = 0$ (Model A, figure 5.10), there is a deviation to the extent of about 20^0 in the middle layers. At layer index 1 (corresponding to layers in the vicinity of z=D), the angle is close to zero, and effective tilt angle (θ_{eff}) due to the corrugation at $z = 0$ also seems to be close to 0^0. However the director configuration shows that the director is tilted away from normal in the regions away from anchoring influences. Simulations with decreasing thickness bring down the extent of deviation, as does further lowering of temperature at the same thickness. Within Model A, figure 5.10 shows the variation of director angle for different anchoring angles θ_D. It may be seen that director orientation changes gradually from the anchoring angle at the top substrate towards the appropriate θ_{eff} value at the bottom surface, though not linearly.

In contrast, in the case of Model B (figure 5.11) the effective tilt angle due to the bottom substrate seem to depend on the anchoring angle θ_D at the top flat substrate. Of course this case was not considered earlier in the continuum model and therefore can not be compared with respect to expected variations. For example for $\theta_D = 0$ (Model B), the director tilt increases progressively as the grating surface is reached (to

a value of about 30^0) before it drops suddenly to about 20^0 near the grating surface. Such variations of layerwise director orientations, for different θ_D values in this model are depicted in figure 5.11. The conclusion from Model A, for which the expected configuration for $\theta_D = 0$ is already predicted (viz, H phase), is that in real systems at finite temperatures, incorporating a Hamiltonian model which permits interactions among mesogenic units spanning the 3-dimensional space, H-phase seems to be an idealization realizable when fluctuation phenomena do not play any significant role, and the equilibrium structure, being determined by microstates strictly comparing to the free energy minimum, does not exhibit therefore any deviations.

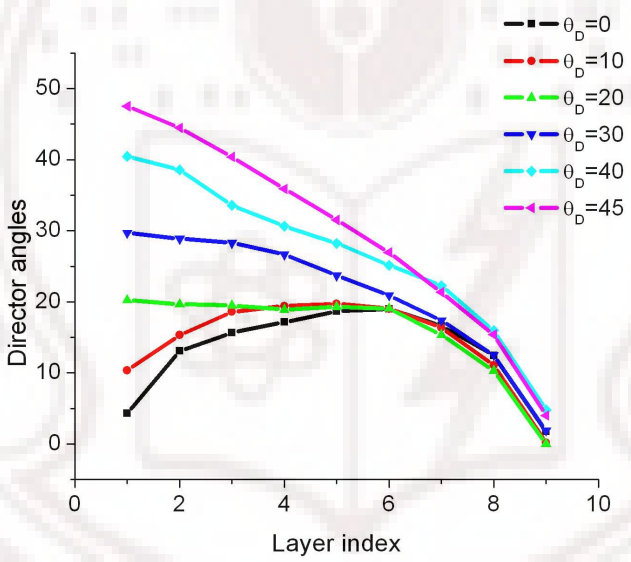

Figure 5.10 Layer-wise director angles at temperature $T = 0.6$ for $\theta_D(0^0$ to $45^0)$ for Model A. Indexing of the layers started with top substrate $z = 0$. Only alternate layers are plotted for clarity.

By extracting canonical ensembles at different temperatures (with a temperature resolution of 0.001) we computed the variation of the layer-wise director angle across the width of the film and plotted them in figure 5.12 as a 3-dimensional stack plot, to indicate the development of the structure of the film as the sample is cooled to a more

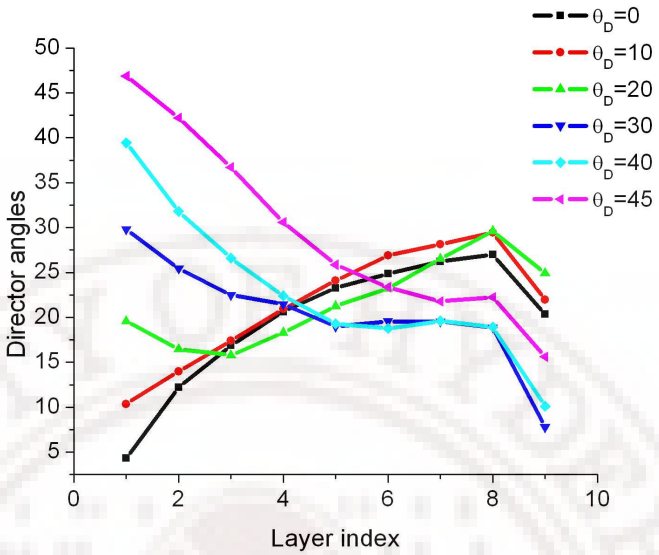

Figure 5.11 Layer-wise director angles at temperature $T = 0.6$ for $\theta_D(0^0$ to $45^0)$ for Model B. Layers are indexed starting from top substrate (z=D) to bottom (z=0) substrate. Only alternate layers are plotted for clarity

ordered nematic phase. At least in Model A for which predictions from continuum theory are available, it may be seen that at finite temperatures, (particularly when the nematic order is not saturated and itself fluctuating in amplitude), the description of the configuration as H-phase is not realisable, and perhaps as the nematic order saturates at very low temperatures (where continuum theory predictions are expected to be valid) the H-phase tends to form asymptotically. For example, at a fairly low temperatures where the nematic order is about 0.75 (at $T = 0.6$; figure 5.5), the director orientations in the middle layers differ significantly from the homeotropic arrangement (figure 5.12).

Figure 5.13 depicts the distribution of microstates contained in the entropic ensemble in Model A and Model B (at $\theta_D = 0^0$) with respect to their energy sorted as per their uniaxial and phase biaxial order parameter values. Figure 5.14 presents these distributions for the case of $\theta_D = 45^0$. Noting that the extent of dstribution of

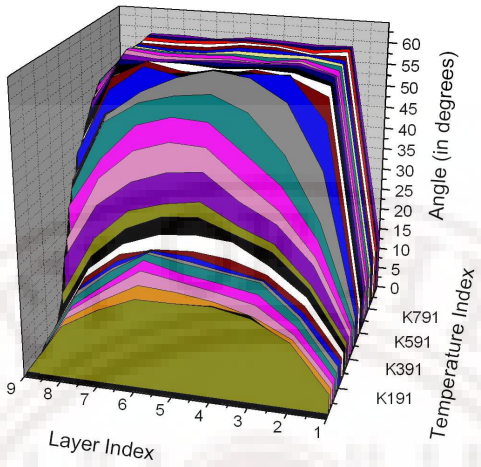

Figure 5.12 Layer-wise director angles at various temperatures for $\theta_D = 0^0$. Layers are indexed starting from top substrate (z=D) to bottom (z=0) substrate.

these states over the corresponding order parameters at a given energy (bin) value is a measure of their susceptibility, it may be noted that in Model A homeotropic anchoring at the top substrate ($\theta_D = 0^0$) has a tendency to form a fairly pure uniaxial phase: the fluctuations in this case with respect to uniaxial order diminish noticeably at low temperatures while there is no significant distribution of microstates in this system with respect to biaxiality parameter (figure 5.13). In contrast, for the same Model at $\theta_D = 45^0$, figure 5.14, the uniaxial order has higher degree of fluctuations, while permitting microstates distributed, somewhat widely, over a finite range of biaxiality parameter. This suggests the onset of a small biaxiality with relatively shallow free energy profiles allowing for larger excursions in the order parameters. In Model B, on the other hand, similar scenario (corresponding to Model A at $\theta_D = 45^0$ already exists at $\theta_D = 0^0$ (figures 5.13 and 5.14). With increase of θ_D to 45^0, this model acquires a much wider distribution of microstates with respect to both the order prameters

(figure 5.14), and more prominently the biaxiality parameters has a higher average value with longer range of fluctuations. These observations are of course borne out by the corresponding derived variables (figures 5.5 and 5.9).

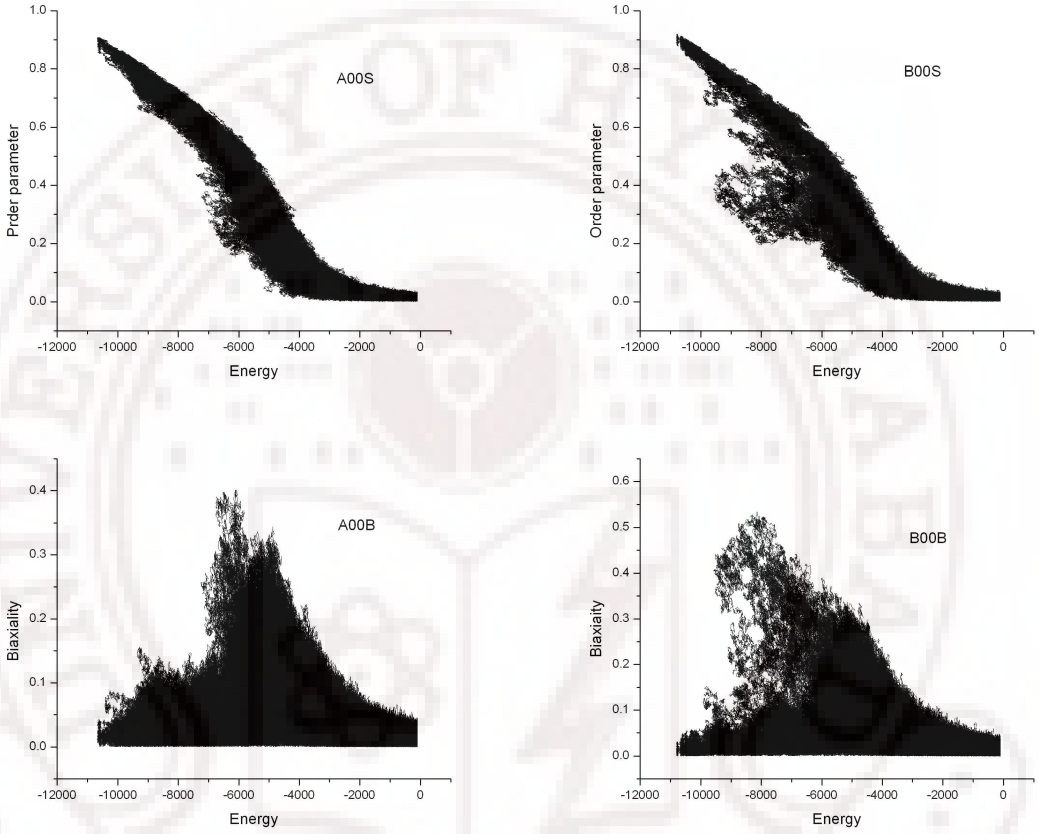

Figure 5.13 Microstates pertaining to uniaxial (top) and biaxial (bottom) order parameters obtained from the non-Boltzmann ensembles for $\theta_D = 0^0$ for Model A(left) and Model B (right) respectively.

Making use of the DoS of these systems, we compute the free energy as a function of, say, the unixial order in both the models (at $\theta_D = 0^0$ and 45^0), for various values of temperatures bracketing the IN transition. Figures 5.15 and 5.16 show a stacked plot of these profiles. Each of these graphs show the gradual shift of free energy minimum at very low order values (in the isotropic phase) to more ordered phases as

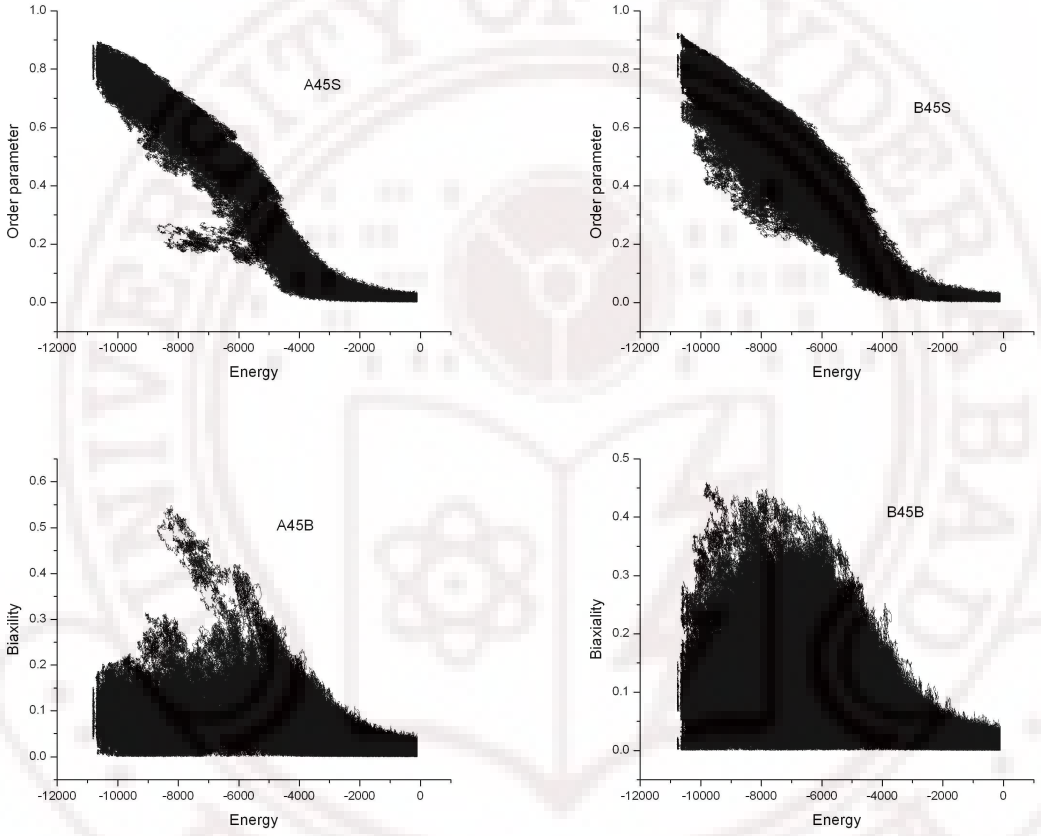

Figure 5.14 Microstates pertaining to uniaxial (top) and biaxial (bottom) order parameters obtained from the non-Boltzmann ensembles for $\theta_D = 45^0$ for Model A(left) and Model B (right) respectively.

the temperature is cooled.

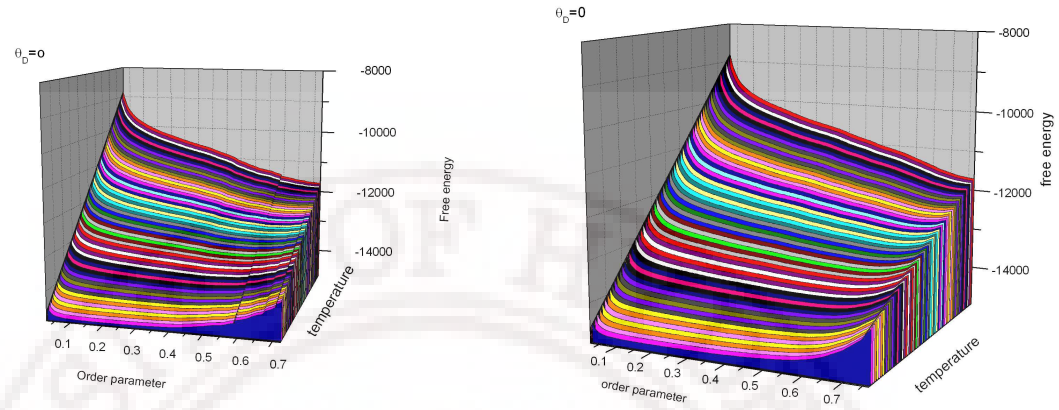

Figure 5.15 Free energy profiles for $\theta_D = 0^0$ as a function of order parameter and temperature for Models A (left) and B (right) respectively

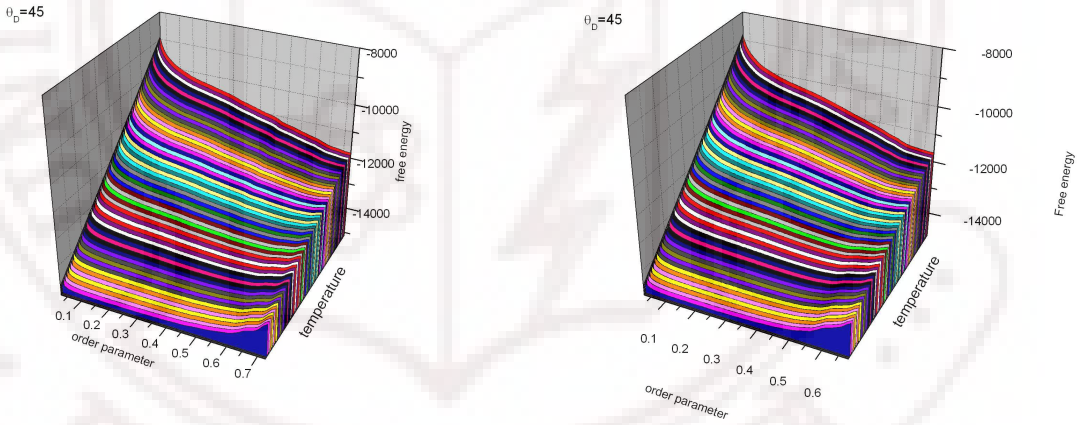

Figure 5.16 Free energy profiles for $\theta_D = 45^0$ as a function of order parameter and temperature for Models A (left) and B (right) respectively

These MC simulations based on a simple lattice model, mimicking the boundary conditions of Model A for example, show that the H phase expected of the Model from considerations of a two dimensional system on grounds of continuum theory is an asymptotic limit of the chosen model at very low temperatures. In nematics with modest amount of orientational order the director configurations deviate considerably.

Secondly, the relative phase of the geometric structure with respect to the chemical pattern has significant effect on the formation of director structures, as well as the apparent θ_{eff} experienced at the lower substrate (figure 5.11). Further, such modifications seem to induce phase biaxiality in the system. This work has been reported recently [40, 41].

5.2 Liquid crystals confined to spherical substrates

In this section, we consider the case of a thin film of liquid crystal covering the surface of a spherical substrate. The substrate induces homeotropic anchoring (radial alignment on the spherical surface), while the outer surface of the liquid crystal experiences free boundary conditions. Such curved films of LC's are found on porous surfaces. As per the notation of the previous section, this corresponds to a geometrically structured substrate with homogeneous chemical texture. The objective is to study the effect on the NI phase transition behaviour of the system as one attempts to achieve delicate balance between the radial ordering induced by the surface interaction and the natural tendency of the system to align uniaxially as the nematic phase forms. To quantify the relative importance of these two interactions in a given macrostate, we define two order parameters appropriately to distinguish between uniaxial and radial ordering of the liquid crystal molecules. The factors that influence the above balance include the radius (r) of the substrate and the anchoring strength at the surface (ϵ_s) on one hand determining the nature and extent of elastic distortion induced in the system, and on the other the thickness of the film (d) controlling the inherent ordering mechanism. We study the thermal behaviour of this film at different anchoring strengths for a film geometry chosen after experimentation with respect to r and d to facilitate curious observable anchoring effects. Experimental and theoretical studies on such systems, restricted to different host geometries, were reported earlier, and continue to excite interest in the NI transition phenomena in such confined systems [42, 43].

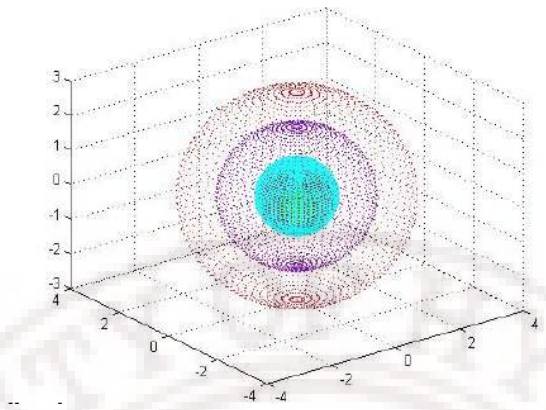

Figure 5.17 Schematic model of the thin liquid crystal film (violet) pasted on a spherical substrate (cyan). Outer surface (red) induces free boundary conditions

5.2.1 Lattice model

This system is modelled on a three dimensional cubic lattice. We consider a sphere embedded inside a cubic lattice, see figure 5.17; the lattice sites interior to the sphere form a core of radius r, representing the substrate. All the liquid crystal molecules located inside this sphere have frozen orientations, directed radially towards the center of the sphere. Chosen number of layers (say, d lattice spacings) of the lattice sites concentric to the substrate outside the sphere, constitute the thin spherical liquid crystal film, and each such site holds a freewheeling liquid crystal molecule. The substrate particles impose homeotropic boundary condition on the inner surface of the curved thin film; the outer surface of the film is allowed to experience free boundary conditions. The substrate molecules do not obviously participate in the Monte Carlo steps but their presence is felt implicitly due to the homeotropic boundary conditions they impose onto the innermost layer of the film. Similarly, all the lattice sites falling outside the spherical substrate and the thin film of molecules (i.e. those molecules whose position vectors have magnitudes greater than $r + d$) are considered as 'ghost spins'. These ghost spins do not take part in the Monte Carlo steps and their presence

is not felt by the outermost layer of the liquid crystal film. For simplicity we let the interactions between the mesogenic units be described by the LL potential. Thus the random walk in the configurational space of this system is restricted to changes in the orientation of the LC molecules confined in the thin spherical shell constructed as above. The mesogenic unit placed at each lattice site in this film is as usual represented by a headless unit vector u_i, and typically represents a group of liquid crystal molecules (mesoscopic level description). The Hamiltonian is expressed as a sum of pair-wise nearest neighbour interactions among these units, given by

$$U = -\sum_{i,j} \epsilon_{ij}(\frac{3}{2}(u_i.u_j)^2 - \frac{1}{2}). \tag{5.2}$$

We set the energy scale by choosing $\epsilon_{ij} = 1$, when the spins i and j are nearest liquid crystal neighbor molecules. $\epsilon_{ij} = \epsilon_s \in [0, 2]$, when the spins i and j are at the interface of the liquid crystal and substrate molecules. $\epsilon_{ij} = 0$, when the interacting units are not nearest neighbors, as well as when the LC units are at the outer surface. The temperature T in the simulations is as usual expressed in reduced units.

The substrate imposes radial order on the film while the mutual interactions among the liquid crystal molecules tend to align them uniaxially when $T \leqslant T_{NI}$. These two ordering mechanisms have variable influence on the liquid crystal film depending on the relative values of uniaxial order induced (via the lower value of T chosen) and the influence of the inner spherical surface via the anchoring strength, ϵ_s. We perform Monte Carlo simulation of this model by employing the Wang-Landau method [33, 34] to study the effect of such competing influences on the isotropic-nematic transition and the resultant low temperature nematic ordering. We calculate relevant thermodynamic properties, like orientational order parameter (both axial as well as radial), average energy $\langle E \rangle$, specific heat C_V and nematic susceptibility χ (say, of uniaxial order).

5.2.2 Monte Carlo Simulation

Initially we explored the thermal behaviour of the system by canonical sampling method, as a function of the surface anchoring strength ϵ_s systematically varied over the range $[0, 2]$. We found that the T_{NI} shifts towards higher temperatures with increase in the anchoring strength as could be noted from the C_V profiles. After experimenting with canonical methods to obtain optimum values for r and d which can yield interesting results at low temperatures in the nematic phase, we proceed to investigate this film with the chosen geometry employing WL algorithm [33, 34] to build entropic ensembles. We thus observe variation of different physical parameters with temperatures with high resolution, as well as obtain the collection of microstates of the entropic ensemble to examine them as sorted out with respect to different order parameters. The details are presented below.

5.2.3 Results and Discussions

We thus consider a thin LC film of thickness $d = 3$ lattice units confined on a spherical substrate of radius $r = 3$ lattice units. Due to the lattice nature of the model the substrate surface as well as the film thickness will not be smooth, as has been the case in all such toy models investigated earlier with lattice Hamiltonians. The number of mesogenic units participate in the MC simulations is 800. We applied Wang-Landau algorithm to study this confined system with the surface anchoring strength ϵ_s varying from 0 to 2. A uniform non-Boltzmann ensemble of atleast three million microstates is generated as rule, while the production run was extended upto ten million microstates whenever the system seemed to exhibit frustration due to the competition between the two ordering mechanisms. Through the usual reweighting procedures canonical ensembles were extracted as a function of temperature with high resolution, and are

used to compute different physical variables of interest, as discussed below.

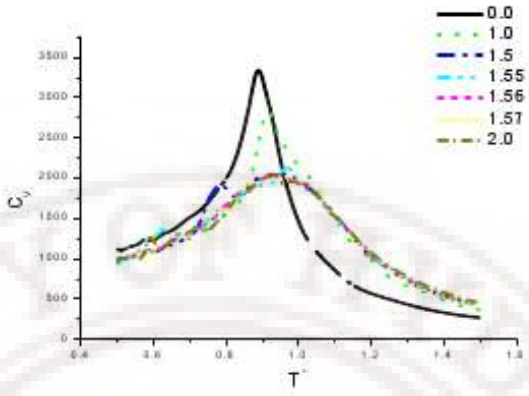

Figure 5.18 Specific heat C_V versus temperature for various values of anchoring strengths; C_V has been obtained from the energy fluctuations.

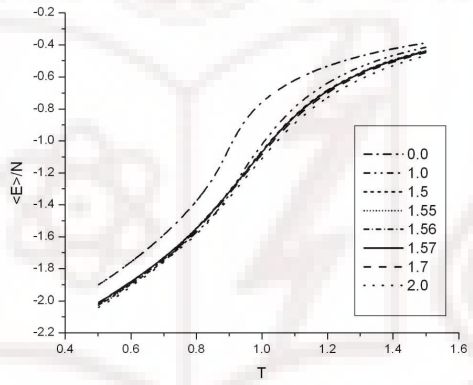

Figure 5.19 Average energy per particle $\langle E \rangle$ versus temperature for anchoring strength values $\epsilon_s = 0.0$ *to* 2.0

The variation of C_V with temperature as ϵ_s is increased (between 0 and 2) is shown in the figure 5.18. The peak of C_V centred at a temperature of about 0.9, and relatively quite sharp at $\epsilon_s = 0$ shifts to 0.92 (approximately) when the radial anchoring strength is set to unity, and the profile is broader. As ϵ_s is now progressively increased further, the profile degenerates into a broad hump centred roughly around 0.935. Thus according to the variation of energy fluctuation behaviour, the introduc-

tion of radial anchoring pushes the IN transition up percetibly as the influence of the boundary condition increases and the transition is smeared out at higher values of ϵ_s. The corresponding variation of the average energy of the system is also shown in figure 5.19. Now to capture the corresponding variation in the orientational order of the system, we introduce two order parameters: axial order (S_A) and radial order (S_R). S_A represents the degree of uniaxial order along the director $\hat{n}$, defined as

$$S_A = \frac{1}{N}\sum_{i=1}^{N} P_2[cos(\hat{u}_i \cdot \hat{n})] \tag{5.3}$$

where $\hat{u}_i$ represents the orientation of the mesogenic units at site i, and the summation is over the number N of units in the curved film. In the MC simulation a further averaging is of course carried out over the canonical ensemble. We introduce another order parameter (S_R) which is a measure of the degree of radial order present in the system, defined as

$$S_R = \frac{1}{N}\sum_{i=1}^{N} P_2[cos(\hat{u}_i \cdot \hat{r}_i)] \tag{5.4}$$

where $\hat{r}_i$ represents a unit vector located at the site i, and oriented radially at that site. Obviously in a large enough system (permitting adequate spatial averaging) perfect order of one type corresponds to the absence of the other. In real systems, and at finite temperatures, however non-zero values of both S_A and S_R can exist representing, quantitatively, the amount of the two types of the orders. We present the variations of S_A and S_R with temperatures (as ϵ_s is increased) in figures 5.20 and 5.20, respectively.

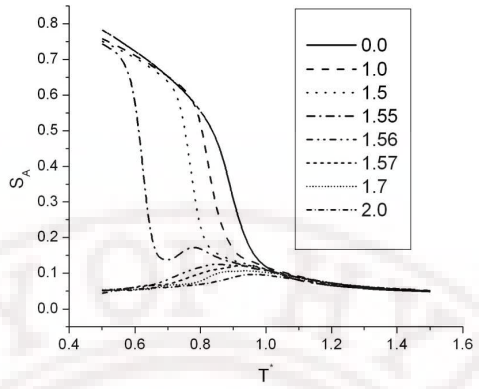

Figure 5.20 Axial orientational order parameter S_A versus temperature for various values of anchoring strengths $\epsilon_s = 0.0$ *to* 2.0.

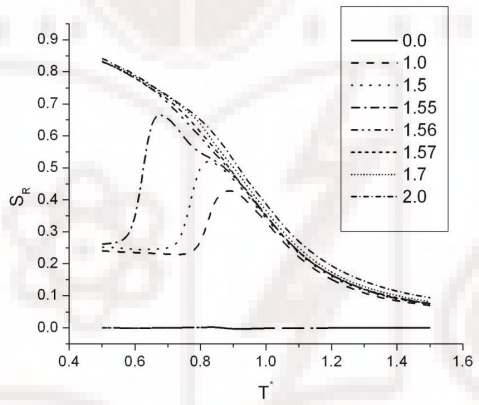

Figure 5.21 Radial orientational order parameter S_R versus temperature for various values of anchoring strengths $\epsilon_s = 0.0$ *to* 2.0.

At $\epsilon_s = 0$, i.e., in the absence of the anchoring influence of the surface, S_A shows a transitional behaviour corresponding to the IN transition. As expected S_R essentially remains zero for this case. As ϵ_s is now increased, the radial anchoring influences this transition differently as far these two order parameters are concerned. With increasing ϵ_s, as the sample is cooled from the isotropic phase, the radial order tries to build initially; After sufficient cooling, the extent of cooling required depending on the

value of ϵ_s, the radial order S_R abruptly drops to a low value (at about 0.25), with a concurrent and simultaneous increase in S_A. This may be seen as an initial formation of a paranematic order influenced by the surface anchoring, followed by the dominance of elastic properties at low enough temperatures. Data on these variations at different values of ϵ_s are shown in these figures, and the corresponding susceptibilities (χ_A and χ_R, obtained from the fluctuations of S_A and S_R) are plotted in figures 5.22 and 5.23. It may be seen from these plots that upto a value of $\epsilon_s = 1.55$, increase of ϵ_s from zero upwards encourages initially paranematic order, followed by a low temperature abrupt changes from radial to axial director structures. Such abrupt change also leave signatures in the corresponding susceptibilities. Beyond $\epsilon_s = 1.55$ this scenario

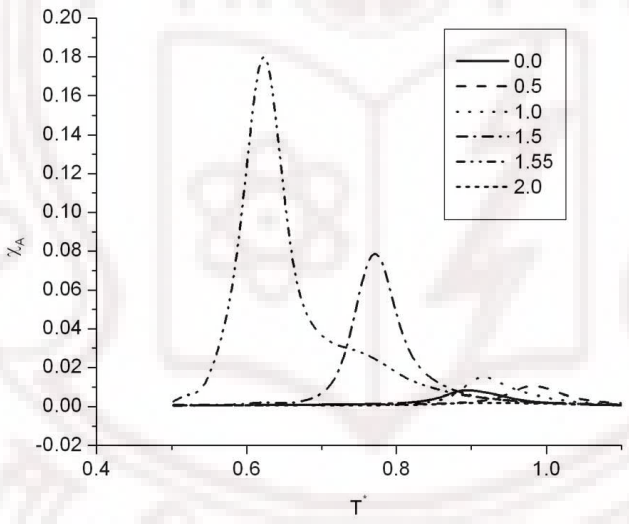

Figure 5.22 Fluctuations in the axial order parameter χ_A for anchoring strengths ranging from $\epsilon_s = 0.0$ *to* 2.0

undergoes a qualitative change. The paranematic radial order S_R building at the onset of IN transition continues to grow smoothly as the temperature is cooled, while the axial order S_A fails to build at low temperatures. Actually at $\epsilon_s = 1.56$, S_A tries to build to a nominal value (~ 0.1) before dropping down. As ϵ_s is varied to 2.0,

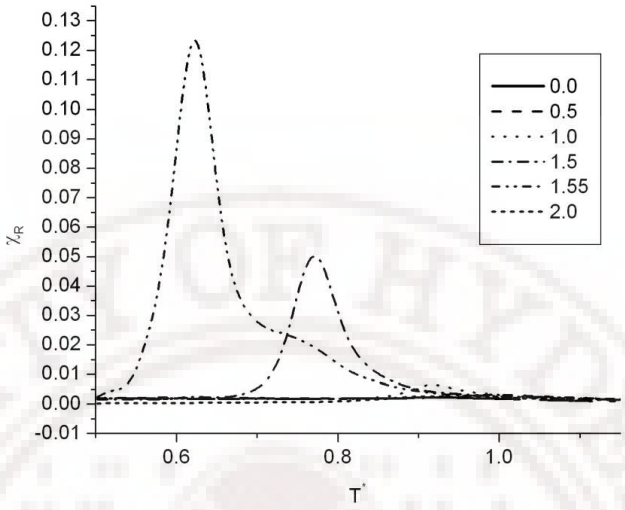

Figure 5.23 Fluctuations in the radial order parameter χ_R for anchoring strengths ranging from $\epsilon_s = 0.0$ *to* 2.0

it is just the smooth build up of radial order alone with decrease in temperature. The disappearence of the phase transitional behaviour, mentioned in connection with the temperature variation of C_V (figure 5.18), is also evidenced by the absence of susceptibility peaks (of S_A and S_R) beyond $\epsilon_s = 1.55$ (figures 5.22 and 5.23). These features are illustrated by plotting the temperature variation of S_A and S_R in the same plot, for chosen values of ϵ_s (figure 5.24). The qualtitative difference between the plots corresponding to $\epsilon_s = 1.55$ and $\epsilon_s = 1.56$ is evident. The microstates in the entropic ensembles of this system at three anchoring values ($\epsilon_s = 1.55$, 1.56 and 1.57) are depicted in figure 5.25, as distributed in the 2-d planes of $S_A - E$ and $S_R - E$ for each of the anchoring strengths. From the variation of the average energy with temperature (at $\epsilon_s = 1.55$), it was concluded that the density of states computed from WL algorithm spans microstates satisfactorily upto a lowest energy of the system equal to -1700. This corresponds to the ability of reweighting procedure to extend to a lowest temperatures equal to about 0.3. Thus all the temperature ranges reported

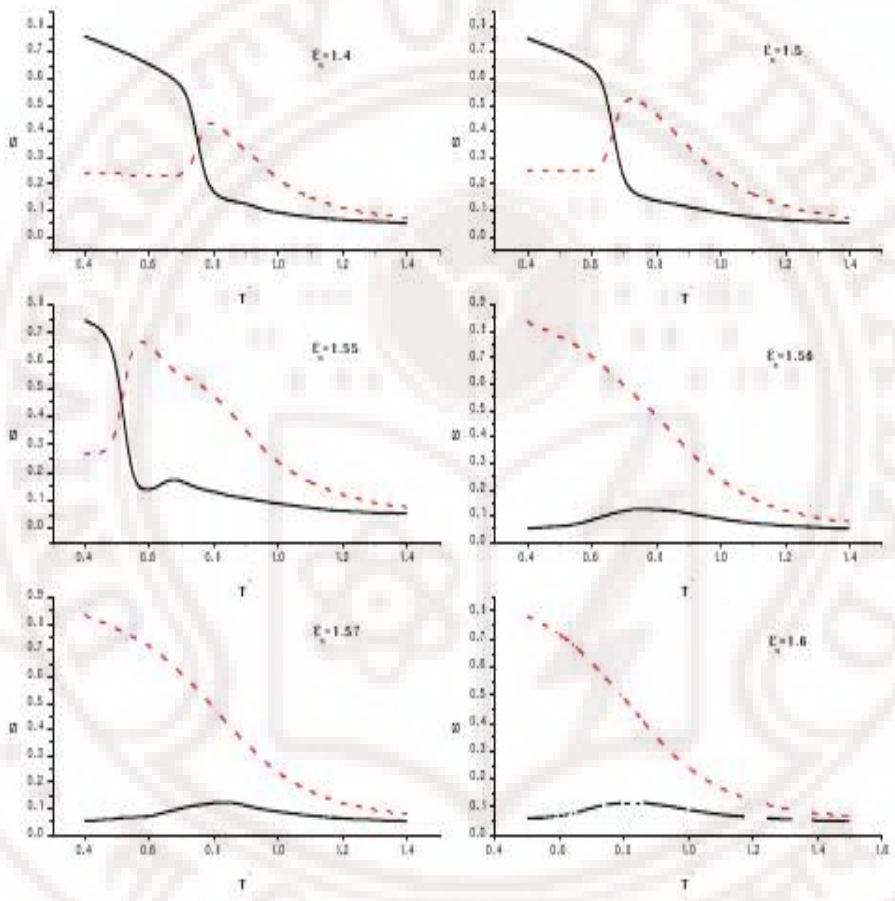

Figure 5.24 Variation of axial (solid lines) and radial order parameters (dotted lines) for anchoring strengths $\epsilon_s = 1.55,\ 1.56$ *and* 1.57

were restricted to a lowest temperature 0.4 or higher. Now, focussing on figure 5.25, and considering the distribution of microstates in the energy region upwards -1700, it may be seen that the average macroscopic behaviour of the system with respect to the temperature variation of S_A and S_R in the neighbourhood of $\epsilon_s = 1.55$ is borne out clearly by the distribution of hte microstates. Further it is very interesting to note that in these three sets of plots, there are certain (narrow) energy regions wherein the microstates are distributed with respect to these order parameters with distinct gaps in between. Since the variations in S_A and S_R are complementary in nature, this indicates that there are iso-energetic director structures with different degrees of order with no connecting microstates. This of course assumes that the collection of microstates in the entropic ensemble is exhaustive and representative. Considering the flatness of the histograms, and the number of microstates (10^7 states) collected, it is believed that these distributions do lead to the observations made above. The free energy profiles computed from the average energy and the density of states are plotted as a function of energy of the system at different temperatures (figure 5.26), showing progressive shift of the minimum to lower energies as the temperature is lowered. In the normal case of a system with a single (unique) order parameter representing the symmetry and director structure of the system, there exists a one-to-one mapping between the order parameters and energies, and hence these free energy profiles can as well be depicted with respect to the order of the system. However, in the present case of a special system with two competing parameters, one building at the cost of the other and with temperature dependence being influenced by the anchoring strength ϵ_s, such depiction of free-energy is not feasible, and perhaps not helpful.

Finally, we compute the quadrupolar perturbed ^2H NMR spectrum in the rigid lattice limit, assuming a typical quadrupolar interaction strength, and the ^2H nucleus to be on the rigid core of the rod-like molecule. Fig 5.27 shows such computed spectra,

as the order in the film changes from a perfectly axial to perfectly radial structure, indicating expected change in the NMR spectrum that can perhaps serve as a guide in an experiment. Considering this film as a nematic system cooled to low enough

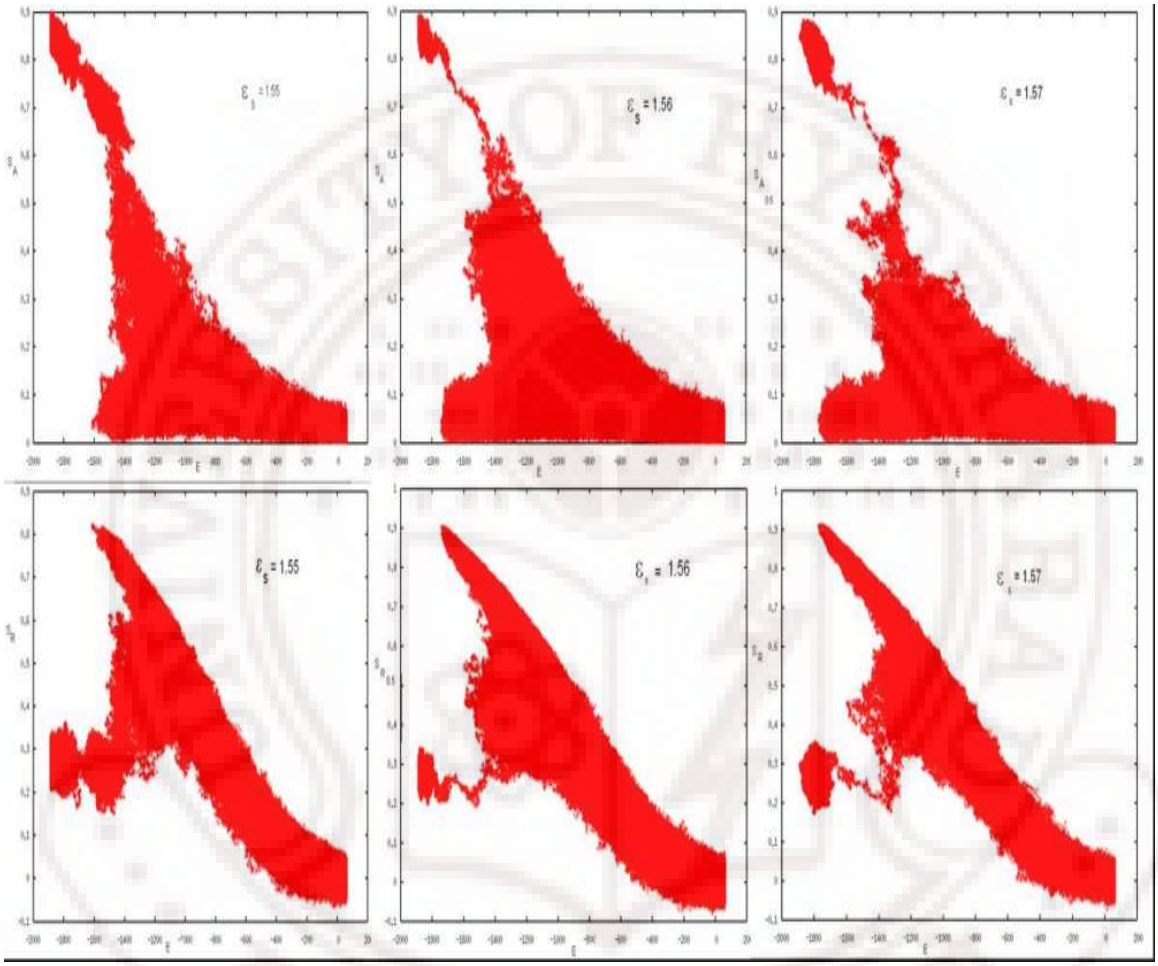

Figure 5.25 Multi-canonical ensembles collected during the production run for $\epsilon_s = 1.55,\ 1.56$ *and* 1.57

temperatures (say corresponding to $T = 0.4$ in the present case), we observe that there is a sudden transition from a well defined axial director structure ($S_A = 0.75$, $S_R = 0.25$, at $\epsilon_s = 1.55$) to a radially ordered director structure ($S_A = 0.05$, $S_R = 0.85$, at $\epsilon_s = 1.56$), as shown in the fig 5.24, triggered by a small change in the anchoring strength. This may be seen as the threshold value of ϵ_s below which, for the given

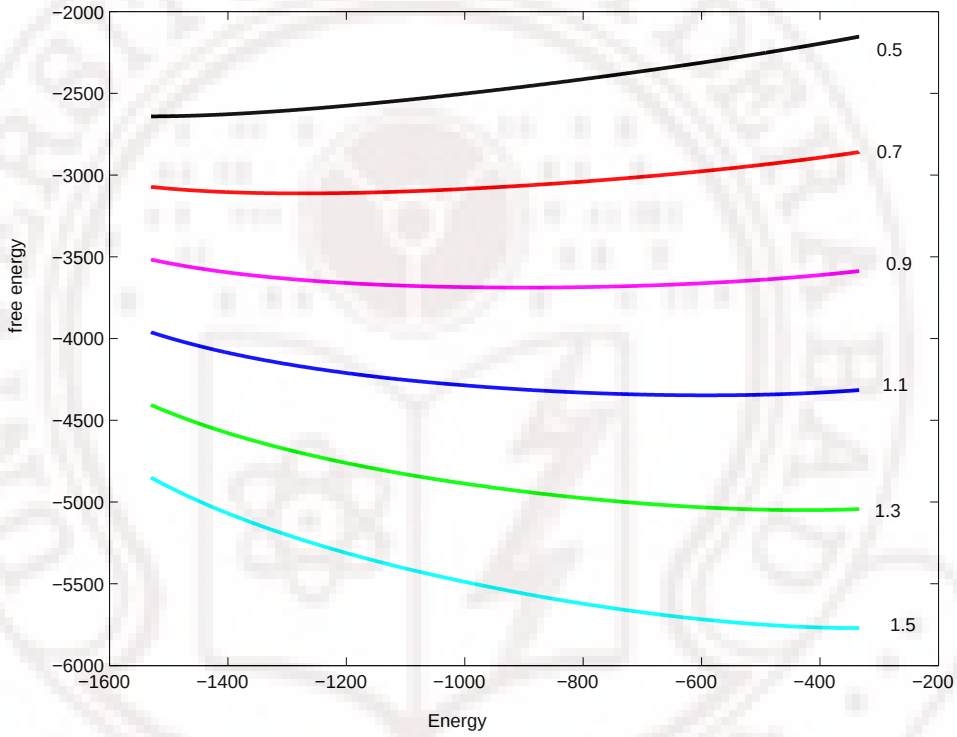

Figure 5.26 Free energy profiles as a function of energy for $\epsilon = 1.55$ at various temperatures bracketing the NI trnasition.

geometry of the film, elastic property of the medium forces a predominant axial order. Above this value of ϵ_s, surface anchoring effects dominate and the thermally driven phase transition degenerates into a simple non-singular development of radial order on cooling the system. From the perspective of anchoring strength as the control parameter, this behaviour corresponds to an anchoring driven transition between two qualitatively different director structures. This work was reported earlier in [44].

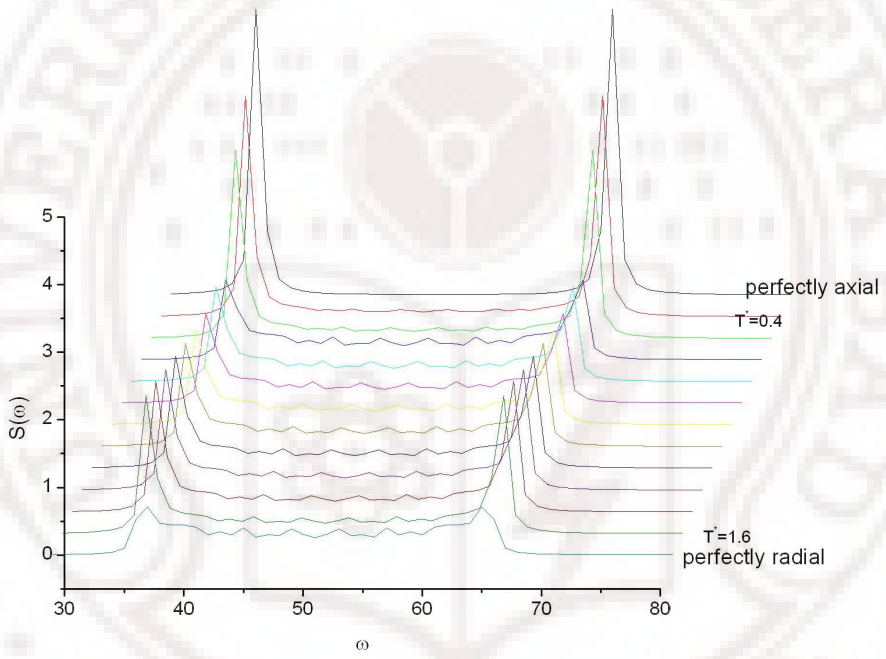

Figure 5.27 Simulated DNMR spectrum for various anchoring strengths.

Bibliography

[1] B. Jerome, *Phys. Rep.* **54**, 391 (1991).

[2] P. Sheng, *Phys. Rev. A.* **26**:1610, 1982; *Phys. Rev. Lett.*, **37**:1059, (1976).

[3] P. I. C. Texeira and T. J. Sluckin, *J. Chem. Phys.* **97**, 1498 (1992); P. I. C. Texeira and T. J. Sluckin, *J. Chem. Phys.* **97**, 1510 (1992); A. Poniewierski and T. J. Sluckin, *Mol. Cryst. Liq. Cryst.* **111**, 373-386 (1984); G. R. Luckhurst, T. J. Sluckin and H. B.Zewdie, *Mol. Phys.* **59**, 657-678 (1986); M. M. Telo da Gama, P.Tarazona, M. P. Allen and R. Evans, *Mol. Phys.* **71**, 801-821 (1990); M. P. Allen, *Mol. Simulation*, **4**, 61-78 (1989).

[4] M. P. Allen, *Mol. Simulation*, **4**, 61-78 (1989).

[5] Z. Zhang, A. Chakrabarti, O. G. Mouristen and M. J. Zuckermann, *Phys. Rev. E* **53**, 2461 (1996); T. Gruhn and M. Schoen, *Phys. Rev. E* **55**, 2861 (1997); T. Gruhn and M. Schoen, *Mol. Phys.* **93**, 681 (1998); G. D. Wall and D. J. Cleaver, *Mol. Phys.* **101**, 1105 (2003); D.J.Cleaver and P. I. C. Texeira, *Chem. Phys. Lett.* **338**, 1 (2001).

[6] T. Rasing and I. Musevic, *Surfaces and Interfaces of Liquid Crystals*, (Springer, Berlin, 2004).

[7] C. Uche, S. J. Elston and L. Parry-Jones, *J. Phys. D: Appl. Phys.* **38**, 2283 (2005).

[8] C. Tsakonas, et. al., *Appl. Phys. Lett.*, **90**, 111913 (2007).

[9] S. Ladak, A. Davidson, et. al., *J. Phys. D: Appl. Phys.* **42**, 085114 (2009).

[10] R. Barberi, et. al., *J. Appl. Phys.* **84**, 3, 1321 (1998).

[11] J-H.Kim, et. al., *Appl Phys. Lett.* **78**, 20, 3055 (2001).

[12] G. Barbero, G. Skacej , A. L. Alexe-Ionescu and S. Zumer, *Phys. Rev. E* **60**, 628 (1999).

[13] C. V. Brown, M. J. Towler, V. C. Hui, and G. P. Bryan-Brown, *Liq. Cryst.* **27**, 233 (2000).

[14] C. V. Brown, L. A. Parry-jones, S. J. Elston, and S. J. Wilkins, *Mol. Cryst. Liq. Cryst* **410**, 945 (2004).

[15] L. A. Parry-Jones, E. G. Edwards, S. J. Elston, and C. V. Brown, *Appl. Phys. Lett.* **82**, 1476 (2003); L. A. Parry-Jones, E. G. Edwards, and C. V. Brown, *Mol. Cryst. Liq. Cryst.* **410**, 955 (2004).

[16] P. Patricio, M. M. Telo da Gamma, and S. Dietrich, *Phys. Rev. Lett.* **88**, 245502 (2002).

[17] X. Lu, Q. Lu, Z. Zhu, J. Yin, and Zongguang Wang, *Chem. Phys. Lett.* **377**, 433 (2003).

[18] D. H. Chung, T. Fukuda, *et. al., J. Appl. Phys.***92**, 1841 (2002).

[19] G. Barbero, T. Beic, A. L. Alex-Ionescu and R. Moldovan, *J. Phys. II.* **2**, 2011 (1992).

[20] T. Z. Qian and P. Sheng, *Phys. Rev. Lett.* **77**, 4567 (1996); T. Z. Qian and P. Sheng, *Phys. Rev. E.* **55**, 7111 (1997).

[21] V. K. Gupta and N. L. Abbott, *Science* 276, 1533 (1997).

[22] S. Kondrat and A. Poniewierski, *Phys. Rev. E.*, **64**, 031709 (2001).

[23] A. Poniewierski and S. Kondrat, *J. Mol. Liq.* **112**, 61 (2004).

[24] O. K. C. Tsui, F. K. Lee, B. Zhang, and Ping Sheng, *Phys. ev. E***69**, 021704 (2004).

[25] S. Kondrat, A. Poniewierski and L. Harnau, *Eur. Phys. J. E* **10**, 163 - 170 (2003).

[26] L. Harnau, S. Kondrat and A. Poniewierski, *Phys. Rev. E.*, **72**, 011701 (2005).

[27] T. J. Atherton and J. R. Sambles, *Phys. Rev. E.*, **74**, 022701 (2006).

[28] L. Harnau, S. Kondrat and A. Poniewierski, *Phys. Rev. E.*, **76**, 051701 (2007).

[29] F. C. Frank, *Discuss. Faraday Soc.* **25**, 19 (1958).

[30] P. G. de Gennes and J. Prost, *The Physics of liquid crystals*, 2nd ed., Clarendon, Oxford (1993).

[31] A. Rapini and M. Papoular, *J. Phys. (Paris)*, Colloq. **30**, C4-54 (1959).

[32] F. Barmes and D. J. Cleaver, *Phys. Rev. E* **69**, 061705 (2004); F. Barmes and D. J. Cleaver, *Chem. Phys. Lett.* **425**, 44 (2006).

[33] F. Wang, and D. P. Landau, *Phys. Rev. Lett.* **86** 2050 (2001); F. Wang and D. P. Landau, *Phys. Rev. E* **64** 056101 (2001).

[34] D. Jayasri, V. S. S. Sastry and K. P. N. Murthy, *Phys. Rev. E* **72**, 036702 (2005). P. Poulain, F. Calvo, et. al., *Phys Rev E* **73** 056704 (2006).

[35] P. A. Lebwohl and G. Lasher, *Phys. Rev. A* **6**, 426 (1972).

[36] C. Zhou, T. C. Schulthess, S. Torbrugge, and D. P. Landau, *Phys. Rev. Lett.* **96**, 120201 (2006).

[37] M. E. J. Newmann and G. T. Barkema, *Monte Carlo methods on statistical physics*, Clarendon press, Oxford (1999).

[38] K. P. N. Murthy, *Monte Carlo methods in statistical physics*, Universities press, India (2004).

[39] G. R. Luckhurst and G. Saelli, *Mol. Cryst. Liq. Cryst.* **395**, 183-192 (2003); G. R. Luckhurst and S. Romano, *Liq. Cryst.* **26**, 6, 871-884 (1999).

[40] D. Jayasri, V.S. S. Sastry and K. P. N. Murthy, CMFM 09, BHU, Varanasi (2009).

[41] D. Jayasri, Regina Jose, V.S. S. Sastry and K. P. N. Murthy, ECLC 09, Colmar, France (2009).

[42] G. P. Crawford and S. Zumer,*Liquid crystals in complex geometries*, Taylor and Francis, London (1996).

[43] P. Ziherl and S. Zumer, *Phys. Rev. Lett.* **78**, 4, 682-685 (1996).

[44] D. Jayasri, V. S. S. Sastry and K. P. N. Murthy, ILCC 06, Keystone, Colarado (2006); D. Jayasri, V. S. S. Sastry and K. P. N. Murthy, 22nd DAE symposium on solid state physics, Mysore (2008).

Chapter 6

Conclusions

Prediction of macroscopic behaviour of physical systems based on Monte Carlo simulations typically rely on building canonical ensembles of microstates appropriate to the given Hamiltonian and under the given boundary conditions. The efficacy of the method depends on the ability of the algorithm employed to perform effective random walk in the relevant configuration space, sampling representative microstates relevant to the ensemble in a realistic time frame. This procedure is thus limited by the topology of the relevant free energy surface that the system presents under the given physical constraints. In systems undergoing phase transitions, or those which are frustrated due to competing external conditions, this topology might introduce several minima separated by barriers. As the barrier height becomes appreciable for purposes of sampling (which is typically the case as the system size goes up), this algorithm is beset with the task of trying to sample two relevant regions of configuration space separated by regions reminiscent of quasi-ergodicity. This issue can be addressed at least notionally by realizing that a sampling carried out with uniform distribution along the energy axis is insensitive to these barriers. Developments of different algorithms over the last two decades try to implement this idea to differ-

ent degrees of adaptation of the concept as well as varying degree of efficacy. The entropic sampling method, implemented by the algorithm suggested by Wang and Landau (WL), is one such recent technique, and seems promising to tackle these problems.

In this context, the first objective of the thesis has been to apply the WL algorithm to liquid crystal systems. As has been noted earlier in other cases, application of the entropic sampling methods to systems requiring continuous random walk in the configuration space is not straight forward, primarily attributed as due to the very many number of microstates that are available to the system, and without further algorithmic modifications WL algorithm has been found to be efficient only for small liquid crystal systems. We report here certain modifications requiring repeated application of WL cycles with appropriate (the so-called) modification factors. We find that the modified WL scheme can lead to satisfactory results to reasonably large sizes of lattice ($25 \times 25 \times 25$) within an acceptable time frame ($\sim$ 300 CPU hours). In this process we also implemented the innovative idea, suggested for magnetic systems, of frontier sampling which accelerates the process of convergence within the scheme of WL algorithm. We report details of implementation of this algorithm taking the example of a liquid crystal represented by the Lebwohl-Lasher lattice Hamiltonian. The efficacy and accuracy of this technique has been validated satisfactorily by carrying out prototype runs on a lattice size of $20 \times 20 \times 20$. For testing the robustness of this modified algorithm, we also considered a liquid crystal system confined to a porous medium, undergoing transition from the isotropic to the nematic (IN) phase. We introduced randomly quenched disorder to mimic the confinement effects, as has been proposed earlier, and simulated satisfactorily such systems in respect of the effect of confinement on the IN transition temperatures. The second objective has been to apply the entropic sampling technique as developed above to two different

liquid crystal systems: liquid crystal elastomers described by a coarse-grained lattice model and liquid crystal films bounded by substrates which have both geometric and chemical patterns. Liquid crystal elastomers (LCE), recently investigated based on canonical sampling methods by employing two distinct lattice Hamiltonian models, present certain challenging problems for the entropic methods. To start with, there are two degrees of freedom to be sampled, namely the orientational dynamics of the mesogenic units (forming part of the polymer chains) and the global strain to which this dynamics is coupled via (random) cross-links between polymer chains. This requires a two-dimensional random walk, with both Monte Carlo variables requiring continuous steps. The second issue arises due to the recognition that terms in one of the Hamiltonians, which depend on the global strain, are indeed of entropic origin, and hence are (linearly) temperature dependent. This calls for a different way of implementing the entropic algorithm, in contrast to what has been done hitherto. The present work aims at tackling these two issues and reports simulation results based on these two lattice Hamiltonians of LCE, revisited with the entropic methods.

The thermal behaviour of the LCE based on the first model Hamiltonian (which incorporates the contributions from elastic degrees of freedom as pure energetic terms) has been computed over a wide temperature region (with high resolution in temperature) by first constructing the two-dimensional density of states and hence the entropic ensemble, and subsequent reweighting of these states to obtain canonical ensembles at the chosen temperatures. We find a few interesting features of this Hamiltonian based on these simulations: 1. the homogeneous part of this Hamiltonian (without external fields and stresses, and without randomly quenched disorder) with the coupling strength γ set to unity, as was used in the reported canonical simulations, predicts a non-linear coupling between the two parameters leading to unusually high strains in contrast to the experimentally reported values; 2. the origin for this behaviour

appears possibly due to an unrealistic choice of the coupling constant, which at the chosen value of unity corresponds to the assumption of extreme shape anisotropy of the polymer chains (in terms of its definition in the Hamiltonian); 3. reduction of γ has the effect of making this coupling between the two order parameters progressively linear, which is expected based on other theoretical considerations; 4. decrease of γ has qualitatively the same effect on the transition behaviour (softening of the transition and changes in the transition temperature) as that of introducing different types of inhomogeneities; and 5. the presence of heterogeneities within the system (as introduced in the earlier work) hence need not be the only cause for this Hamiltonian to make contact with the experimental data, and 6. these results indicate the desirability of also including factors other than shape anisotropy of polymer chains in determining the degree of coupling between the two order parameters. It should be noted that the contribution to the pure elastic energy is still entropic even within this model and the temperature dependence is indeed embedded in the definition of the shear modulus appearing in the expression, though taken as a constant for purposes of simulation.

The second model of LCE investigated here treats the contributions from strain, as well as its coupling to the orientational order, as entropic in nature based on its origin from rubber elasticity in such systems. Further, the coupling parameter contains, besides a free parameter (χ) a deformation-dependent term which is qualitatively different from the first Hamiltonian model, bounded to finite limits over the entire range of the strain. Monte Carlo simulations carried out earlier on this model report in detail the thermal behaviour of this system with a certain choice of the model parameters [polymer cross-link density ($\alpha = 0.3$) and the free parameter ($\chi = 0.5$)], consistent with experimental conditions. We applied the entropic sampling procedure on this system and the salient features of this work are: 1. the mixed nature of

the Hamiltonian terms is dealt with by dividing the computation into two parts: the energetic origin of the pure orientational part of the Hamiltonian is used to compute the density of states as before, and the entropic nature of the second term is exploited to compute the probability distribution along the strain axis; 2. the combined density of states in the space of orientational order and strain is then constructed by combining these two probabilities, which due to their assigned distinct origins are treated independent; 3. the entropic ensembles obtained by performing random walk in this 2-dimensional space, biased by the density of states, are used to obtain canonical ensembles which are localized distributions in this 2-d space, and the results extracted from this model (with the above chosen values of α and χ) agree very well with the canonical results reported earlier; and 4. such simulations are carried out varying the values of α and χ, each over the range $[0, 1]$ and one at a time, to study the effect of the cross-linking density (which sets the energy scale of the elastic term with respect to the anisotropic interaction of the constituent mesogenic units) and the free coupling constant (which depends on several other factors pertinent to the specific system, besides in principle on the cross-link density itself), and the results which are found to be on expected lines validate the procedure suggested to tackle such mixed Hamiltonians.

The application of entropic sampling technique to liquid crystals subjected to boundary conditions from patterned substrates encompassed two systems. In the first system, the liquid crystal is bounded between a flat surface with anchoring influence at the desired tilt angle and a patterned substrate (which has a geometric structure and variable chemical influence along the structure). The results obtained from the present simulations bring out the following features: 1. the nearly homeotropic equilibrium structures with this geometry (the so-called H-structures) predicted based on continuum model (and on the reduction of the model to two dimensions owing to

the symmetry of the film) do not seem to be wholly realizable; 2. the temperature evolution of the director structure of the film indicates that even in the very low temperature nematic phases [for example, at $T = 0.4$, with $T_{NI} \sim 1.12$ for 3-d LL model] director distortions away from the normal occur in the middle of the film, though progressively decreasing with temperature; 3. the relative phase of the chemical pattern with respect to the geometric pattern plays a significant role in determining the director structure, and in assigning the effective anchoring angle to be used at the patterned substrate while replacing the actual surface with a planar substrate; 4. such confinement introduces phase biaxiality in the medium and it can be substantial depending on the patterning conditions; and 5. the free energy profiles computed from the density of states show the onset of the transition, and the distribution of microstates collected in the entropic ensemble, sorted out according to the parameters of interest, bring the above mentioned features into focus.

The liquid crystal film pasted on a spherical substrate is a toy model to study the effect of two competing molecular mechanisms on the thermal behaviour of the system. To this end, the number of mesogenic units that participate in the simulation (via the thickness of the film), and the degree of the distorting effect of the surface (via the radius of the sphere) are first experimented with (employing canonical simulations), looking for evidences of such competition. The results of the present investigations on this film show some interesting features: 1. in the absence of the influence of the spherical substrate (by making its anchoring strength zero) the film exhibits a well defined NI transition, the ordering being brought out by the interacting mesogenic units (LL interaction) placed on the thin spherical shell; 2. progressive introduction of radial anchoring has the effect of promoting the radial order initially on cooling, which finally yields to the strong enough axial order at low enough temperatures; 3. this trend continues until a threshold level of anchoring is reached, beyond which the radial

ordering persists (at the cost of axial order) even at the lowest temperature reached in the simulation; 4. viewed as a phenomenon of a sufficiently cooled nematic, this corresponds to a sudden transition from axial director structure to radial structure due to changes in the anchoring strength; 5. the distribution of microstates in the entropic ensemble shown with respect to their energy and sorted according to the different order parameters, indicate the presence of microstates of the same energy distributed in different regions of configuration space and distinctly separated with respect to their orientational ordering; and 6. it is possible to obtain comprehensive maps of microstates through the entropic sampling technique, and such investigations seem to offer a promising way of probing the configuration space in frustrated systems with rugged free energy landscapes.

In summary, this thesis makes a modest attempt at developing computational tools to extend entropic sampling methods to liquid crystal systems of moderate size, and tries to illustrate its applicability with a few examples.

Appendix A

Numerical tricks to avoid overflow errors

Let g_i denote the number of microstates in the i^{th} energy bin and $\alpha_i = log(g_i)$ the corresponding microcanonical entropy. Let us define $\xi = log(\alpha_i)$. To avoid errors due to overflow in the computations, we perform the entire simulation in terms of ξ. The acceptance probability p and the weight factor used in the reweighting procedure are written in terms of ξ. Berg's addition method [1] is used to calculate these parameters in log-log scale as described below. According to [1], if we have two values $a = log(A)$ and $b = log(B)$ we can calculate $c = log(C)$ and $d = log(D)$ where $C = A + B$ and $D = A - B$ as:

1. Let $x = max(a, b)$ and $y = min(a, b)$. Then,

$$\begin{aligned} c &= x + log[1 + exp(y - x)] \\ C &= exp(c) = exp[x + log\{1 + exp(y - x)\}] \end{aligned} \tag{A.1}$$

2. $exp(d) = sign(a - b) \times exp[x + log\{1 - exp(y - x)\}]$

Let the current microstate belong to an energy bin c and the trial microstate to a bin t. The acceptance probability of the trial microstate in the Wang-Landau algorithm is then given by

$$p = \begin{cases} 1 & \text{if } \xi_t \leq \xi_c \\ exp\Big[- exp\big\{\xi_t + log\big(1 - exp(-(\xi_t - \xi_c))\big)\big\}\Big] & \text{if } \xi_c < \xi_t \end{cases} \tag{A.2}$$

If the visited microstate has an energy which belongs to say i-th bin, then ξ_i is updated to $\xi_i + log(log(f))$ where f is the so-called modification factor or Wang-Landau factor for that run.

The reweighting of the grand ensemble of microstates generated during the production run is carried out in log-log scale as follows. Let $\mathcal{C}$ be the microstate under consideration. Let the energy $E = E(\mathcal{C})$ of the microstate belongs to the bin c. Let ξ_c be the value of ξ in that bin. The weight factor (say, $W(C)$) used for reweighting the microstates obtained from the grand ensemble is given by

$$W(C) = \begin{cases} exp\Big[exp\big[\xi_c + log\{1 - exp(-\Delta_1)\}\big]\Big] & \text{where } \Delta_1 = \xi_c - log(\beta E) \geq 0 \\ exp\Big[exp\big[log(\beta E) + log\{1 - exp(-\Delta_2)\}\big]\Big] & \text{where } \Delta_2 = log(\beta E) - \xi_c \geq 0 \end{cases} \tag{A.3}$$

The average of any macroscopic property O is calculated employing the reweighting formula using the weight factor $W(C)$ as shown below:

$$\langle O \rangle = \frac{\sum_C O(C) W(C)}{\sum_C W(C)} \tag{A.4}$$

1. B. A. Berg, arxiv: cond-mat/0206333v2 (2002).